

University of Alberta

On Mixing and Demulsifier Performance in Oil Sands Froth Treatment

by

Patrick G. Laplante

A thesis submitted to the Faculty of Graduate Studies and Research
in partial fulfillment of the requirements for the degree of

Master of Science in Chemical Engineering

Department of Chemical and Materials Engineering

© Patrick G. Laplante
Fall 2011
Edmonton, Alberta

Permission is hereby granted to the University of Alberta Libraries to reproduce single copies of this thesis and to lend or sell such copies for private, scholarly or scientific research purposes only.

Where the thesis is converted to, or otherwise made available in digital form, the University of Alberta will advise potential users of the thesis of these terms.

The author reserves all other publication and other rights in association with the copyright in the thesis and, except as herein before provided, neither the thesis nor any substantial portion thereof may be printed or otherwise reproduced in any material form whatsoever without the author's prior written permission.

On Mixing and Demulsifier Performance in Oil Sands Froth Treatment

Abstract

The impact of mixing on diluted bitumen de-watering is studied in two stages using a fractional factorial design of experiments. The first stage evaluates the relative effects of bulk demulsifier dosage, local maximum energy dissipation, and mixing time. The second stage of experiments evaluates the relative effects of bulk demulsifier dosage, local maximum energy dissipation, mixing time, and the injection concentration of the demulsifier. Shaker table results did not compare well with results obtained using a stirred tank. A shear and sedimentation test cell (SSTC) is designed to conduct mixing and settling in the same vessel while providing a large ratio of impeller volume to tank volume. The bulk concentration of demulsifier is the dominant effect, but favourable levels of local maximum energy dissipation, mixing time, and injection concentration are necessary to optimize demulsifier performance. Solids removal is shown to be a function of water removal.

Table of Contents

Chapter 1 : Mixing and the Oil Sands	1
1.1 Oilsands Extraction: An Overview	4
1.1.1 Mining Operations.....	4
1.1.2 Water-Based Extraction	4
1.1.3 Froth Treatment - A Brief Overview	5
1.2 Mixing and Multi-Phase Systems: An Overview	6
1.2.1 Characterisation of Fluid mixing.....	6
1.2.2 General Mixing Calculations for Newtonian Fluids.....	6
1.2.3 Suspension of Liquids and Solids	9
1.2.4 Size Distribution of Suspended Liquids and Solids.....	10
1.2.5 Drop Breakup in Liquid-Liquid Dispersions	12
1.2.6 Coalescence and Flocculation in Multiphase Systems	13
1.2.7 Liquid-Liquid Dissolution	15
1.3 Naphtha Based Froth Treatment	16
1.3.1 W/O Emulsion Stability	17
1.3.2 Chemical W/O Emulsion Breakers.....	18
1.3.3 Mixing Studies in Froth Treatment	19
1.4 Knowledge Gaps	19
Chapter 2 : Evaluation of Mixing Effects on Bitumen Clarification – Phase 1 21	
2.1 Experimental Setup:	22
2.1.1 Pre-Mixing Protocol.....	22
2.1.2 Mixing Protocol	26
2.1.3 Design of Experiments.....	29

2.1.4	Karl-Fischer Titration.....	32
2.2	Results/Discussion	33
2.2.1	Batch Gravity Settling Results.....	33
2.2.2	Mixing and Demulsifier Effects on Settling.....	36
2.2.3	The Nature of the Oil-Water Interface.....	41
2.2.4	Material Balance Considerations from OWS Analysis	45
2.2.5	Karl Fischer and O/W/S Water Content Comparison.....	46
2.2.6	Solids Reduction by Water Removal.....	49
2.3	Conclusions.....	50
Chapter 3 : Evaluation of Mixing Effects on Bitumen Clarification –		
Phase 2 52		
3.1	Experimental Design	53
3.1.1	Pre-Mixing Protocol.....	55
3.1.2	SSTC Design and Mixing Protocol.....	55
3.1.3	Design of Experiments.....	61
3.1.4	Karl-Fischer Titration.....	64
3.2	Results/Discussion	65
3.2.1	Mixing and Demulsifier Effects on Settling.....	68
3.2.2	Lumped Parameter Multiple Linear Regression (MLR)	78
3.2.3	Initial Settling and Other Design Considerations.....	80
3.2.4	The Nature of the Oil-Water Interface.....	82
3.2.5	Solids Reduction and Characteristics	85
3.3	Conclusions.....	88
A.	PHASE 1 EXPERIMENTAL DATA.....	89
B.	PHASE 2 EXPERIMENTAL DATA.....	97

C. PRE-MIXING EXPERIMENTS 109

List of Figures

Figure 1-1: The dimensions of segregation, reproduced from (Kresta 2010) with permission..... 6

Figure 2-1: Experimental setup and procedure..... 24

Figure 2-2: Sample image at 100x magnification following pre-mixing protocol..... 26

Figure 2-3: Variable coding for Box-Behnken fractional 29

Figure 2-4: Kam Controls Karl-Fischer calibration 32

Figure 2-5: Consolidated batch gravity settling results; product water content decreases as a function of time. Variable order: (X_C, X_ϵ, X_t) 34

Figure 2-6: Consolidated batch gravity settling results; product water content decreases as a function of time. Variable order: (X_C, X_ϵ, X_t) 34

Figure 2-7: Three repeated center point runs: there is good repeatability between runs. 35

Figure 2-8: Representative batch gravity settling profiles for demulsifier concentrations of 0, 50, and 100 ppm. Average final water concentrations are 1.64%, 0.68%, and 0.34% respectively. Variable order: (BC, ϵ, t) 36

Figure 2-9: Main regression coefficients with 95% confidence intervals as a function of time – absolute water content (wt%) 37

Figure 2-10: Quadratic regression coefficients with 95% confidence intervals as a function of time – absolute water content (wt%) 38

Figure 2-11: Main regression coefficients with 95% confidence intervals as a function of time – water reduction (%) 38

Figure 2-12: Quadratic regression coefficients with 95% confidence intervals as a function of time – water reduction (%)	39
Figure 2-13: Water content as a function of water reduction at a normalized height of $h/Z=0.2$	44
Figure 2-14: Water content as a function of water reduction at a normalized height of $h/Z=0.1$	44
Figure 2-15: Material balance closure errors for water, solids, naphtha, and bitumen; the error in total hydrocarbons measured is minimal	46
Figure 2-16: Standard deviation of Karl-Fisher measurements normalized by average measurement; each measurement was repeated 3 times	47
Figure 2-17: Comparison of initial water content measured with KF titration and OWS analysis; OWS analysis over predicts compared to KF titration	48
Figure 2-18: Product water reduction for each experimental run, from Karl-Fisher titration data and OWS analysis; OWS analysis underpredicts product water reduction compared to KF titration	48
Figure 2-19: Initial solids content as a function of initial water content	49
Figure 2-20: Final solids content as a function of final water content; a linear trend is observed	50
Figure 3-1: Schematic of experimental setup and procedure; the sample is pre-mixed and heated to 76.5 °C and then transferred to two SSTC's. Demulsifier is injected mixed with the diluted bitumen, and the sample is allowed to settle for 60 minutes.	54
Figure 3-2: Sample image at 100x magnification following pre-mixing protocol.....	56
Figure 3-3: SSTC design schematic; the glass stirred tank has a volume of 1L, a tank diameter T of 7.5 cm, and $T/12$ baffles. A $\frac{1}{4}$ in shaft is supported at the tank bottom using a steady bearing. Stainless steel $\frac{3}{8}$ "	

sampling and injection ports protrude from the tank lid. The tank is jacketed to allow for easy circulation of heating fluid. Impellers are equally spaced between distance $D/3$ from tank bottom and D below fluid surface.

..... 58

Figure 3-4: Power number measurements as a function of Reynolds' number for 5 A310 impellers, 5 Rushton impellers, and 6 Intermig impellers. Test Fluid: ethylene glycol at 25 °C (6 cSt). Data reproduced with permission (Machado and Kresta 2011). 60

Figure 3-5: Diluted bitumen water content during batch gravity settling, centre point repeats (5); repeated runs provide an estimate of variability from run to run 66

Figure 3-6: Diluted bitumen water content during batch gravity settling, 54 experimental runs included..... 66

Figure 3-7: Diluted bitumen water content during batch gravity settling, with final water content exceeding 1 wt%. Unfavourable mixing conditions can render 26 ppm of demulsifier as ineffective as 2 ppm demulsifier. Variable order: (X_{BC} , X_{ϵ} , X_t , and X_{IC})..... 67

Figure 3-8: Diluted bitumen water content during batch gravity settling, with final water content less than 0.5 wt%; favourable mixing conditions can yield similar results using 26 ppm and 50 ppm of demulsifier. Variable order: (X_{BC} , X_{ϵ} , X_t , and X_{IC})..... 68

Figure 3-9: Regression coefficients and their confidence intervals for four variable multiple linear regression; significant main effects include bulk concentration (BC), mixing intensity (ϵ), mixing time (t), and injection concentration (IC) 70

Figure 3-10: Diluted bitumen water content during batch gravity settling, bulk concentration (BC) and mixing intensity (ϵ) block; intense mixing and greater demulsifier dosage are preferred. Variable order: (X_{BC} , X_{ϵ} , X_t , and X_{IC}). 71

Figure 3-11: Diluted bitumen water content during batch gravity settling, bulk concentration (BC) and mixing time (t) block; longer mixing time and greater demulsifier dosage are preferred. Variable order: (X_{BC} , X_{ϵ} , X_t , and X_{IC}). 72

Figure 3-12: Diluted bitumen water content during batch gravity settling, bulk concentration (BC) and injection concentration (IC) block; greater demulsifier dosage is preferred. Variable order: (X_{BC} , X_{ϵ} , X_t , and X_{IC})..... 72

Figure 3-13: Diluted bitumen water content during batch gravity settling, mixing intensity (ϵ) and mixing time (t) block; intense mixing and longer mixing time are preferred. Variable order: (X_{BC} , X_{ϵ} , X_t , and X_{IC}). 73

Figure 3-14: Diluted bitumen water content during batch gravity settling, mixing intensity (ϵ) and injection concentration (IC) block; intense mixing and less concentrated injections are preferred. Variable order: (X_{BC} , X_{ϵ} , X_t , and X_{IC}). 73

Figure 3-15: Diluted bitumen water content during batch gravity settling, mixing time (t) and injection concentration (IC) block; intense mixing and longer mixing time are preferred. Variable order: (X_{BC} , X_{ϵ} , X_t , and X_{IC})... 74

Figure 3-16: Microscope images before and after 60 minutes batch gravity settling at 100x magnification; final water content decreases as floc size increases 76

Figure 3-17: Microscope images obtained from samples at the bottom of the SSTC; the sampled bottom is observed to be a combination of normal diluted bitumen product, larger droplets, and packed flocs of water and solids 77

Figure 3-18: Regression coefficients for three variable multiple linear regression; significant main effects include bulk concentration (BC), energy dissipation (w), and injection concentration (IC) 79

Figure 3-19: Adjusted R^2 values as a function of time for both 4 and 3 factor multiple linear regressions 79

Figure 3-20: Initial water removal rate, water content immediately following initial settling (C_s) and final water content (C_f) can be determined by isolating linear trends in the data 80

Figure 3-21: Observed initial settling rate as a function of water content; initial settling rate increases drastically with reducing final water content 81

Figure 3-22: Initial settled water content is approximately 0.2 wt% greater than final water content after 60 minutes settling;..... 82

Figure 3-23: Water content at $h/Z=0.2$ following 60 minutes batch gravity settling; water content is approximately equal to final water content as measured from 1.25" from the surface of the SSTC. Solids content correlates with water content. 84

Figure 3-24: Water content at $h/Z=0.1$ following 60 minutes batch gravity settling; there is an abrupt rise in tailings water content following sufficient water content reduction 84

Figure 3-25: Water content at $h/Z=0$ following 60 minutes batch gravity settling; water content increases with decreased final water content in fanning motion (due to high variance in the tailings layer) 85

Figure 3-26: Initial solids content as a function of initial water content; initial solids vary from 1-1.2% while initial water varies from 1.8-2.2% with no correlation..... 86

Figure 3-27: Product solids content (product) as a function of final water content; solids content varies linearly with water content 86

Figure 3-28: Product solids content (middlings) as a function of final water content; solids content varies linearly with water content 87

Figure 3-29: Product solids content (bottoms) as a function of final water content; solids do not correlate well with water content 87

List of Tables

Table 1-1: Power numbers of various impellers under turbulent conditions with 4 standard baffles adapted from (Paul et al. 2004)	8
Table 2-1: Properties and composition of diluted bitumen	23
Table 2-2: Pre-mixing tank dimensions and mixing parameters	25
Table 2-3: Mixing specifications for each mixing configuration. For shaker flasks, 1 L Erlenmeyer flasks are filled to the 500 mL level.	28
Table 2-4: Experimental conditions at each of three levels	30
Table 2-5: Box-Behnken factorial design runs; two-variable pairs are separated into orthogonal blocks.....	31
Table 2-6: A summary of significant effects on batch gravity settling for 1-60 minutes (absolute water content).....	42
Table 2-7: A summary of significant effects on batch gravity settling for 1-60 minutes (water content reduction)	43
Table 2-8: Material balance closure error statistics	45
Table 3-1: Properties and composition of diluted bitumen	53
Table 3-2: Pre-mixing tank dimensions and mixing parameters	57
Table 3-3: SSTC geometry and mixing specifications	59
Table 3-4: Box-Behnken factorial design runs	63
Table 3-5: Variable coding for Box-Behnken fractional.....	64
Table A-1: Batch gravity settling data in wt% water (corr.)	89
Table A-2: Vertical concentration profile data in wt% water (corr.) at normalized height h/Z	90
Table A-3: OWS Data	92
Table B-1: Batch gravity settling data in wt% water (corr.)	97

Table B-2: Vertical concentration profile data in wt% water (corr.) 101
 Table B-3: Solids Content Data 105

List of Symbols

B_d	agglomerate birth rate (class size d)
D_d	agglomerate death rate (class size d)
N_p	power number
N_Q	flow number
N_{js}	just-suspended speed (s^{-1})
\bar{U}	average fluid velocity (m/s)
V_{IMP}	impeller volume (m)
V_{TANK}	tank volume (m)
V_s	settling velocity (m/s)
X_{BC}	bulk concentration
X_C	bulk concentration
X_{IC}	injection concentration
X_t	mixing time
X_ε	mixing intensity
d_{32}	sauter mean diameter (m)

d_i	class size (m)
d_p	mass-mean particle diameter (m)
g_c	gravitational constant, (m/s ²)
n_i	number of drops in a size class i
C	off-bottom clearance (m)
D	impeller Diameter (m)
H	tank height, (m)
M	mass (kg)
N	shaft rotational speed, (s ⁻¹)
P	energy dissipation (W)
Q	volumetric flow rate (m ³ /s)
Re	Reynolds' number
S	impeller submergence (m)
S	Zweitering constant
T	tank width, (m)
We	Weber number
X	mass ratio of suspended solids to liquids
t	time (s)
β	regression coefficient

ε	local energy dissipation rate (W/kg)
η	kolmogorov length scale (m)
θ	dimensionless mixing time
μ	viscosity, (Pa*s)
ν	kinematic viscosity (m ² /s)
ρ	density, (kg/m ³)
ε_{max}	local maximum energy dissipation rate (W/kg)
θ_{95}	dimensionless mixing time to 95% homogeneity
σ	interfacial tension (kJ/m ²)

Chapter 1 : Mixing and the Oil Sands

Alberta's oilsands are an important part of the world's petroleum resources. Alberta's annual production of crude oil is expected to increase from 1.6 million barrels per day in 2010 to 3.5 million barrels per day in 2020 (ERCB 2011). The remaining estimated proved reserves as of 2007 were 179 billion barrels, second only to Saudi Arabia (Radler 2006). Given the world's increasing dependency on oil, Alberta's oilsands will continue to play an important role in the world economy.

What are the oilsands? The oilsands are exactly what they sound like: black, oily sand. Eight cups of sands mixed with two cups cold molasses will give you a rough idea of the texture. The oil is extracted from these

black sands to yield liquid called bitumen with the consistency of the molasses you mixed with the sand. With further processing this black liquid will become a variety of products, ranging from the oil in your car, the gasoline in the car tank, and the plastics which make up your car.

Mixing is the act of agitating a continuous fluid-like component. There are many types of mixing, including fluid mixing, solids mixing, and fluidization of solids with a gas. Although fluidization and solids mixing are large fields of study in their own right, most industrial operations relevant to the process industry involve the mixing of two fluids. Therefore, fluid mixing has received of a great amount of attention for the past fifty or so years.

Fluid mixing can be broadly categorized as a combination of the following processes: liquid-liquid mixing, solid-liquid mixing, or gas-liquid mixing. With respect to liquid-liquid mixing, the liquids may be miscible, immiscible, or partially miscible. Miscible liquids will form one continuous phase, while immiscible liquids will form a continuous phase and a dispersed phase. Partially miscible liquids will dissolve up to a solubility limit, with the excess forming a second phase. Solid-liquid mixing is largely concerned with the drawdown, suspension, and dispersion of solids in a continuous liquid phase. Gas-liquid mixing concerns the successful drawdown and/or dispersion of a gas into a much denser and incompressible liquid phase. One or more of the liquid, solid, or gas components mentioned above may be reacting, dissolving, precipitating, or diffusing into the other component. Non-continuous components may be broken up, agglomerated, suspended, or drawn down. The solid, liquid, and gas pairings mentioned above are highly idealized, and it is often the case that many of these mixing operations are performed simultaneously. Growing numbers of pharmaceutical, cosmetic, industrial, and consumer products are created every year with increasingly complex combinations of mixing operations. Complex mixing operations are often needed to achieve favourable physical or chemical properties. For example, hand creams might be processed by aerating a liquid-liquid dispersion, which is

already stabilized by a colloidal suspension of solids. Furthermore, this liquid-liquid dispersion may contain an additional emulsified liquid phase. While mixing operations are vital to process performance, it is important to remember that they are always part of a greater picture and that it takes at least two components and a goal to mix.

Natural resources are more often than not a combination of many liquid and solid phases, a prime example being the extraction of bitumen from Athabasca oilsands. In the extraction of bitumen from oilsands, a solid-liquid-liquid mixing operation is used to extract liquid bitumen from the solid sands. This liquid bitumen is suspended in the hot water used to extract it. It may also be stabilized by additional solids. This suspension will be aerated in a liquid-liquid-solid-gas operation to yield bitumen froth containing bitumen, water, solids and bubbles of air. This is often accomplished with the aid of chemical dispersion aids, which may or may not be miscible in the process water. The consequences of this water-based extraction process will be carried forward and the froth will undergo many additional mixing operations in order to create a refined product. The bitumen will be diluted and the oil and sand will be separated using many miscible or immiscible chemicals. The processes, possibilities, and physical mechanisms are in theory infinite. This study is concerned with the removal of water and fine solids from naphtha-diluted bitumen. The water and solids are stabilized by a variety of organic and inorganic contaminants naturally occurring in the bitumen. The damage and corrosion which occurs when these solids and salty water are not separated warrants the use of expensive chemical demulsifiers which are often concentrated and must be dissolved into the continuous phase. This step is only one of many in the production of refined products from oilsands ore and is a prime example of a chemically interacting liquid-liquid-liquid-solid mixing problem.

1.1 Oilsands Extraction: An Overview

Athabasca heavy crude is produced by extracting bitumen from oil sands. Deposits can either be mined if they are sufficiently shallow or they can be extracted in situ if they are sufficiently deep. The goal of any commercial oilsands extraction operation is to produce a bitumen product fit for upgrading. Bitumen feed to the upgrader should have as little residual water, salts, and solids as possible in order to avoid corrosion and wear of the upgrading equipment.

1.1.1 Mining Operations

Oil sands consist of ~6-15% bitumen and the balance solids. The solids can be clays, fines, and most notably sand. There is often accompanying water. Water is an important part of Athabasca oil sands in particular as it forms a fine film, separating the bitumen from the solids and facilitates subsequent processing. Approximately twenty percent of the remaining established oil sands reserves are mineable while the remaining 80% are recoverable through in-situ extraction operations (ERCB 2011). Mined oil sands are removed by truck and shovel methods and are transported to the nearest extraction plant as a thick water and oil sands slurry by pipeline, also called hydrotransport. Hydrotransport is a convenient way to reduce oil sands lumps to a manageable size for Clark Water Extraction.

1.1.2 Water-Based Extraction

Clark Water Extraction is the primary extraction method for separating oil from mineable oil sands. Oil is extracted from the sand with the use of hot water, surfactants and pH modifiers. Small bubbles of air are used to entrain bitumen to the top of the slurry, forming a froth containing roughly 60% oil, 30% water, and 10% solids plus additional air. The air is removed with further processing. While very high rates of bitumen recovery are

possible it is important to note that the ore grade (bitumen content), fines content, ionic composition, weathering, and ageing all significantly affect bitumen recovery (Liu et al. 2005). A comprehensive review of water-based extraction by Masliyah et al. (2004) is recommended for all interested readers.

1.1.3 Froth Treatment - A Brief Overview

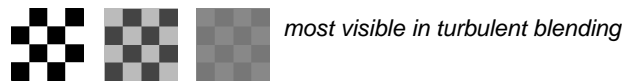
Bitumen froth is not immediately available for refining or even transport for several reasons: the viscosity of the fluid is very elevated, the salts present in the aqueous portion of the froth leads tends to corrode most processing equipment, and fine solids present in the froth will tend to accumulate and cause abrasion to process vessels, piping, and equipment. Froth treatment consists of two steps: a dilution step followed by an optional clarification step. Froth is typically diluted with either naphtha in naphthenic froth treatment or an alkane in paraffinic froth treatment. Both methods of dilution will lead to a much lower viscosity and will allow for settling of most of the water and solids. Naphthenic froth treatment will remove less water and solids, but will lead to a higher oil recovery. This high recovery also leads to less tailings disposal issues. Paraffinic processes precipitate asphaltenes and produce much clearer diluted bitumen (containing less water and solids). Paraffinic solvents are also more expensive and less readily available than naphtha. These processes generally require more solvent than the naphthenic processes. The solvent is evaporated from the bitumen prior to upgrading. Bitumen from the naphthenic process is typically coked, while the clearer and more valuable bitumen from the paraffinic process is typically hydrogenated. Those seeking more information on the selection of froth treatment processes are referred to a review by Shelfantook (2004).

1.2 Mixing and Multi-Phase Systems: An Overview

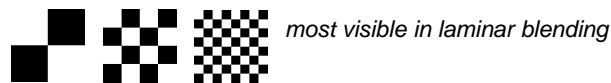
1.2.1 Characterisation of Fluid mixing

Fluid mixing is a diverse field. What is considered properly mixed varies from system to system. What ultimately matters is the goal of the process. This goal can be as simple as obtaining a homogenous mixture of two miscible fluids, or as complicated as destabilizing a solid-stabilized micro-emulsion. The latter would be considered a form of “un-mixing” or separation by most. Many parameters have been used to describe the degree or quality of mixing. A recent review by Kukukova et al. (2009) describes mixing in terms of three parameters: the intensity of segregation, the scale of segregation, and the exposure of the dispersed phase. These parameters are best described in Figure 1-1.

1. Intensity of segregation drops



2. Scale of segregation drops



3. Exposure increases



Figure 1-1: The dimensions of segregation, reproduced from (Kresta 2010) with permission

1.2.2 General Mixing Calculations for Newtonian Fluids

Fluid mixing problems can be generalized because, despite many differences, the continuous phase remains a fluid. This fluid may have a high or low viscosity, which may be Newtonian or non-Newtonian in

nature. Shear-thinning fluids can lead to cavern formation, while shear-thickening fluids are very difficult to process and can lead to severe equipment damage. Excluding these two fluid rheologies, we observe either laminar or turbulent mixing conditions. The pumping power of an impeller stirred tank is characterised by the flow number (Paul et al. 2004), defined as

$$N_Q = \frac{Q}{ND^3} \quad 1-1$$

where Q is the average volumetric flow rate through the impeller (m^3/s); N the shaft rotational speed (s^{-1}); D the impeller diameter (m). The energy consumption in an impeller stirred tank is characterised by the power number (Paul et al. 2004), which is defined as

$$N_P = \frac{P}{\rho N^3 D^5} \quad 1-2$$

where P is the shaft power consumed by the impeller (W); N the shaft rotational speed (s^{-1}); D the impeller diameter (m); ρ the fluid density (kg/m^3). Both the power number and flow number are dependent largely on impeller and tank geometry. Impeller geometry also determines whether the flow is radial (Rushton turbine impeller) or axial (hydrofoil impeller). There are also drastic differences in both flow and power numbers in laminar and turbulent flow. The mixing regime or level of turbulence can be estimated using a common dimensionless number, the Reynolds' number, which is the ratio of inertial to viscous forces. In a stirred tank, the Reynolds' number is defined as (Paul et al. 2004)

$$Re = \frac{\rho ND^2}{\mu} \quad 1-3$$

where μ is the fluid viscosity (Pa.s). Laminar mixing takes place below a Reynolds' number of 10 while fully turbulent mixing takes place at a Reynolds' number greater than 20,000. The two mixing regimes are separated by a transitional region, where local turbulence is experienced near the impeller. At fully turbulent Reynolds' numbers the bulk flow characteristics become independent of viscous forces. Accordingly, the flow numbers and power numbers converge to a constant value reflecting their full proportionality to inertial forces. While typical turbulent flow numbers fall between 0.5-0.8, power numbers vary more widely with impeller geometry. Table 1-1 shows that power number can vary by an order of magnitude over an assortment of commonly used impellers.

Table 1-1: Power numbers of various impellers under turbulent conditions with 4 standard baffles adapted from (Paul et al. 2004)

Impeller Type	N_p
Lightnin A310	0.3
Chemineer HE3	0.3
45° PBT; 4 blades	1.3
Rushton; 6 blades	5

For the simple case of turbulent blending of miscible Newtonian fluids in a stirred tank ($H=T$), the blend time to reach 95% homogeneity in a mixture has been well correlated for all impeller types by Grenville (1992) as

$$N\theta_{95} = \frac{5.20}{N_p^{1/3}} \left(\frac{T^2}{D^2} \right) \quad \text{Re} > 10,000 \quad \mathbf{1-4}$$

$$N\theta_{95} = \frac{183^2}{N_p^{2/3} Re} \left(\frac{T^2}{D^2} \right) \quad 10,000 > \text{Re} > 200 \quad \mathbf{1-5}$$

where T is the tank diameter (m) and H the tank height (m). The Reynolds' number limit of 10,000 varies according to the transitional Reynolds' number.

Static mixers and rotor stators can also be used for turbulent mixing applications. Various inline mixing devices are available for different levels of agitation. Static mixers are of particular interest as they enjoy greater consistency, lower capital and operational costs, lower maintenance costs, and occupy a smaller footprint in a plant environment. These benefits come at the expense of flexibility and residence time. Design correlations for static mixers are well documented and in the Handbook of Industrial Mixing Chapter 12 (Paul et al. 2004).

1.2.3 Suspension of Liquids and Solids

Immiscible liquid-liquid and liquid-solid systems share a lot in common, and the physics surrounding the two are more or less identical. The difference lies mostly in the density of the solid phase which causes suspension issues, and the immobile nature of solids which makes coalescence impossible. Immiscible liquids are also prone to adopt a spherical shape to minimize the energy of the system, while this is often not possible with solids (crystalline shapes are more common, and spherical shapes are rare in amorphous solids). Nevertheless, correlations and mechanistic equations can often be corrected for non-spherical distributions.

First it is best to ask whether or not the dispersed phase can be suspended. In many systems suspension or dispersion is ultimate goal of mixing. An estimate of the "just suspended speed" or N_{js} in a liquid-solid system was formulated by Zweitering (1958) as

$$N_{js} = S\nu^{0.1} \left[\frac{g_c(\rho_s - \rho_l)}{\rho_l} \right]^{0.45} X^{0.13} d_p^{0.2} D^{-0.85} \quad \mathbf{1-6}$$

where X is the mass ratio of suspended solids to liquid x 100 (kg solid/ kg liquid); d_p the mass-mean particle diameter, $(d_p)_{43}$ (m); D the impeller diameter (m); S the dimensionless number which is a function of impeller type, as well as D/T and off-bottom clearance; ν the kinematic viscosity (m^2/s); g_c the gravitational acceleration constant (m/s^2); ρ_s and ρ_l the solid and liquid density, respectively. Using a similar approach the minimum speed required to suspend one liquid into another was given by Skelland and Seksaria (1978)

$$\frac{N_{min} D^{0.5}}{g^{0.5}} = C_{20} \left(\frac{T}{D} \right)^{\alpha_5} \left(\frac{\mu_c}{\mu_d} \right)^{1/9} \left(\frac{\Delta\rho}{\rho_c} \right)^{0.25} \left(\frac{\sigma}{D^2 \rho_c g} \right)^{0.3} \quad \mathbf{1-7}$$

Drawdown of solids or liquids is another concern in liquid-liquid and liquid-solid mixing. This is topic is beyond the scope of this work, as we are concerned with a dispersed phase of equal or greater density than the continuous fluid. Interested readers are referred to the Handbook of Industrial Mixing for further reading (Paul et al. 2004).

1.2.4 Size Distribution of Suspended Liquids and Solids

Mixing operations in liquid-liquid and liquid-solid systems are often concerned with maintaining a specified dispersed phase size distribution. While suspended drops of liquid assume a spherical shape and are separated by a distinct interface, solid particles agglomerate in loosely packed groups called flocs. Voids within the floc are filled with fluid from the continuous phase, and so flocs are rarely spherical in nature. Liquid drops may also form flocs which may coalesce into large drops if favoured by physical forces at the liquid-liquid interface. For convenience, both

drops and flocs will be referred to as agglomerates. What applies to one will often apply to the other with limitations and corrections for physical properties and surface area.

It is well understood that the breakup of agglomerates in turbulent mixing is largely dependent on energy dissipation in the system. Turbulent eddies which are significantly smaller than the agglomerate size will break the agglomerate if the energy dissipated by the eddy overcomes the cohesive forces of the agglomerate. The length scale of the smallest eddies is estimated by the Kolmogorov length scale defined as

$$\eta = \left(\frac{\nu^3}{\varepsilon} \right)^{1/4} \quad \mathbf{1-8}$$

where ν is the kinematic viscosity (m^2/s) and ε the local dissipation rate of turbulent kinetic energy. At this length scale the viscous forces in the eddy are equal to the inertial forces due to turbulent velocity fluctuations (Paul et al. 2004). It is important to note that these turbulent eddies are the smallest of many larger turbulent eddies. The maximum agglomerate size in a breakup-dominated system will be some multiple of the Kolmogorov length scale, while the smallest agglomerate sizes will be limited to the Kolmogorov scale and other fragments produced during breakup (Zhou and Kresta 1998). The application of this result to a stirred tank is not without difficulty, however. The energy dissipation in a stirred tank has been found to vary by up to a factor of 100 (Zhou and Kresta 1996). The maximum and minimum energy dissipations of some commonly used impeller geometries have also been quantified by Zhou and Kresta (1996). In cases where no correlations exist it is possible to obtain a reasonable estimate of the maximum energy dissipation by assuming all energy will be dissipated in the impeller volume. That is,

$$\varepsilon_{max} \sim \frac{P}{\rho V_{Impeller}} = \frac{N_p N^3 D^3}{H_{Impeller}} \quad 1-9$$

where $H_{Impeller}$ is the vertical height of the impeller. This approach has been found to estimate maximum energy dissipation within a factor of 2 (Paul et al. 2004).

Agglomerates are most commonly found in a distribution of sizes. Characteristic diameters must be used to represent these distributions in the most physically relevant way. Although the average diameter can be used in some limited cases, it is not very physically relevant. In liquid-liquid dispersions, the most commonly used diameter is the Sauter mean diameter, d_{32} , defined as

$$d_{32} = \frac{\sum_{i=1}^{i=m} n_i d_i^3}{\sum_{i=1}^{i=m} n_i d_i^2} \quad 1-10$$

where m is the number of size classes corresponding to the drop size distribution, n_i the number of drops and d_i the drop diameter of drops in class size i. The Sauter mean diameter is often used because relates the total volume of the dispersed liquid to the total surface area of the dispersed liquid.

1.2.5 Drop Breakup in Liquid-Liquid Dispersions

Drop breakup has been the subject of rigorous study. Nevertheless, the variety of breakage mechanisms, stabilization, surface interactions and other factors continue to challenge researchers. In liquid-liquid systems, Chen and Middleman (1967) and others validated the Weber number correlation, which states that for geometrically similar, non-coalescing systems

$$\frac{d_{32}}{D} \propto We^{-3/5} \quad 1-11$$

where $We = \rho_c N^2 D^3 / \sigma$ is the Weber number, the ratio of inertial (disruptive) to surface (cohesive) forces and σ the interfacial tension between the two dispersed liquids. This relation assumed a proportional relationship between d_{32} and d_{max} , an assumption that holds true if geometric similarity is maintained. Davies (1987) correlated a rough estimate of ε_{max} with the maximum stable drop size, and illustrated that

$$d_{max} \propto \varepsilon_{max}^{-2/5} \quad 1-12$$

The rate at which breakage occurs is bound to increase as circulation time goes down. It will increase as the distance from the equilibrium drop size distribution goes up. Accordingly, researchers have approached this problem in a way similar to reaction kinetics:

$$\frac{d\Omega}{d\theta} \propto -C_1 \Omega^{C_2} \text{ where } \Omega = \frac{d_{32}(t) - d_{32}^{\infty}}{d_{32}^{\infty}} \text{ and } \theta = Nt \quad 1-13$$

where N is the impeller speed, $d_{32}(t)$ the Sauter mean diameter of the dispersed phase at time t and d_{32}^{∞} its value at equilibrium. Exponential decay functions with a value of C_2 equal to 1 and 2 have been reported (Paul et al. 2004). The decay rate can also be computed using computational fluid dynamics (CFD) given a known breakage rate.

1.2.6 Coalescence and Flocculation in Multiphase Systems

When coalescence and flocculation are involved in a multiphase system, the only practical way to describe the system is with CFD and Population Balance Equations. Population balance equations can be used to describe systems where a combination of breakup and agglomeration occur. The

most general form of the population balance for a discrete volume can be written

$$\frac{\partial n_d}{\partial t} + \nabla \cdot (\bar{U}n_d) - B_d + D_d = 0 \quad \mathbf{1-14}$$

Where for a given agglomerate size, n_d is the number of agglomerates, \bar{U} the velocity normally at the surface of a discrete volume, B_d the birth rate, and D_d the death rate of the agglomerates. This equation is essentially a mathematical material balance that must be exact, assuming that agglomerates can only be introduced into a discrete volume by breakup, coalescence/flocculation, and fluid motion. The particles in the multiphase system are often assumed to be spherical where determining collision frequencies. Equation 1-14 also assumes the dispersed phase to be incompressible, and in this form does not take into account additions to the dispersed phase through condensation, precipitation, and other forms of mass transfer. Given that this equation must hold true for each agglomerate size present in the mixture, the drop size distribution is often discretized into bins rather than using continuous functions. Various approaches to implementing population balances in CFD simulations have been outlined by Ramakrishna (2001).

In breakage controlled systems, the size distribution decreases until it is no longer affected by the shear-induced breakage and the maximum size present approaches the Kolmogorov length scale. In coalescing systems a kinetic steady state is achieved by balancing breakage and coalescence throughout the entire system. Agglomeration rates have typically been expressed in two parts, particle/particle collision frequency and coalescence/agglomeration efficiency. Likewise, breakage rates have been divided into two steps, eddy/particle collision frequency and breakage efficiency.

While population balances will not be utilized in this study it is illustrative to expand on the general equation. Tavlarides & Tsouris (1994) reviewed breakage rates and coalescence rates relating to implementation of population balances in liquid-liquid systems. Flocculating systems have also been described using similar equations (Chin et al. 1998; Zhang and Li 2003). While these equations are very complicated, the underlying message is quite simple: breakup occurs when eddies and aggregates collide, while coalescence/flocculation occurs when two aggregates collide. Whether or not they occur depends on their velocity and trajectory. In turbulent mixing, trajectory is random, and so the collision frequency of any two items can be estimated through collision statistics. In general, breakup rates increase with increased mixing intensity while particles collide more frequently but agglomerate with less efficiency at higher mixing intensities.

1.2.7 Liquid-Liquid Dissolution

Liquid dissolution problems occur when one fluid is not fully miscible with another. Given enough time they will completely mix. Rahidnia and Balasubramaniam (2004) demonstrated that for a water/glycerine system, the diffusivity of glycerine in water depends linearly on the concentration of glycerine being dissolved. Ibemere and Kresta (2007) showed that the miscibility gap between two fluids depended more on the difference in concentration between the dispersed phase and the bulk, as well as the solubility limit of the dispersed liquid. Intuitively it is easy to see that higher rates of energy dissipation will increase the dissolution rate as the contact area between the phases increases. The dissolution time will also be greater than the blend time. Liquid dissolution problems are mesomixing problems. The injection concentration of the dispersed phase will greatly affect the dissolution time.

1.3 *Naphtha Based Froth Treatment*

The goal of froth treatment is to remove water and solids from bitumen froth in order to reduce corrosion and abrasion in subsequent processing steps. Water tends to accumulate in small droplets while solids tend to either remain as individual non-spherical particles or to agglomerate into loosely packed flocs. Separation principles in bitumen dewatering are based on Stokes Law,

$$V_s = \frac{1}{18} \frac{(\rho_p - \rho_f)}{\mu} gD^2 \quad \mathbf{1-15}$$

where V_s is the terminal settling velocity of a spherical particle, ρ_p and ρ_f the densities of the settling particle and the continuous fluid, μ the continuous fluid viscosity, g the acceleration due to gravity, and D the particle diameter. The first step in froth treatment is to dilute hot bitumen with hot solvent. The high temperature and the dilution with solvent both reduce viscosity and decrease density of the continuous hydrocarbon phase, among other things. In naphtha based processes this step reduces water and solids content from 30% and 10% respectively to 2-4% and 1-2% respectively. The remaining water and solids are kinetically stable and will not settle from solution in a practical amount of time. A typical naphthenic froth treatment process operates at 80 °C and has a naphtha to bitumen ratio (N/B) of 0.7 by mass. The water and solids may be separated using either inclined plate settlers (longer settling times) or centrifuges (higher costs).

Ideally the final water and solids content should be decreased even further. Diluted bitumen clarification involves removing additional water and solids from diluted bitumen containing 2-4% water and 1-2% solids. This is done by attacking the stability of the emulsion chemically in order to induce settling.

1.3.1 W/O Emulsion Stability

The stability of water droplets in diluted bitumen emulsions has been studied extensively. Earlier works reviewed by Menon and Wasan (1988) hinted at a sludge layer at the water/oil interface which prevented the coalescence of droplets. A later study by Bhardwaj and Hartland (1994) confirmed that stabilizing agents in the bitumen slowly migrated to the surface of the water droplets, which demonstrated that emulsion ageing contributed to emulsion stability. The initial sludge layer was later demonstrated as being rigid given a sufficiently high concentration of naturally stabilizing material (Yeung et al. 1999). Later studies on emulsion stability focused on the rheology of the interface and on the stabilizing effects of asphaltenes, resins, and fine solids.

The contribution of asphaltenes to water in oil (w/o) emulsion stability has perhaps received the most attention in literature. Stabilization with asphaltenes depends on the concentration of soluble asphaltenes in solution. Paraffinic solvents were found to greatly reduce the solubility of asphaltenes (Yarranton et al. 2000) and this discovery gave rise to paraffinic froth treatment processes. Asphaltenes were later separated into two categories: water-soluble asphaltenes and water-insoluble asphaltenes. Water-insoluble asphaltenes were found to be key contributors to emulsion stability (Gu et al. 2002). Slightly flocculated asphaltenes were found to create a thicker viscoelastic film at the interface (Xia et al. 2004). The combination of asphaltenes and resins at the o/w interface were found to produce more stable emulsions (Khristov et al. 2000).

Solids are key contributors to emulsion stability. Fine solids of intermediate hydrophobicity dispersed in the organic phase have been shown to produce stable water in oil emulsions (Yan et al. 2001). Sufficient coarse solids loadings will also stabilize emulsions given enough asphaltenes to stabilize the solids at the w/o interphase (Sztukowski and

Yarranton 2005). While solids, asphaltenes, and resins play a very large role in emulsion stabilization it is important to remember that many other surface active components are present in water and bitumen systems, such as naphthenic acids, salts, and artificial surfactants.

1.3.2 Chemical W/O Emulsion Breakers

Chemical demulsification is an effective means of removing water from diluted bitumen. The demulsifying agents can either cause water droplets to coalesce and settle or to flocculate and settle in flocs. Coalescing and flocculating additives can be used in combination to obtain better results (Peña et al. 2005). Feng et al. (2010) demonstrated demulsification by flocculation and subsequent coalescence. With coalescing demulsifiers it is necessary to enhance the mobility of the interphase to facilitate film drainage (Krawczyk et al. 1991). Demulsifier partitioning describes the way in which a demulsifier interacts with the oil/water interface. Demulsifiers approaching intermediate levels of partitioning are most effective (Kim and Wasan 1996). In addition to a good partitioning between phases, higher molecular weight demulsifiers are preferred to low molecular weight demulsifiers (Bhardwaj and Hartland 1993). The salinity of the dispersed water is also an important consideration, since higher salinity systems require a reduced amount of demulsifier (Borges et al. 2009). Some more recent studies have focused on producing environmentally friendly demulsifiers (Feng et al. 2009).

Coalescing systems settle according to Stokes law, while flocculated water and solids exhibit different settling mechanics (Long et al. 2002). A modification to Stokes law can be used to account for the non-sphericity and the porosity of the flocs (Rahmani et al. 2005). Flocculating systems are more susceptible to overdosing and are more likely to produce a “rag layer”, an interfacial layer of neutral density between the oil-rich product

and water-rich settled phase (Czarnecki et al. 2007; Saadatmand et al. 2008).

1.3.3 *Mixing Studies in Froth Treatment*

Mixing studies related to froth treatment are relatively rare. Bhardwaj and Hartland demonstrated that for water in diluted bitumen systems, very large mixing times may not be necessary since most of the coalescence occurs in the first few minutes, after which any additional coalescence occurs over a much larger period of time (1994). Mason et al. (1995) studied the effects of mixing time and demulsifier dosage on the drop size distribution of water in diluted bitumen. The floc size distribution of asphaltenes has been shown to vary with shear rate in laminar flow regimes. (Rahmani et al. 2003; Rahmani et al. 2004). Rastegari et al. (2004) also studied the kinetics of asphaltene flocculation by varying ratios of toluene and heptane as solvents at different levels of shear. From these studies we can infer that shear effects, mixing time, and demulsifier dosage are important variables to explore.

1.4 *Knowledge Gaps*

There are many knowledge gaps in the field of mixing with respect to oilsands froth treatment. Oilsands research has often improperly characterised mixing parameters. Some studies use mixing conditions that either undershoot or overshoot industrial mixing conditions. For example, shaker tables are common during initial testing of demulsifiers, but such tests underestimate the blending power and energy dissipation levels present in industrial mixing operations. Methods of mixing are often poorly characterised geometries, such as magnetic stirrers, jar tests, unbaffled stirred vessels, and non-standard impellers. Often certain key specifications such as physical dimensions of the impeller or tank are missing. In addition, not all demulsifiers are tested under the same mixing conditions. These mismatched mixing conditions, combined with missing

key information makes it very difficult to compare demulsifier performance on the same mixing basis. Therefore a standard test cell in which to perform mixer settler experiments would provide a common, fully scale-able basis for comparison of demulsifiers. The scale-ability would allow researchers to proceed to the pilot scale with greater physical insight. The common basis would also allow for proper evaluation of mixing variables on demulsifier performance.

A standard method of demulsifier addition to the system has not yet been developed. While in most studies demulsifier will be injected via syringe or sampling tube, the injection concentration of demulsifier, if it is specified, varies from study to study. In some studies concentrated demulsifier solutions are injected while others chose to dilute the demulsifier in a solvent, such as xylene. Dissolving a demulsifier additive in solvent before addition into the system will greatly reduce demulsifier dissolution time and will ensure a more homogeneous dispersion of demulsifier into the system. Injection concentrations of 1-5% active ingredient are common. The solvent medium for demulsifier addition can also vary. The type of solvent used is an injection medium is known to affect the performance of demulsifier, as shown by Pacheco et al. (2011).

The purpose of this study is to evaluate the relative effects of mixing intensity (i.e. maximum energy dissipation), mixing time, bulk demulsifier dosage, and injection concentration on diluted bitumen clarification for a commercial demulsifier. The initial study was used to evaluate the relative effects of the first three variables. A second study considers the effect of injection concentration of demulsifier in combination with the other three variables. A shear and sedimentation test cell (SSTC) is developed in an effort to standardize mixing protocols in demulsifier testing.

Chapter 2 : Evaluation of Mixing Effects on Bitumen Clarification – Phase 1

The purpose of the first stage of experiments was two-fold: to study the impact of mixing on demulsifier performance in diluted bitumen clarification and to determine whether a shaker flask apparatus is a reliable method to compare mixing conditions. Demulsifiers are typically evaluated in terms of dosage and response. They are rarely evaluated at multiple mixing intensities, though performance is sometimes quantified according to mixing time after addition. A standard stirred tank and a shaker flask apparatus will be used to evaluate the relative effects of bulk demulsifier concentration, mixing intensity, and mixing time in diluted bitumen clarification.

2.1 Experimental Setup:

The experimental procedure can be divided into three stages: sample preparation, demulsifier dispersion, and batch gravity settling at 76.5 °C. A schematic of the mixing protocol is shown in Figure 2-1. A single batch of Syncrude froth treatment inclined plate settler (IPS) product diluted bitumen samples was used for all experiments. The properties and composition of diluted bitumen after pre-mixing are shown in Table 2-1. The IPS product diluted bitumen composition was obtained using a combination of Karl-Fisher titration, Dean Stark oil, water, and solids (O/W/S) analysis, and known density measurements following sample preparation. The diluted bitumen as supplied had a naphtha to bitumen ratio (N/B) of 0.7 by weight. The viscosity of diluted bitumen was measured at 80°C using a Fenske viscometer, giving results which are consistent with previous viscosity measurements for diluted bitumen froth (Seyer and Gyte 1989).

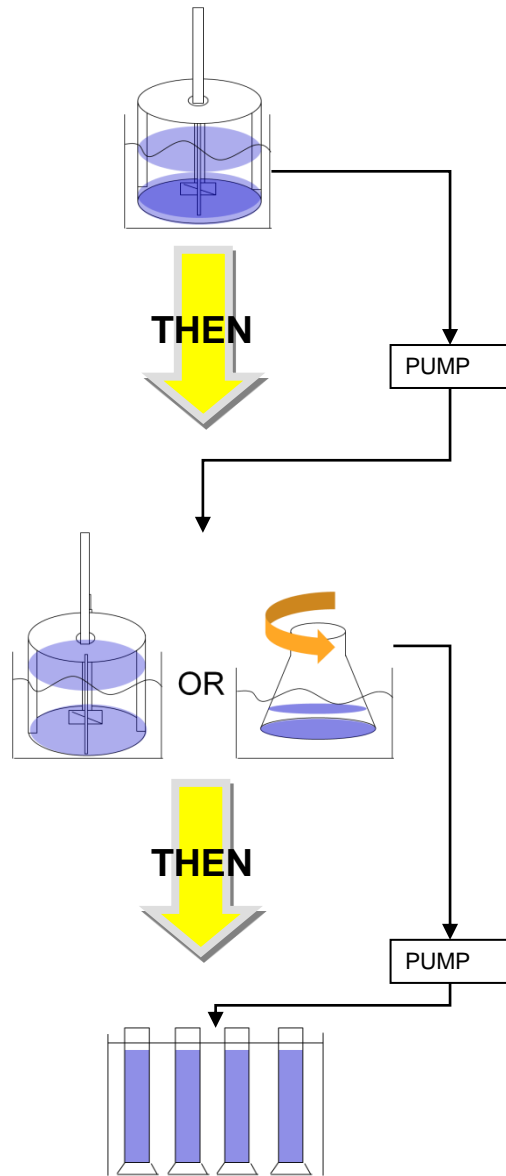
2.1.1 Pre-Mixing Protocol

The diluted bitumen is re-suspended at a high energy dissipation level in order to provide a “worst case” emulsification scenario. This worst case scenario is quantified in Table 2-2. A single 2.7L sample in a 4 L paint can was heated for 30 minutes without mixing and for 15 minutes with pre-mixing to 76.5 °C, after which the temperature is held constant for the duration of the experiment. The sample cans were stored upside down at 5°C, and re-agitated by shaking thoroughly by hand before heating. Pre-mixing was found to have a substantial effect on initial water content by re-suspending settled solids and water. This is shown in Appendix C. The diluted bitumen was re-suspended using a 45° pitched blade turbine (PBTD) impeller. Standard T/10 baffles were attached to a modified paint can lid to promote turbulence. A sample was withdrawn following pre-mixing for O/W/S analysis and Karl-Fisher titration. A small sample was

retained using a hydrophobic treated glass slide and an untreated cover slip for microscopy. Figure 2-2 is a representative image of the diluted bitumen following the pre-mixing protocol at 100x magnification; large and small water droplets and fine solids are evenly dispersed throughout the sample.

Table 2-1: Properties and composition of diluted bitumen

Average Water Content $\pm \sigma$ (wt%)	3.5-4.1
Average Solids $\pm \sigma$ (wt%)	1.6-2.0
Average Hydrocarbons Content $\pm \sigma$ (wt%)	93.9-94.9
N/B	0.7
Density, 80 °C (kg/m ³)	860
Viscosity, 80 °C (cSt)	6.1



Step 1: Pre-Mixing

- IPS Product diluted bitumen sample (N/B=0.7) is re-suspended.
- Storage time is important – water and solids in diluted bitumen samples settle with time. Sample cans were stored upside down to simplify resuspension.
- Sample is shaken manually and then agitated at 1000 rpm using an 8 cm pitched blade turbine (PBSD) impeller ($H=0.66 \cdot T$) for 15 minutes, where H is the tank height and T is the tank width.
- Sample is preheated to 60 °C before agitation, and then brought to 76.5 °C for the premixing step.

Step 2: Demulsifier Addition

- Transfer to new stirred tank ($H=T$) or shaker flask.
- Inject 5 mL demulsifier solution into diluted bitumen. to achieve **demulsifier concentration X_C** .
- Agitate at **mixing intensity X_E** for **mixing time X_t** .

Step 3: Batch Gravity Settling (BGS)

- Four repeated runs are performed.
- Product layer is sampled at 1, 3, 5, 10, 30, and 60 minutes, 2.5 cm below the surface.
- Product layer (top) and tails layer (bottom) kept for Dean Stark Oil/Water/Solids (OWS) analysis

Step 4: Analysis

- Water content determined by Karl-Fisher titration.
- Microscope images are acquired for each step.
- Oil/water/solids by Dean-Stark technique, analysis in progress

Figure 2-1: Experimental setup and procedure

Table 2-2: Pre-mixing tank dimensions and mixing parameters

Impeller Type	PBTD (45)
Tank diameter, T (m)	0.16
Impeller diameter, D (m)	0.08
Liquid height (H)	0.11
Off-bottom clearance, C (m)	0.04
Total Impeller Volume, V_{IMP} (m ³)	8.04E-05
Power Number, N_P	1.30
Impeller speed, N (rpm)	1000
$P/\rho V_{TANK}$ (W/kg)	9.20
$P/\rho V_{IMP}$ (W/kg)	245
Reynolds Number, Re	17558
Mixing time (min)	15

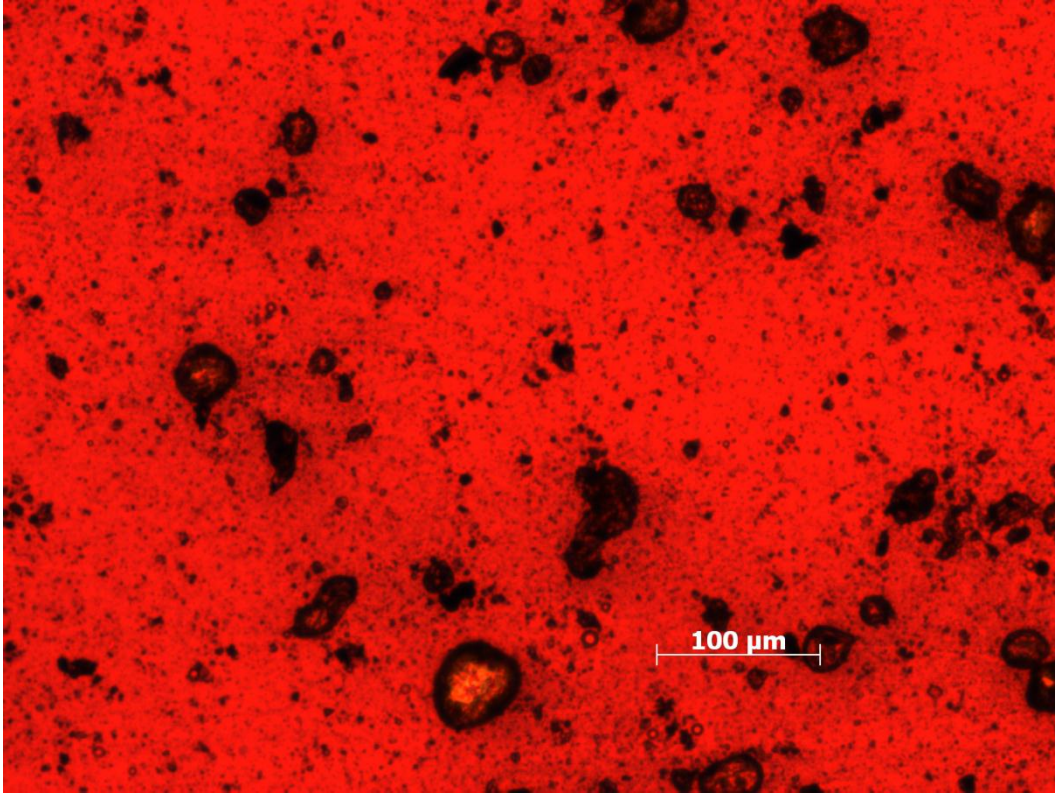


Figure 2-2: Sample image at 100x magnification following pre-mixing protocol

2.1.2 Mixing Protocol

Following pre-mixing, the sample was transferred to either a stirred tank or two shaker flasks for demulsifier dispersion using a Masterflex pump and disposable neoprene tubing. The 1 L shaker flasks were used for their low mixing intensity characteristics. The stirred tank contained T/10 Baffles while the shaker flasks remained un-baffled. The stirred tank and shaker flasks were immersed in an open ethylene glycol bath shaker bath, and the heating fluid covered half of the liquid height. Following the appropriate mixing a portion of the mixed sample was transferred to four graduated cylinders for batch gravity settling using a Masterflex pump and disposable neoprene tubing. The graduated cylinders were allowed to settle for 1h after which the top and bottom halves of the cylinders were collected for

analysis. The cylinders were also sampled from a height of 2.5 cm below the liquid surface at 1, 3, 5, 10, 30, and 60 minutes for water content determination using a 1 mL tapered auto-pipette tip. The fill height of a single cylinder is 14 cm.

Three independent variables were studied for the experiment: bulk demulsifier concentration per unit mass (BC), mixing intensity (ϵ_{max}), and mixing time (t). The bulk concentration is calculated on a mass basis. An estimate of ϵ_{max} is obtained from Zhou and Kresta (1996) assuming the maximum energy dissipation at the impeller is 21 times larger than the average energy dissipation in the stirred tank. The demulsifier was injected shortly after the impeller was turned on (or shaker flasks in rotation) using a 5 mL auto-pipette with a 5 mL auto-pipette tip. The stock demulsifier solution (39 wt% in xylenes) was dissolved in xylenes to achieve the proper dosage in a 5 mL injection. This was done in order to minimize dissolution effects in this initial study. The injection takes place over 2 seconds directly above the upper impeller blade tip to promote high initial dispersion of demulsifier.

Each variable was varied at three levels over a wide range to allow for the detection of quadratic effects. Demulsifier A was added to the diluted bitumen at a dosage of 0, 50, and 100 ppm, which covers the active range of the majority of commercial demulsifiers.

The three mixing intensity levels were selected according to their maximum energy dissipation levels. These levels are set to approximate the maximum energy dissipation found in process piping: minimal agitation (shaker flasks) through with a static mixer (PBSD). Shaker flasks have been used by other researchers to approximate the energy dissipation rates found in ocean waves. A study by Kaku et al. (2006) measured maximum energy dissipation levels of 0.75 W/kg in an un-baffled 150 mL Erlenmeyer flask agitated at 150 rpm at 4/5 capacity⁷. However, there exists no correlation to predict maximum energy dissipation in the shaker

flasks currently in use. Three mixing times of 2, 15, and 28 minutes were used. The majority of energy dissipation occurs in the impeller region of the stirred tank, which occupies roughly 5% of the tank volume assuming an impeller diameter of $D=T/2$ and an impeller height of $D/5$. The increase in fluid velocity in the impeller region reduces the effective residence time in the impeller region to less than 1%, meaning that a volume of fluid will be exposed to the maximum energy dissipation region for around 2-28 seconds. The mixing conditions for the stirred tank and shaker flasks are summarized in Table 2-3.

Table 2-3: Mixing specifications for each mixing configuration. For shaker flasks, 1 L Erlenmeyer flasks are filled to the 500 mL level.

	PBTD	A310	Shaker Table
Tank diameter, T (m)	0.145	0.145	n/a
Impeller diameter, D (m)	0.08	0.08	n/a
Impeller speed, N (rpm)	650	350	150
Liquid height, H (m)	0.145	0.145	n/a
Off-bottom clearance, C (m)	0.06	0.06	n/a
$P/\rho V_{\text{tank}}$ (W/kg)	2.26	0.08	n/a
Max energy dissipation, ε_{max} (W/kg)	40.72	1.55	n/a
Reynolds number, Re	11413	6145	n/a
Mixing time (min)		2, 15, and 28	

2.1.3 Design of Experiments

The variables X_C , X_ϵ , and X_t were coded as -1, 0, and +1. Fifteen experimental points were selected to complete a 3 level Box-Behnken fractional factorial as shown in Figure 2-3, and the experimental conditions corresponding to each level are summarized in Table 2-4. A list of the experiments required is shown in Table 2-5. This arrangement of experimental points provides a quadratic analysis of the design variables with the least amount of experimental effort. This experimental design is orthogonal and rotatable, two important features in surface response methodology. Central design points provide additional degrees of freedom necessary to calculate regression variance.

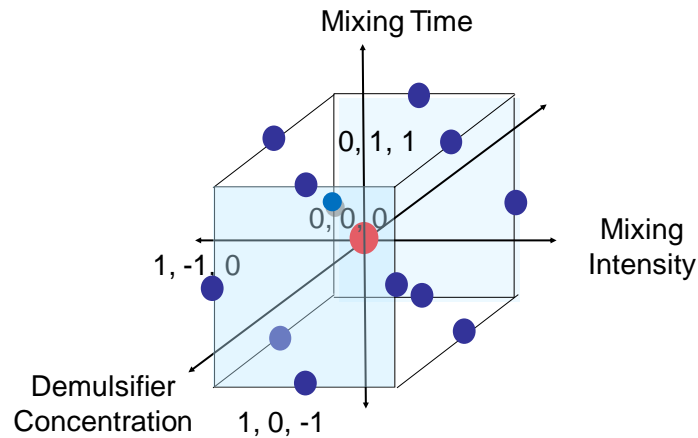


Figure 2-3: Variable coding for Box-Behnken fractional

Table 2-4: Experimental conditions at each of three levels

Variable	-1	0	+1
Bulk Concentration, C (ppm)	0	50	100
Mixing Intensity, ϵ (W/kg)	Low	1.6	41
Mixing Time, t (min)	2	15	28

Table 2-5: Box-Behnken factorial design runs; two-variable pairs are separated into orthogonal blocks

Block/Variable	Bulk Concentration	Mixing Intensity	Mixing Time
	X_C	X_ϵ	X_t
$X_C X_\epsilon$	+1	+1	0
	+1	-1	0
	-1	+1	0
	-1	-1	0
$X_\epsilon X_t$	0	+1	+1
	0	+1	-1
	0	-1	+1
	0	-1	-1
$X_C X_t$	+1	0	+1
	+1	0	-1
	-1	0	+1
	-1	0	-1
Center Points	0	0	0
	0	0	0
	0	0	0

2.1.4 Karl-Fischer Titration

Karl-Fischer titration is used as the standard measure of water content since Dean Stark extraction was determined to lack precision at low water content. Samples are pre-dissolved before analysis using a 1:3 isopropyl alcohol and toluene mixture, which is dried using silica gel and sampled for water content prior to dilution. The samples are analyzed using a Kam Controls Karl Fischer titration apparatus and standard reagents. A calibration curve was generated using standard test samples containing 0.1 wt% water and varying the injection volume, and this calibration curve is shown in Figure 2-4. They are agitated using a vortex mixer for 6 seconds and a 50 μL spring loaded Hamilton syringe is used to inject the sample. Samples are weighed before and after dilution, and syringes are weighed before and after injection.

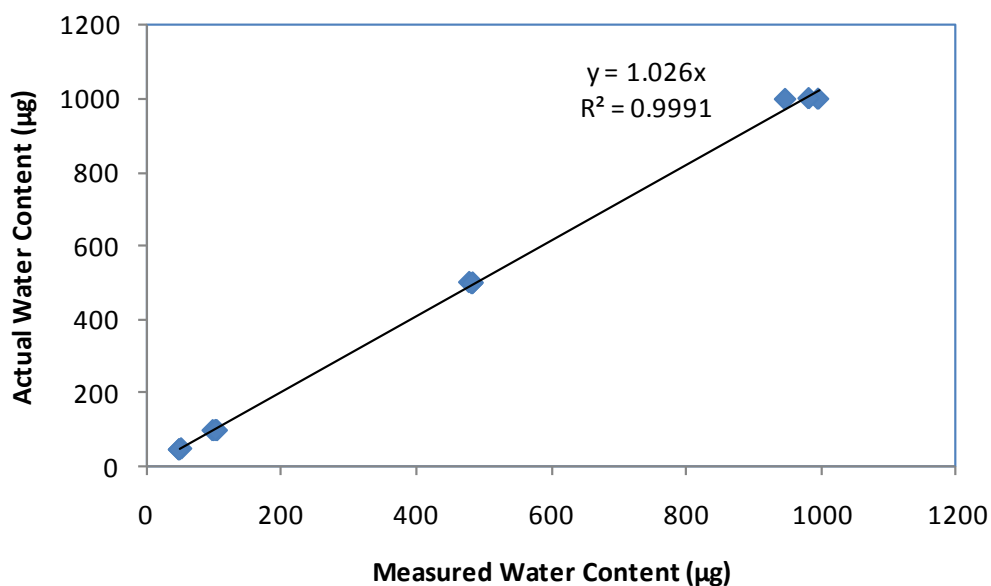


Figure 2-4: Kam Controls Karl-Fischer calibration

2.2 Results/Discussion

A full data set for this study can be found in Appendix A. First, batch gravity settling profiles as measured by Karl-Fischer titration are presented and explored. These profiles are subjected to a multiple linear regression at each instance in time. The vertical water concentration profiles following batch gravity settling are then explored. OWS analysis results are then used with KF titration to examine the material balance and the presence of solids.

2.2.1 Batch Gravity Settling Results

Settling profiles for each settling test are shown in Figure 2-5 as absolute concentrations and Figure 2-6 as water reductions. The water content of each sample was obtained through Karl-Fisher titration. Each settling profile is averaged over four cylinders. This gives a total of 17 runs averaged four times each including the three center point repeats.

Water reduction is heavily dependent on demulsifier dosage. There also appears to be a high initial settling rate followed by a low settling rate.

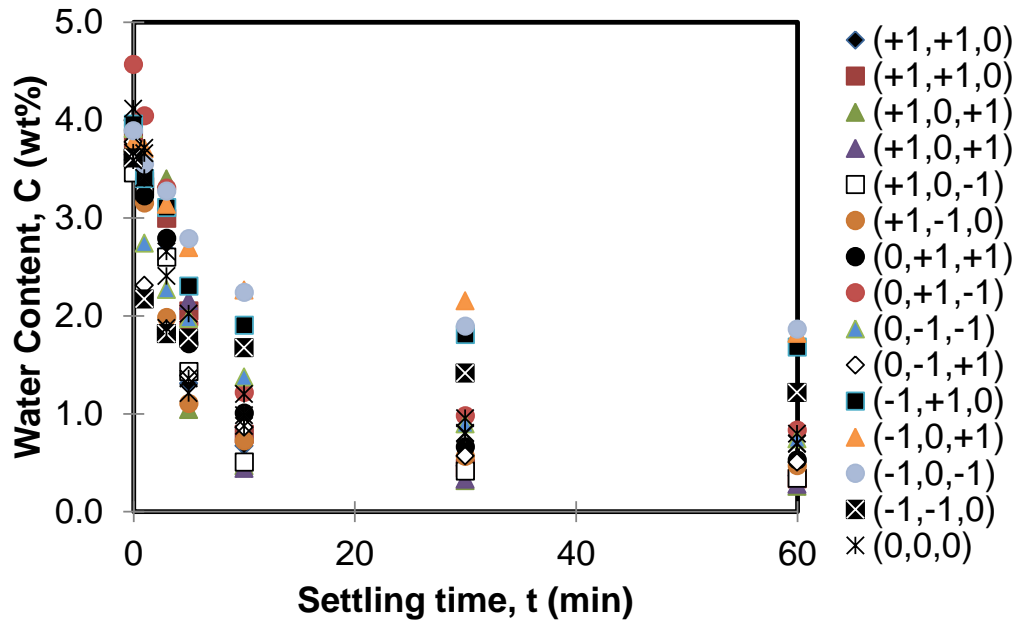


Figure 2-5: Consolidated batch gravity settling results; product water content decreases as a function of time. Variable order: (X_C, X_E, X_I)

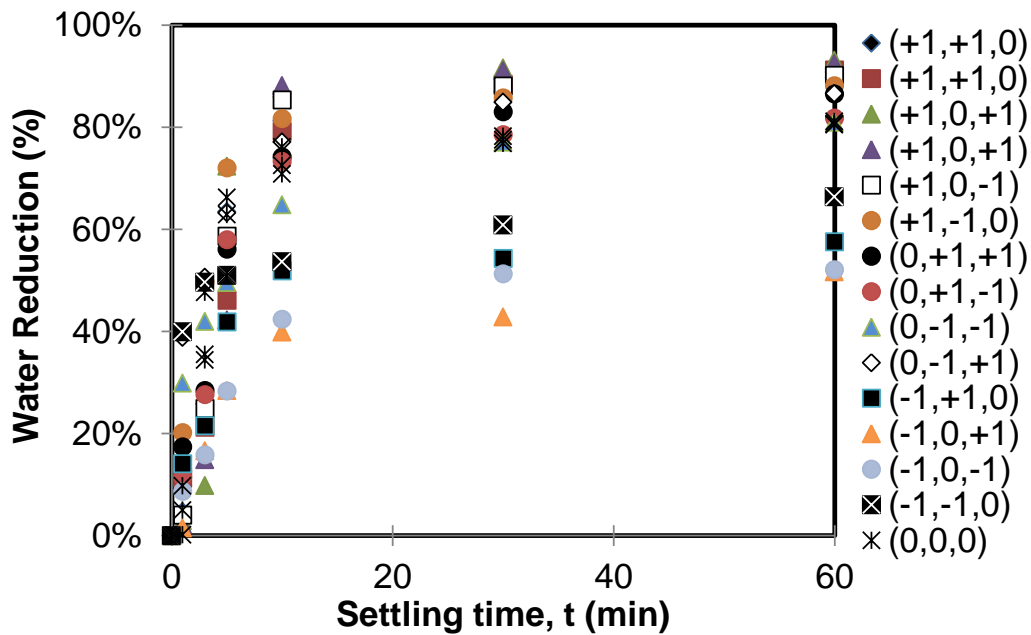


Figure 2-6: Consolidated batch gravity settling results; product water content decreases as a function of time. Variable order: (X_C, X_E, X_I)

The likely reason for these two settling ranges is that larger flocs settle much faster whereas smaller flocs are much less likely to settle. Indeed, there may be no actual settling in the slower settling region. The center point repeats are shown in Figure 2-7. There is good agreement between these runs. Figure 2-8 shows representative settling curves for each dosage of demulsifier. Demulsifier doses of 0, 50, and 100 ppm obtained final product water concentrations of 1.64%, 0.68%, and 0.34% respectively.

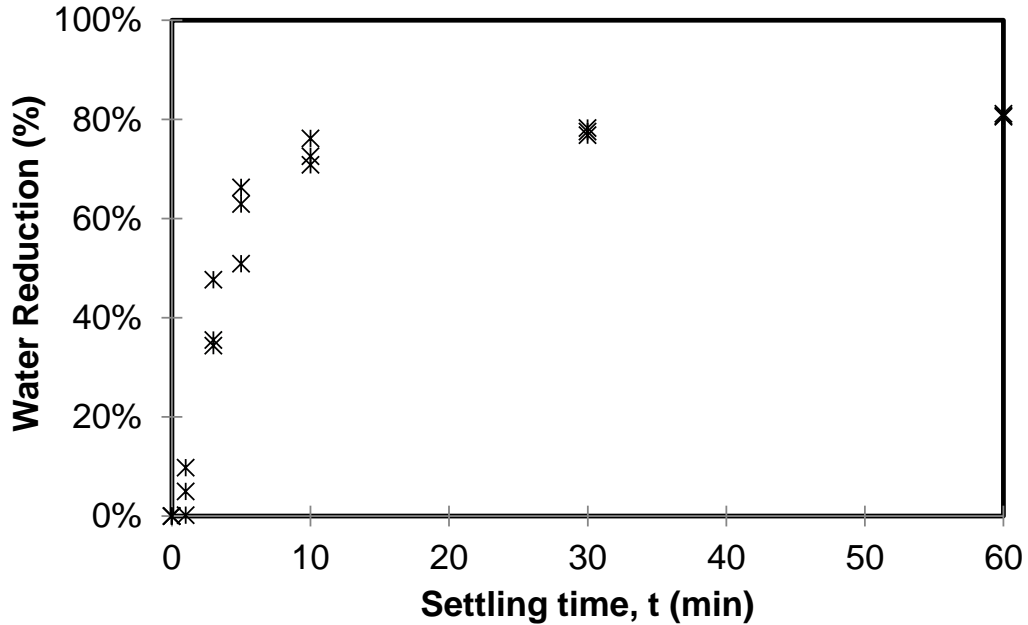


Figure 2-7: Three repeated center point runs: there is good repeatability between runs.

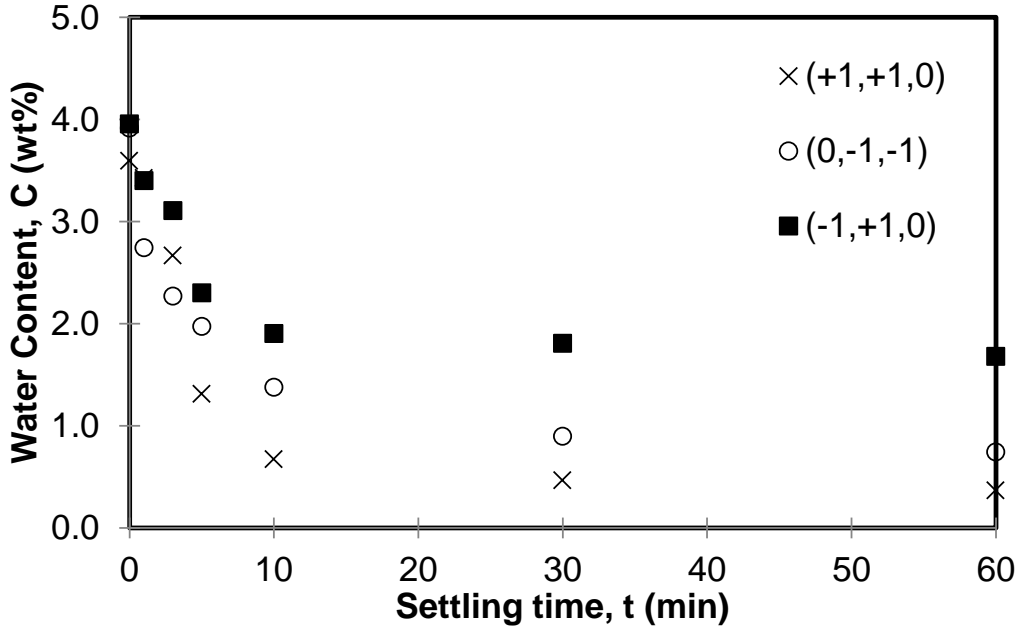


Figure 2-8: Representative batch gravity settling profiles for demulsifier concentrations of 0, 50, and 100 ppm. Average final water concentrations are 1.64%, 0.68%, and 0.34% respectively. Variable order: (BC, ε , t)

2.2.2 Mixing and Demulsifier Effects on Settling

Settling data is available at 1, 3, 5, 10, 30, and 60 minutes of settling time, which allows for the evaluation of effects as a function of time. The multiple linear regression equation is written as

$$\begin{aligned}
 & \% \text{ Reduction or Absolute Reduction} \\
 & = C_0 + \beta_C X_C + \beta_\varepsilon X_\varepsilon + \beta_t X_t + \beta_{CC} X_C^2 + \beta_{\varepsilon\varepsilon} X_\varepsilon^2 + \beta_{tt} X_t^2 \\
 & \quad + \beta_{C\varepsilon} X_C X_\varepsilon + \beta_{Ct} X_C X_t + \beta_{\varepsilon t} X_\varepsilon X_t
 \end{aligned} \tag{2-1}$$

where the subscripts C, ε and t correspond to demulsifier bulk concentration, mixing intensity, and mixing time respectively. The results of the initial factorial analysis for absolute water content can be found in Figure 2-9 and Figure 2-10. Figure 2-11 and Figure 2-12 show the same analysis for percent water reduction in the product. The effects are plotted

with 95% confidence intervals. Effects are discarded as insignificant in the subsequent analysis if the null hypothesis that 0 falls within the confidence interval of the coefficient cannot be rejected. Both approaches would imply that mixing intensity is the dominant main effect during initial settling but disappears after 10 minutes of settling. Bulk concentration is statistically insignificant during initial settling but becomes increasingly significant after 10 minutes of settling. Mixing time is discarded as insignificant. Quadratic effects are detected for bulk concentration and mixing intensity. The quadratic mixing intensity effect is suspect as it only appears once at 1 minute of settling, while the quadratic effect for bulk concentration appears at later settling times. Mixing time also demonstrates a quadratic effect at 3 and 5 minutes of settling. No significant interaction effects are detected as part of the analysis.

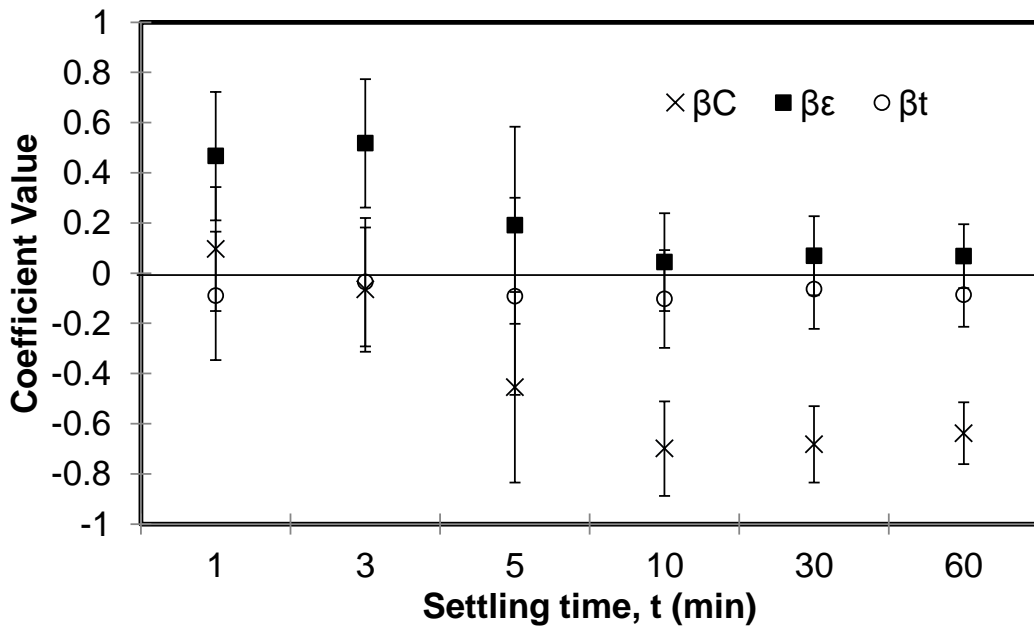


Figure 2-9: Main regression coefficients with 95% confidence intervals as a function of time – absolute water content (wt%)

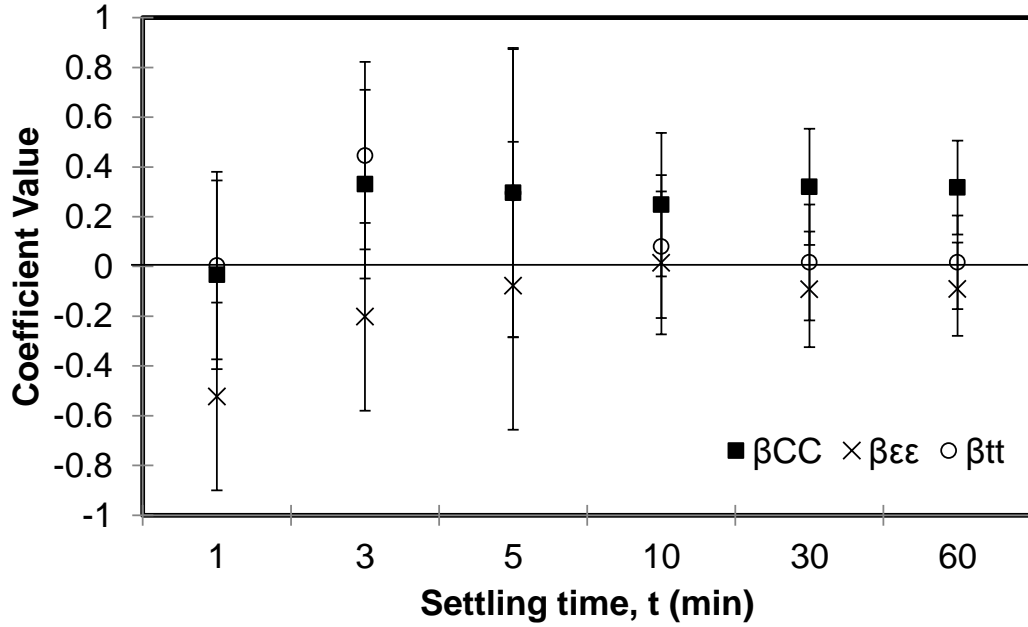


Figure 2-10: Quadratic regression coefficients with 95% confidence intervals as a function of time – absolute water content (wt%)

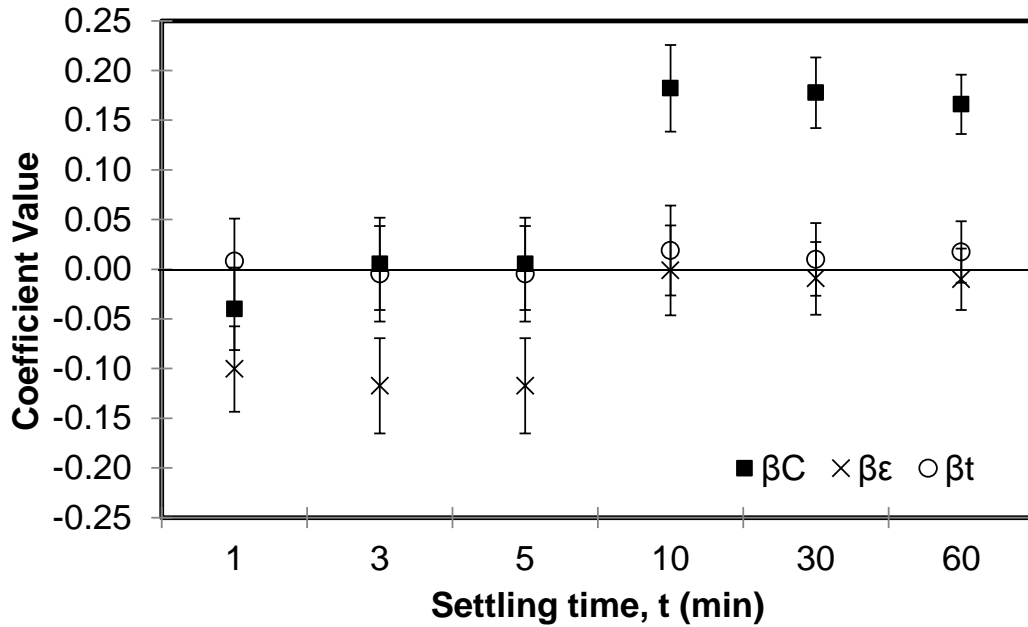


Figure 2-11: Main regression coefficients with 95% confidence intervals as a function of time – water reduction (%)

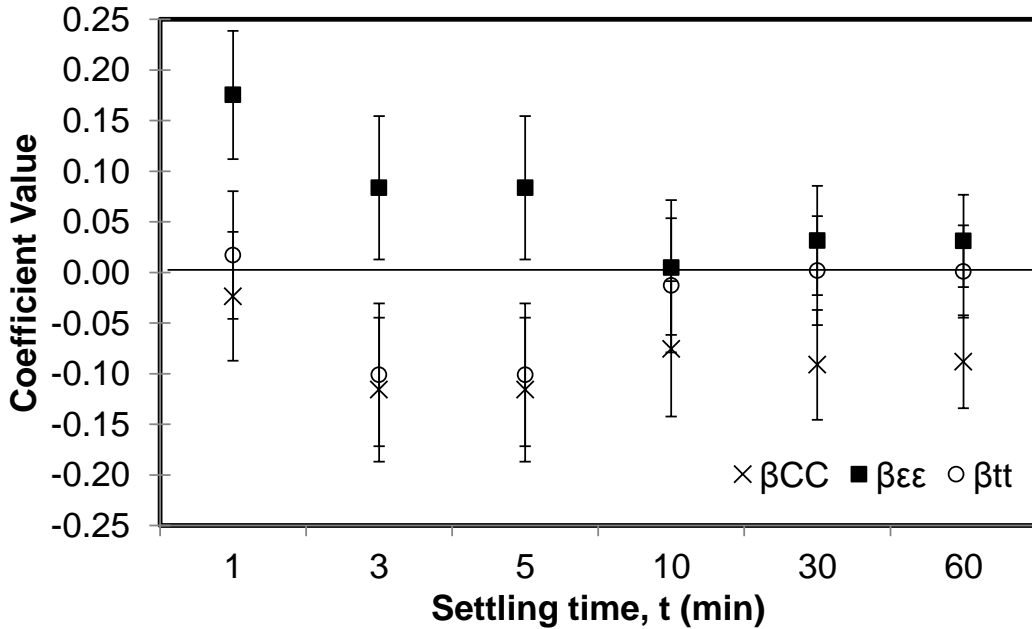


Figure 2-12: Quadratic regression coefficients with 95% confidence intervals as a function of time – water reduction (%)

A more precise estimate of the relevant parameters is obtained after further iterations of the regression, discarding insignificant effects. The results of these iterations are shown in Table 2-6 and Table 2-7. The general trends are as follows:

- Increasing bulk demulsifier concentration increases product water reduction, with an opposite quadratic effect. This effect appears later in the settling process.
- Increasing mixing intensity negatively affects primary settling. The effect disappears later in the settling process.

The first 1-5 minutes of settling are better accounted for when the regression is performed on water reduction as opposed to absolute water content. This difference disappears after 5 minutes of settling where the effects of mixing intensity are less pronounced.

The observed demulsifier effects are expected. An increase in demulsifier dosage should surely lead to increased process performance. The

quadratic behaviour of the demulsifier effect is not unexpected, since demulsifiers can either start interfering with each other at the interface or can start to form micelles at the critical micelle concentration. Mixing intensity is often a key factor in determining equilibrium drop/floc size distributions, as it can both increase breakup and agglomeration. However one would expect this effect to be sustained in later settling stages. It is possible that the demulsifier effect becomes so large that the mixing intensity effect becomes statistically insignificant. The early presence of mixing intensity as a variable could also be due to the experimental design. A shaker flask is used at the lowest mixing intensity level while a stirred tank is used for all other levels. The settling process could already be under way in the shaker flask, leading to an earlier than expected drop in water content.

Reducing the demulsifier dosage range could reveal otherwise dominated effects. Since the effect of demulsifier dosage is quite large, the variance introduced by the variable over its large range could mask other significant effects. Reducing the demulsifier dosage would shorten the range of the variable and reduce overall variance in the system. It is also important to consider that the experimental range for mixing intensity is not normalized linearly. The mixing intensity in the shaker flask is not properly characterised, making it difficult to define the lowest level of mixing intensity in the design. The second stage of this work will consider a linear and well-defined range of mixing intensities, and will reduce demulsifier dosage to better estimate smaller effects. The effects of mixing time may be under-represented due to the high dilution of demulsifier prior to injection. The demulsifier was injected at activities of 4% and 8% (mass basis) for 50 ppm and 100 ppm of demulsifier respectively. Demulsifier dilution is known to have a significant effect on mixing time due to surface effects and local concentration considerations (Ibemere and Kresta 2007). Low activity injections were used in order to minimize these effects in this first stage.

2.2.3 The Nature of the Oil-Water Interface

A profile of water content was measured vertically following one hour of batch gravity settling. While vertical water content may not be directly relevant to process performance it does give us insight into the nature of the oil/water settling interface. Figure 2-13 and Figure 2-14 show water content as a function of water reduction for normalized heights of $h/Z = 0.2$ and 0.1 , respectively, where Z is the total fill height in the cylinder. The fill height is approximately 14 cm. Water concentration measurements are normalized by initial water content. Water content remains equal to the final product water content above a normalized height of $h/Z=0.2$. That is, at all times the “product layer” is at least 80% of the final sample. The water content increases sharply between heights of 0.2 and 0.1 , indicating some sort of rag layer between the oil rich and water rich layers. Given that at most 6.5% of the volume of the cylinder can be occupied by water or solids, these results indicate that the optimal separation height cannot simply be determined through mass balance. This also indicates that either the water-rich phase takes the form of a w/o or o/w emulsion or there exists a large rag layer which will complicate the subsequent settling process. Similar concentration profiles showing a stable suspension followed by a sharp interface have been observed in a previous study where mixing of diluted bitumen was performed with a homogenizer (Feng et al. 2009). A large amount of variability was also observed in this same study. Rag layers have been observed in similar diluted bitumen systems (Czarnecki et al. 2007).

Table 2-6: A summary of significant effects on batch gravity settling for 1-60 minutes (absolute water content)

Time (min)	1		3		5		10		30		60	
	Estim.	95%										
β_C	-	-	-	-	-0.412	0.296	-0.689	0.157	-0.698	0.126	-0.652	0.114
β_ε	0.451	0.205	0.507	0.254	-	-	-	-	-	-	-	-
β_t	-	-	-	-	-	-	-	-	-	-	-	-
β_{CC}	-	-	-	-	-	-	-	-	0.310	0.193	0.309	0.175
$\beta_{\varepsilon\varepsilon}$	-0.542	0.298	-	-	-	-	-	-	-	-	-	-
β_{tt}	-	-	0.492	0.368	-	-	-	-	-	-	-	-
$\beta_{C\varepsilon}$	-	-	-	-	-	-	-	-	-	-	-	-
β_{Ct}	-	-	-	-	-	-	-	-	-	-	-	-
$\beta_{\varepsilon t}$	-	-	-	-	-	-	-	-	-	-	-	-
R²adj	0.67		0.59		0.33		0.84		0.90		0.91	

Table 2-7: A summary of significant effects on batch gravity settling for 1-60 minutes (water content reduction)

Time (min)	1		3		5		10		30		60	
	Estim.	95%										
β_C	-	-	-	-	0.100	0.075	0.169	0.026	0.182	0.030	0.169	0.026
β_ε	-0.103	0.040	-0.117	0.039	-	-	-	-	-	-	-	-
β_t	-	-	-	-	-	-	-	-	-	-	-	-
β_{CC}	-	-	-0.119	0.058	-	-	-0.087	0.041	-0.090	0.046	-0.087	0.041
$\beta_{\varepsilon\varepsilon}$	0.176	0.040	0.088	0.058	-	-	-	-	-	-	-	-
β_{tt}	-	-	-0.105	0.058	-	-	-	-	-	-	-	-
$\beta_{C\varepsilon}$	-	-	-	-	-	-	-	-	-	-	-	-
β_{Ct}	-	-	-	-	-	-	-	-	-	-	-	-
$\beta_{\varepsilon t}$	-	-	-	-	-	-	-	-	-	-	-	-
R²adj	0.81		0.85		0.31		0.90		0.92		0.92	

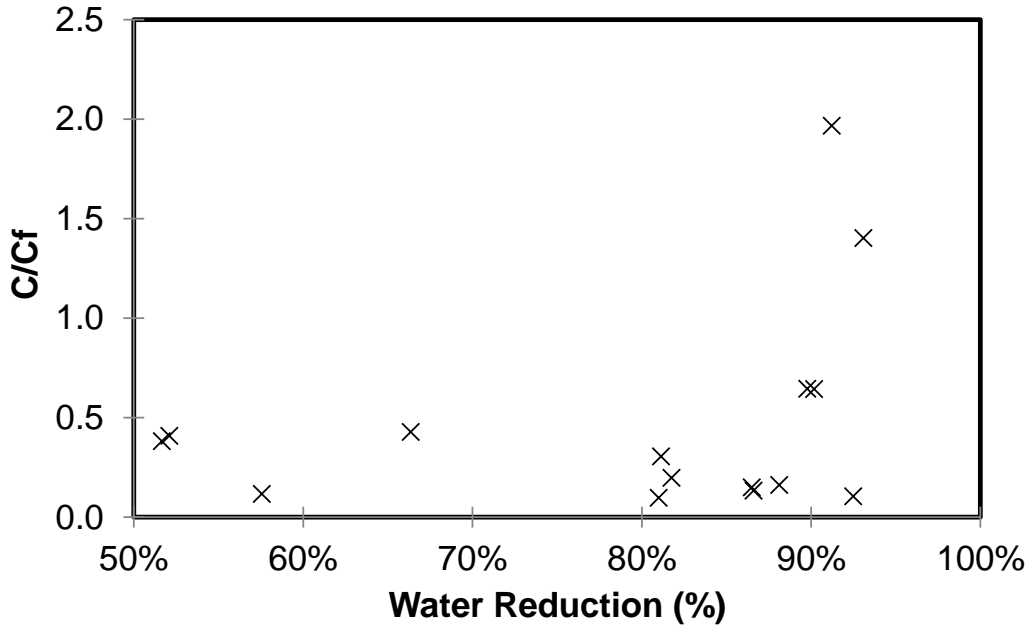


Figure 2-13: Water content as a function of water reduction at a normalized height of $h/Z=0.2$

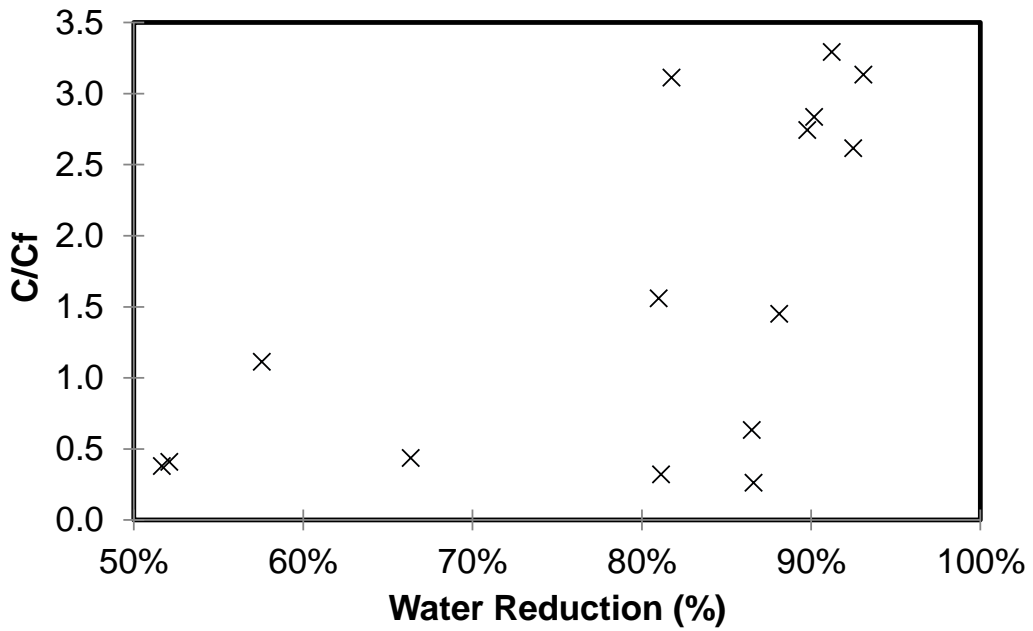


Figure 2-14: Water content as a function of water reduction at a normalized height of $h/Z=0.1$

2.2.4 Material Balance Considerations from OWS Analysis

The resulting top and bottom samples following batch gravity settling for each cylinder were subjected to O/W/S analysis. In this case the product layer is defined as the top 50% of the graduated cylinder, while the bottoms layer is defined as the bottom 50% of each graduated cylinder. A material balance was conducted between the initial, product, and bottoms samples. The closure error for each run is taken as

$$\%Closure\ Error = \frac{M_i - M_P - M_B}{M_i} \quad 2-2$$

where M_i is the initial content assuming a sample mass equal to the top and bottoms samples, M_P is the final content in the product layer, and M_B is the final content in the bottoms layer. Closure error statistics for each component are shown in Table 2-8. Figure 2-15 shows closure errors for all four components in each run, and are presented run by run. Water and naphtha measurements are most prone to error. The results of the mass balance confirm that reasonable amounts of material are lost throughout the experiment and as such mass loss is not a large concern.

Table 2-8: Material balance closure error statistics

Statistic	HC	Water	Solids	Naphtha	Bitumen
Average closure error	-0.3%	6%	-6%	-6%	1%
Standard deviation	1%	15%	10%	24%	8%
Maximum error	3%	36%	23%	76%	22%

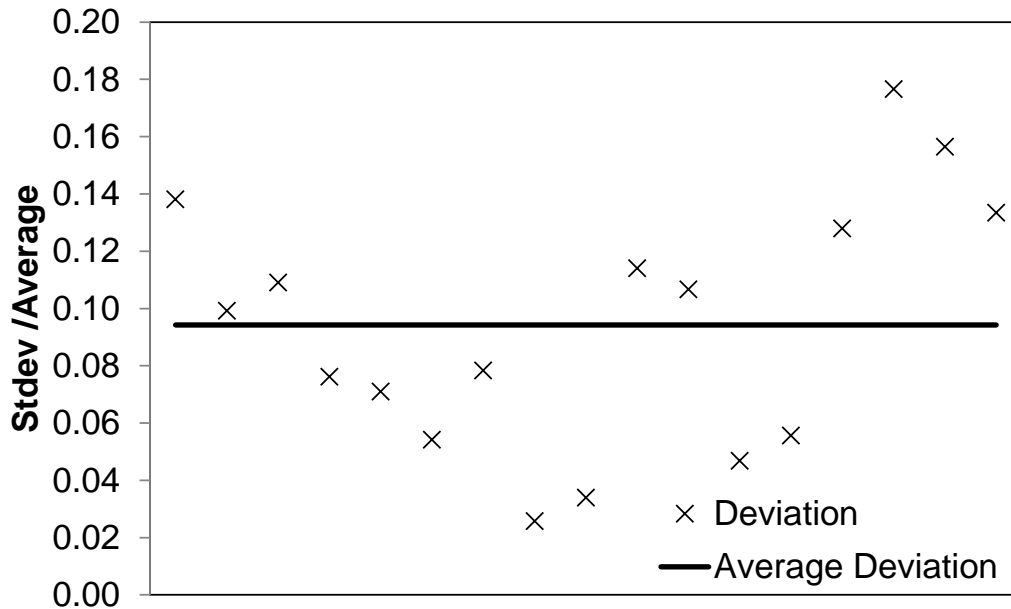


Figure 2-16: Standard deviation of Karl-Fisher measurements normalized by average measurement; each measurement was repeated 3 times

Figure 2-17 compares initial water content measurements from KF titration and OWS analysis. OWS analysis over predicts water content compared to KF titration. It is difficult to say which measurement is most accurate, but it is clear that in this case Karl-Fischer titration is the more precise method. A similar analysis is conducted with water reduction as calculated from both techniques in Figure 2-18. The differences between the two measurement techniques can be quite large. The OWS water content is on average 1.16 times larger than the KF water content, with a standard deviation of 0.18. The stability of the KF titration technique allows for a better regression of the batch gravity settling results. The KF results are more useable than the OWS results and as such are assumed to be the most reliable results for the purpose of this study.

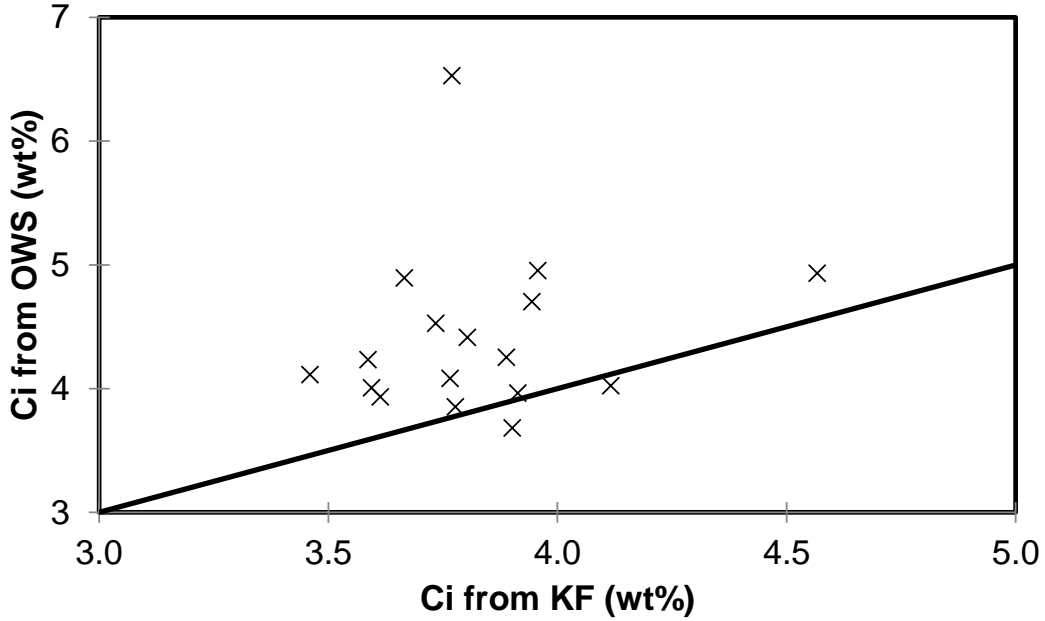


Figure 2-17: Comparison of initial water content measured with KF titration and OWS analysis; OWS analysis over predicts compared to KF titration

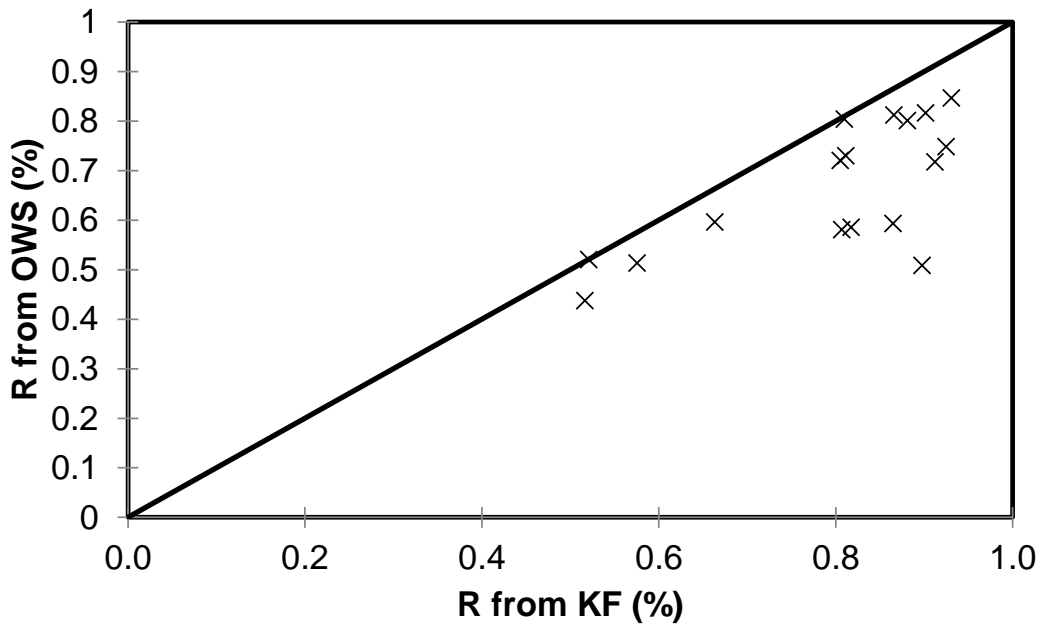


Figure 2-18: Product water reduction for each experimental run, from Karl-Fisher titration data and OWS analysis; OWS analysis underpredicts product water reduction compared to KF titration

2.2.6 Solids Reduction by Water Removal

Diluted bitumen clarification is as much about solids reduction as it is about water reduction. That being said, solids are known to associate with either the aqueous phase or the organic phase depending on wettability. Therefore water removal may serve a dual purpose by removing unwanted solids from the diluted bitumen. Figure 2-19 shows solids content as a function of initial water content in the initial pre-mixed diluted bitumen product. There is no correlation between initial solids and water content. However, following batch gravity settling a linear relationship between solids and water content is observed in Figure 2-20. This indicates that a large portion of solids not associated with the water phase have settled and that a large portion of the remaining solids is associated with the water phase. It is likely that a large portion of the settled solids settled out with the water. This relationship also indicates that any further reduction in water content will yield a corresponding reduction in solids. The correlation indicates that for every 0.1 wt% in water reduction there will be an equal 0.1 wt% reduction in solids.

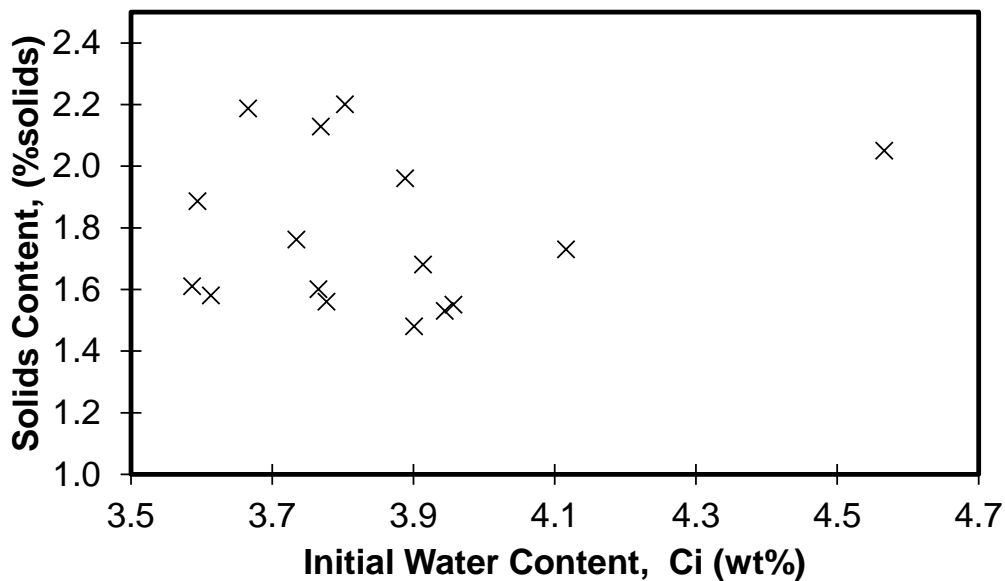


Figure 2-19: Initial solids content as a function of initial water content

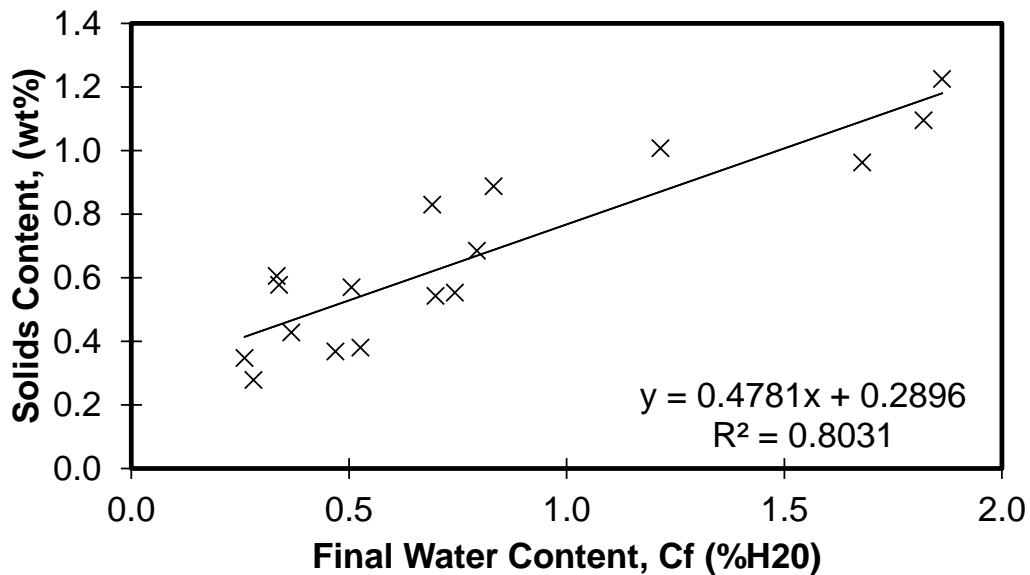


Figure 2-20: Final solids content as a function of final water content; a linear trend is observed

2.3 Conclusions

This study confirms that demulsifier dosage is the dominating variable in diluted bitumen clarification. There is an initial fast settling rate followed by a slower settling rate. Although mixing intensity was detected as a significant effect during the initial settling, this effect was not sustained. It is possible that these inconsistent results are due to either the dominance of demulsifier dosage as an effect or that they are simply due to the inclusion of shaker flasks as part of the experimental procedure. Shaker flasks yield data which are not easily compared to data obtained from stirred tanks.

The study also demonstrated that solids reduction can be achieved through water reduction, and that a linear relationship between water and solids content emerges after sufficient settling.

Future studies of this kind can be improved by: reducing the demulsifier dosage, comparing mixing intensity on a common basis, and including injection concentration in the factorial analysis.

Chapter 3 : Evaluation of Mixing Effects on Bitumen Clarification – Phase 2

The purpose of this study is two-fold: to study the impact of mixing on demulsifier performance in diluted bitumen clarification and to establish a standard mixing/settling apparatus and protocol which will simplify the evaluation of mixing parameters on the lab scale, as well as providing a solid foundation for subsequent scale-up. To this end, a shear and sedimentation test cell (SSTC) has been designed. Demulsifiers are typically evaluated in terms of dosage and response. They are rarely evaluated at multiple mixing intensities, and there is no standardized range of mixing intensities at which to test. There is also no standard

injection concentration of active ingredient at which to inject a demulsifier solution. The SSTC will be used to evaluate the relative effects of bulk concentration, mixing intensity, mixing time and injection concentration in diluted bitumen clarification.

3.1 Experimental Design

The experimental procedure can be divided into three stages: sample preparation, demulsifier dispersion, and batch gravity settling at 76.5 °C. A schematic of the mixing protocol is shown in Figure 3-1. A single batch of Syncrude froth treatment inclined plate settler (IPS) product diluted bitumen samples was used for all experiments. The properties and composition of diluted bitumen after pre-mixing are shown in Table 3-1. The IPS product diluted bitumen composition was obtained using a combination of Karl-Fisher titration, Dean Stark oil, water, and solids (O/W/S) analysis, and known density measurements following sample preparation. The diluted bitumen as supplied had a naphtha to bitumen ratio (N/B) of 0.7 by weight. The viscosity of diluted bitumen was measured at 80 °C using a Fenske viscometer, giving results which are consistent with previous viscosity measurements for diluted bitumen froth (Seyer and Gyte 1989).

Table 3-1: Properties and composition of diluted bitumen

Average Water Content $\pm \sigma$ (wt%)	1.8-2.2
Average Solids $\pm \sigma$ (wt%)	1.0-1.2
Average Hydrocarbons Content $\pm \sigma$ (wt%)	96.6-97.2
N/B	0.7
Density, 80 °C (kg/m ³)	860
Viscosity, 80 °C (cSt)	6.1

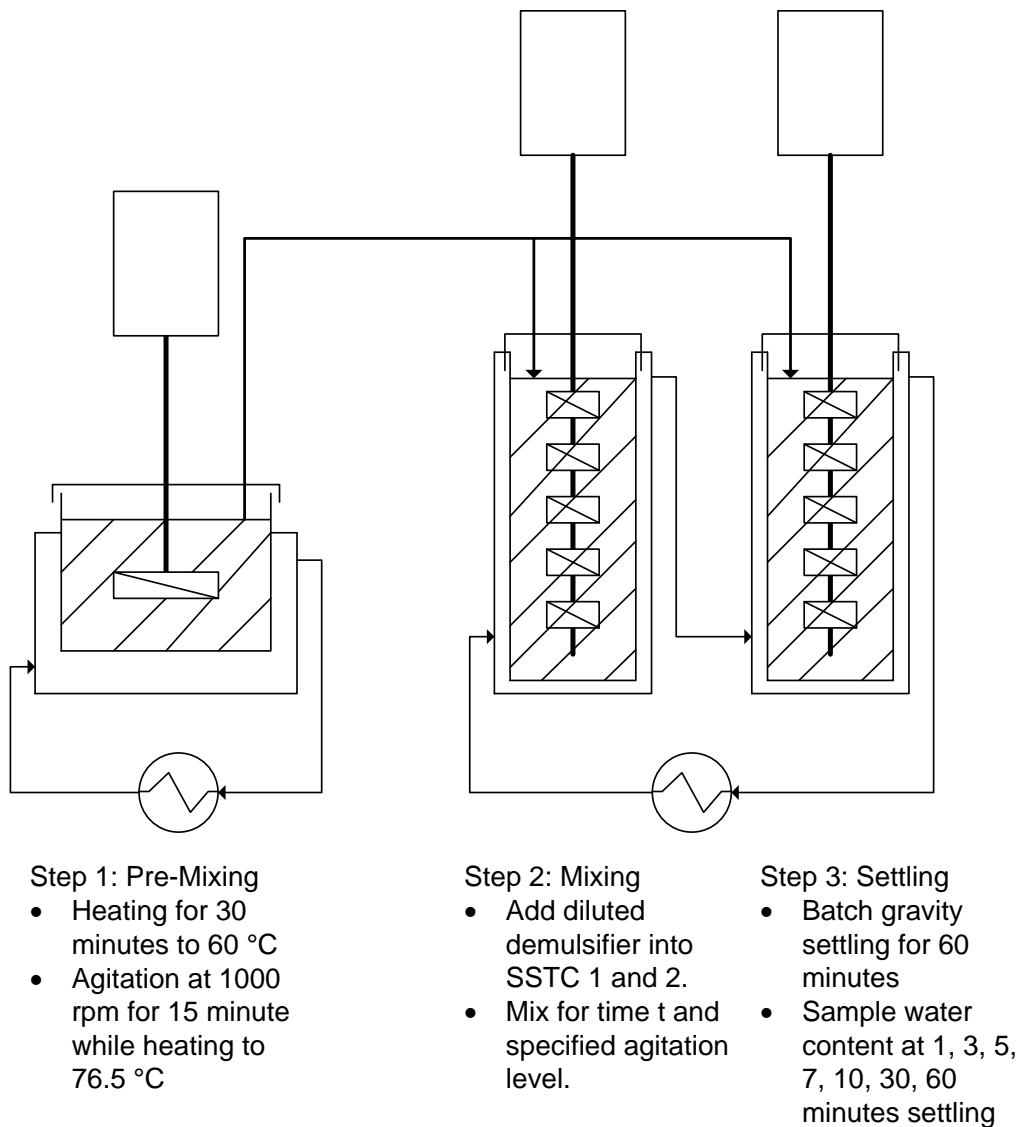


Figure 3-1: Schematic of experimental setup and procedure; the sample is pre-mixed and heated to 76.5 °C and then transferred to two SSTC's. Demulsifier is injected mixed with the diluted bitumen, and the sample is allowed to settle for 60 minutes.

3.1.1 Pre-Mixing Protocol

The diluted bitumen is re-suspended at a high energy dissipation level in order to provide a “worst case” emulsification scenario. The worst case scenario is quantified previously in Table 2-2. A single 2.7L sample in a 4 L paint can was heated for 30 minutes without mixing and for 15 minutes with pre-mixing to 76.5 °C, after which the temperature is held constant for the duration of the experiment. Pre-mixing was found to have a substantial effect on initial water content by re-suspending settled solids and water. This is shown in Appendix C. The diluted bitumen was re-suspended using a 45° pitched blade turbine (PBSD) impeller. Standard T/10 baffles were attached to a modified paint can lid to promote turbulence. A sample was withdrawn following pre-mixing for O/W/S analysis and Karl-Fisher titration. A small sample was retained using a hydrophobic treated glass slide and an untreated cover slip for microscopy. Figure 2-2 is a representative image of the diluted bitumen following the pre-mixing protocol at 100x magnification; large and small water droplets and fine solids are evenly dispersed throughout the sample.

3.1.2 SSTC Design and Mixing Protocol

The pre-mixed diluted bitumen was transferred to two shear and sedimentation test cells (SSTC) for demulsifier dispersion using a Masterflex Pump and disposable tubing. A schematic of the heated SSTC test cell is shown in Figure 3-3. The SSTC tank geometry and mixing specification are shown in Table 3-3. The SSTC consists of a 1 L 3:1 H/T ratio baffled stirred tank, agitated with either 6 Intermig impellers, 5 A310 impellers or 5 Rushton impellers. All three sets of impellers had an off-bottom clearance of 0.017 m and a submergence of 0.038 m. Successive impellers were staggered at 60°, 30°, and 90° to each other for A310s, Rushtons, and Intermigs respectively. The Intermig impellers were supplied by Ekato and are fabricated using stainless steel, while the A310

impellers and Rushton impellers were supplied by Lightnin and are constructed from Resin and are plated with Nickel to minimize chemical attack to the impellers. The power numbers as a function of Reynolds' number for each impeller type were measured using ethylene glycol at 25 °C (kinematic viscosity = 6 cSt) and are shown in Figure 3-4.

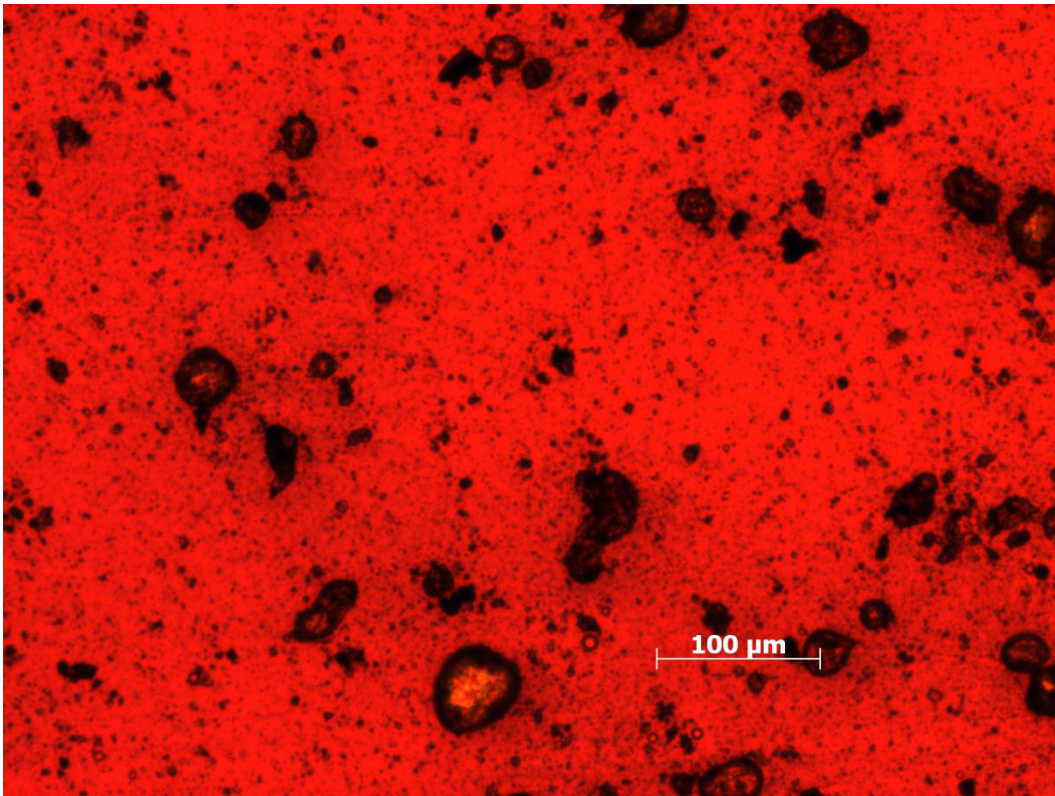


Figure 3-2: Sample image at 100x magnification following pre-mixing protocol

Table 3-2: Pre-mixing tank dimensions and mixing parameters

Impeller Type	PBTD (45)
Tank diameter, T (m)	0.16
Impeller diameter, D (m)	0.08
Liquid height, H (m)	0.11
Off-bottom clearance, C (m)	0.04
Total Impeller Volume, V_{IMP} (m ³)	8.04E-05
Power Number, N_P	1.30
Impeller speed, N (rpm)	1000
$P/\rho V_{TANK}$ (W/kg)	9.20
$P/\rho V_{IMP}$ (W/kg)	245
Reynolds Number, Re	17558
Mixing time (min)	15

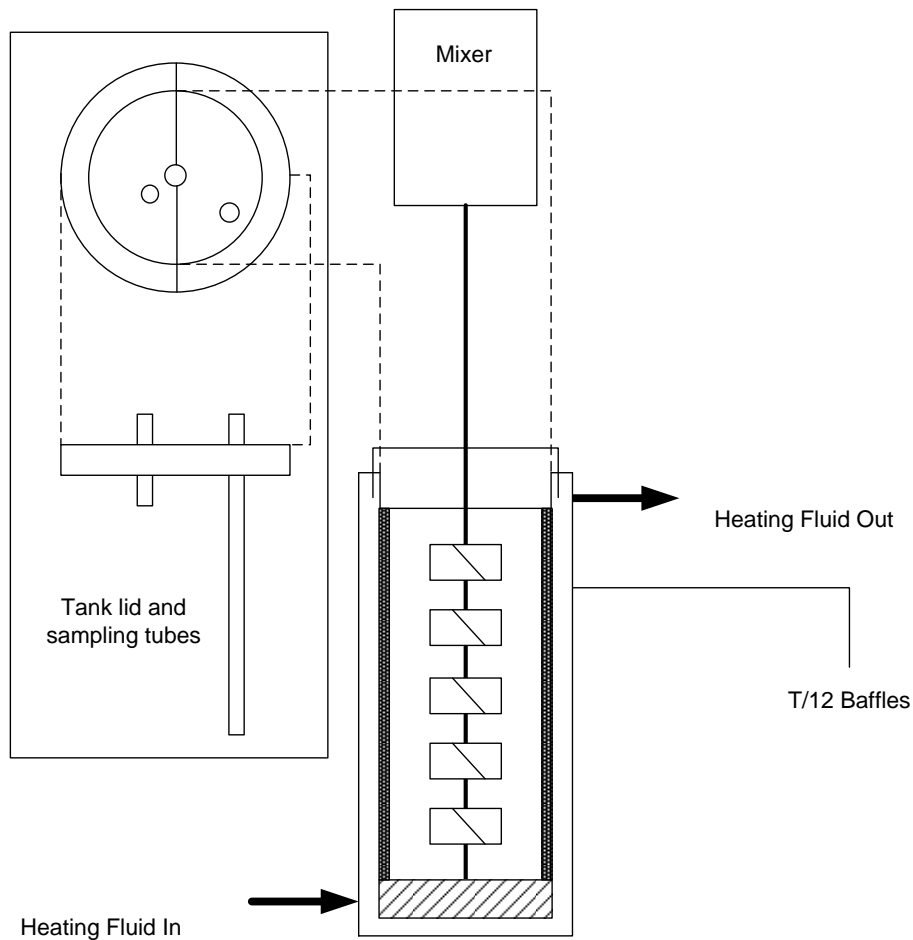


Figure 3-3: SSTC design schematic; the glass stirred tank has a volume of 1L, a tank diameter T of 7.5 cm, and $T/12$ baffles. A $\frac{1}{4}$ in shaft is supported at the tank bottom using a steady bearing. Stainless steel $\frac{3}{8}$ " sampling and injection ports protrude from the tank lid. The tank is jacketed to allow for easy circulation of heating fluid. Impellers are equally spaced between distance $D/3$ from tank bottom and D below fluid surface.

Table 3-3: SSTC geometry and mixing specifications

Impeller Type	Intermig	A310	Rushton
Tank diameter, T (m)	0.075	0.075	0.075
Number of impellers	6	5	5
Impeller diameter, D (m)	0.050	0.038	0.038
Impeller speed, N (rpm)	250	1000	600
Liquid height, H (m)	0.225	0.225	0.225
Off-bottom clear, C (m)	0.017	0.013	0.013
Submergence, S (m)	0.038	0.038	0.038
Tank volume, V_{TANK} (m ³)	9.94E-04	9.94E-04	9.94E-04
Total impeller vol, V_{IMP} (m ³)	1.68E-04	5.23E-05	4.31E-05
Transitional N_p per impeller*	1.3	0.65	4.6
$P/\rho V_{TANK}$ (W/kg)	0.18	1.13	1.71
$\epsilon \sim P/\rho V_{IMP}$ (W/kg)	1.08	21.45	39.48
Reynolds number, Re	1715	3858	2315
Mixing time (min)	2, 6, and 10 min		

**Power number for the SSTC was measured using a Torque Transducer and Ethylene glycol at 20° C with a kinematic viscosity of 6 cSt.*

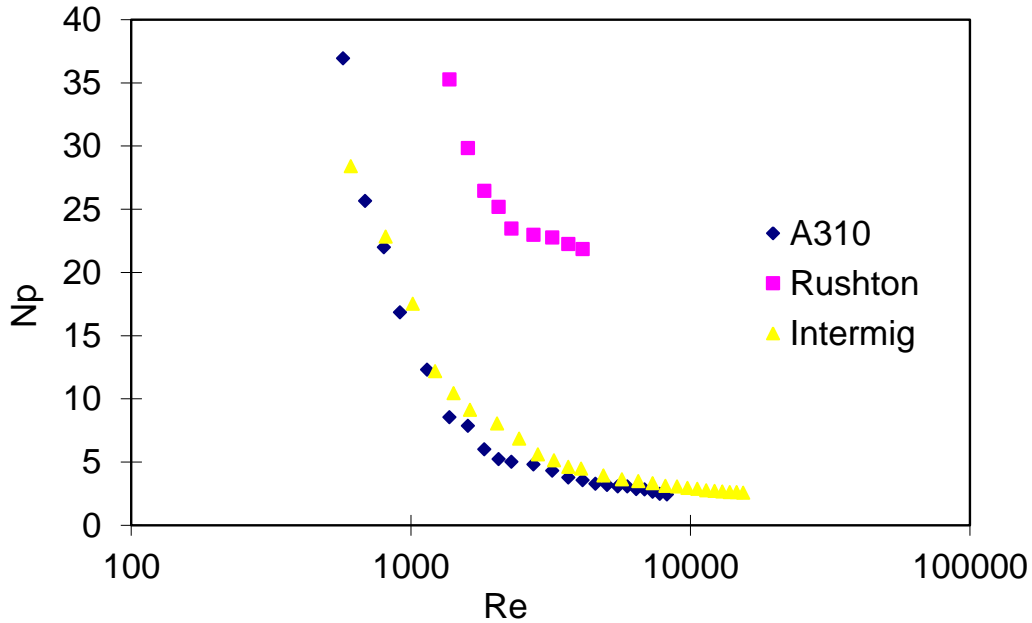


Figure 3-4: Power number measurements as a function of Reynolds' number for 5 A310 impellers, 5 Rushton impellers, and 6 Intermig impellers. Test Fluid: ethylene glycol at 25 °C (6 cSt). Data reproduced with permission (Machado and Kresta 2011).

The advantages of the SSTC over a conventional stirred tank are numerous. An SSTC can be used for smaller sample volumes (1L) where settling height is important. The vessel is also filled with at least five impellers per three standard tank volumes (one standard tank volume is defined as a tank where $H=T$) where as a standard stirred tank would have one impeller per standard tank volume. Accordingly there is an estimated 66% more turbulence per unit volume in the SSTC than the standard stirred tank, and as a result the agitation is more uniform. The viscosity of diluted bitumen is quite high, leading to high-transitional Reynolds' numbers as opposed to fully turbulent conditions. While a shorter and wider tank is expected to provide a higher Reynolds' number at a constant impeller speed N , the large amount of turbulence provided by multiple impellers is expected to compensate for the lower Reynolds' number. The high aspect ratio of the SSTC allows for immediate settling

after mixing without sample transfer. The footprint per stirred tank is also smaller, which allows for several simultaneous experiments.

Four independent variables were studied for the experiment: bulk demulsifier concentration per unit mass (BC), mixing intensity (ε_{max}), mixing time (t), and the injection concentration of demulsifier (IC). Both bulk concentration and injection concentration are calculated on a mass basis. An estimate of ε_{max} is obtained by observing that

$$\varepsilon_{max} \propto \frac{P}{\rho V_{Impeller}} \quad 3-1$$

Demulsifier is injected shortly after the impeller is turned on at the appropriate level, using an appropriately sized syringe or a pipette connected to 0.25" polyethylene tubing. The injection takes place over 2 seconds directly above the upper impeller blade tip to promote high initial dispersion of demulsifier. Mixing continues until the mixing time is reached. Samples are obtained for water content determination and microscope analysis by sampling the bulk mixtures 1.25" below the liquid surface using 0.25" ID polyethylene tubing attached to an auto-pipette. These samples are obtained 60 seconds after demulsifier injection and 30 seconds before the end of mixing.

3.1.3 Design of Experiments

Following the mixing period the diluted bitumen was allowed to settle by gravity for 60 minutes. The diluted bitumen was sampled for water content 3.25 cm below the liquid surface at 1, 3, 5, 7, 10, 30, and 60 minutes using 0.25" polyethylene tubing directed by a steel sampling tube. Microscope images of the samples were obtained at 5, 7, 10, and 60 minutes settling. The liquid was then sampled vertically for water content from top to bottom at 10 equally spaced intervals. Sampling was conducted using 1/4" ID polyethylene tubing guided along 3/8" stainless steel tubing lowered from

the tank lid. The tubing was attached to an auto-pipette by using a pipette tip as an adapter (ensuring an air tight seal). The tubing tip was flat, and samples were withdrawn during agitation directly above the impeller tip for convenience. A 100 mL sample was obtained for OWS analysis at the first, fifth, and ninth sampling interval. Images were obtained from samples at the bottom of the cylinder where a muddy layer was formed.

Each variable was varied at three levels to allow for the detection of quadratic effects. Demulsifier A was added to the diluted bitumen at a dosage BC of 2, 26, and 50 ppm, which is the commercial application range of the demulsifier. The injection concentration IC was varied from 1% injection concentration to 39% (stock solution) active demulsifier diluted in xylenes, by mass. The SSTC mixing configurations shown previously were used to obtain maximum energy dissipations of 1-40 W/kg as given in Table 3-5. This range was selected to cover energy dissipation levels ranging from agitation in an empty pipe to agitation with a static mixer. This energy dissipation range also overlaps with the experimental range of Phase 1. Different impellers are used in order to maintain circulating velocities and Reynolds' numbers while changing energy dissipation levels over a large range. Mixing time was varied from 2-10 minutes, with two minutes being the shortest mixing time possible with this experimental configuration. The variables are coded according to equally spaced intervals using the relationship:

$$X_A = 2 \frac{(A - A_{MIN})}{A_{MAX} - A_{MIN}} - 1 \quad \mathbf{3-2}$$

This coding arrangement yields coded levels of -1, 0, and +1 for each of three design coordinates for each variable. The full Box-Behnken fractional factorial design of experiments is shown in Table 3-4.

Table 3-4: Box-Behnken factorial design runs

Block/Variable	Bulk Concentration	Mixing Intensity	Mixing Time	Injection Concentration
	X_{BC}	X_{ϵ}	X_t	X_{IC}
X_{BC}, X_{ϵ}	-	-	0	0
	-	+	0	0
	+	-	0	0
	+	+	0	0
X_{BC}, X_t	-	0	-	0
	-	0	+	0
	+	0	-	0
	+	0	+	0
X_{BC}, X_{IC}	-	0	0	-
	-	0	0	+
	+	0	0	-
	+	0	0	+
X_{ϵ}, X_t	0	-	-	0
	0	-	+	0
	0	+	-	0
	0	+	+	0
X_{ϵ}, X_{IC}	0	-	0	-
	0	-	0	+
	0	+	0	-
	0	+	0	+
X_t, X_{IC}	0	0	-	-
	0	0	-	+
	0	0	+	-
	0	0	+	+
Central Design Points	0	0	0	0
	0	0	0	0
	0	0	0	0
	0	0	0	0
	0	0	0	0
	0	0	0	0

A summary of the design coding arrangements for all four variables is shown in Table 3-5. The experiments were conducted in two repeated full design blocks, and the order of all experiments within the blocks was randomized.

Table 3-5: Variable coding for Box-Behnken fractional

Variable	-1	0	+1
Bulk Demulsifier Concentration, BC (ppm)	2	26	50
Mixing Intensity, ϵ (W/kg)	1	20	40
Mixing Time, t (min)	2	6	10
Injection Concentration, IC (wt. %)	1	20	39

3.1.4 Karl-Fischer Titration

Karl-Fischer titration is used as the standard measure of water content since Dean Stark extraction was determined to lack precision at water content less than 2%. Samples containing approximately 1 mL diluted bitumen were obtained once after pre-mixing, nine times during the experiment from the top layer for each SSTC, and 10 times following batch gravity settling for each SSTC to give a full water profile over the volume. These are pre-dissolved before analysis using a 1:3 isopropyl alcohol and toluene mixture, which is dried using silica gel and sampled for water content prior to dilution. The samples are analyzed using a Kam Controls Karl Fischer titration apparatus and standard reagents. A calibration curve was generated using standard test samples containing 0.1 wt% water and varying the injection volume, and this calibration curve

is shown previously in Figure 2-4. They are agitated using a vortex mixer for 6 seconds and a 50 μ L spring loaded Hamilton syringe is used to inject the sample. Samples are weighed before and after dilution, and syringes are weighed before and after injections.

3.2 Results/Discussion

The complete set of batch gravity settling data is given in Appendix B. Two full repeated data sets were collected for each Box-Behnken factorial design point. Obvious outliers were removed, while one additional non-design point was retained for analysis. The five centre point repeats shown in Figure 3-5 provide an estimate of the experimental variance (sampling & analysis). Variance between repeated runs is generally observed to decrease with settling time. Figure 3-6 shows all 54 experimental runs as a function of settling time. The only conclusions that can be drawn from this plot are that final water contents fall between 0.31 – 1.55 wt. %, there is a continuous progression from high to low water contents, and that improved product quality depends on faster initial settling. A more informative approach is to consider the best and worst cases of settling.

Figure 3-7 shows all runs resulting in a final water contents greater than 1 wt. %. The majority of these cases are the experiments where the smallest bulk concentration of 2 ppm demulsifier was used. These results did not seem to be greatly affected by any mixing-related variables. Every single case with a bulk concentration of 26 ppm and two unfavourable mixing variables (i.e. low mixing intensity, low mixing time, or high injection concentration) also appears in this set of data. This suggests that addition of demulsifier will have little impact on product quality if the mixing conditions are not properly selected.

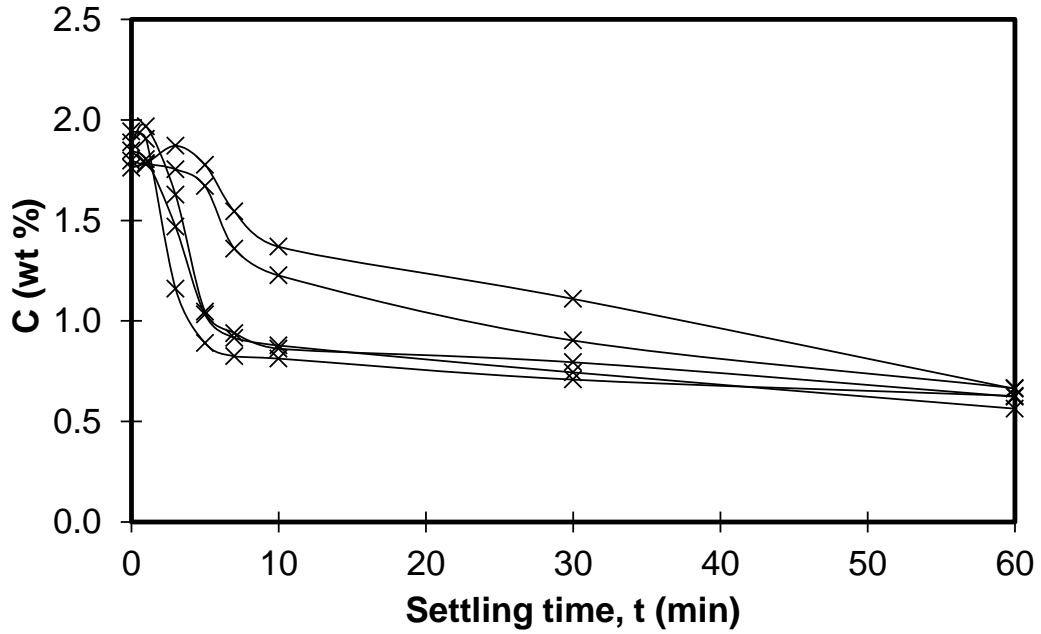


Figure 3-5: Diluted bitumen water content during batch gravity settling, centre point repeats (5); repeated runs provide an estimate of variability from run to run

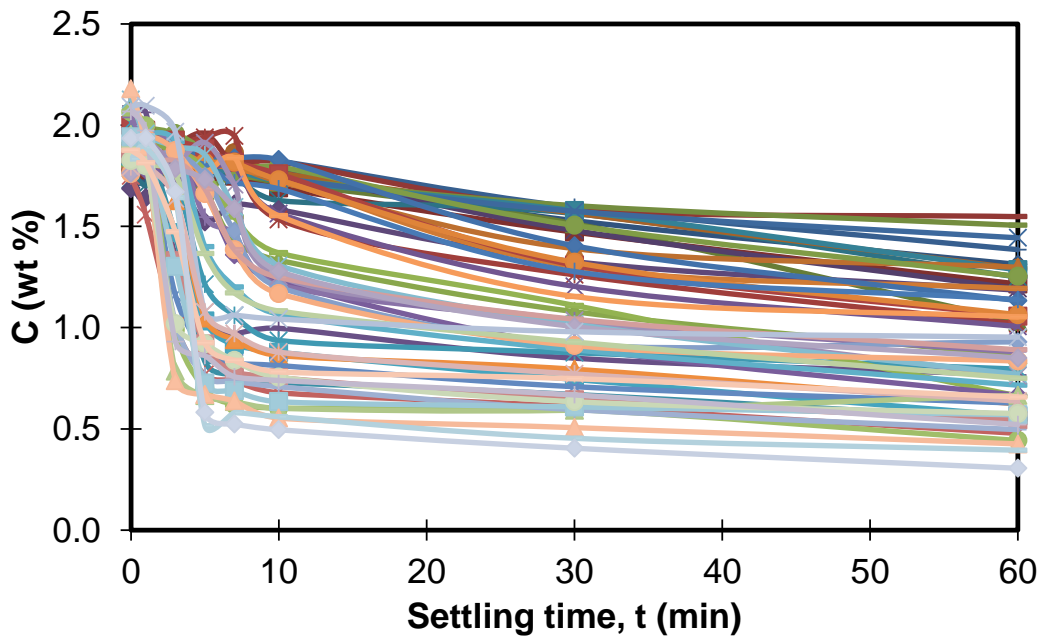


Figure 3-6: Diluted bitumen water content during batch gravity settling, 54 experimental runs included

The best results are shown in Figure 3-8 where all cases of two favourable variables appear (i.e. two of high bulk concentration, high mixing intensity, high mixing time, and low injection concentration). All possible combinations of two variables are observed, and in all cases the remaining two variables are at the mid-level values. These observations summarize three key factors to consider when optimizing diluted bitumen settling operations: firstly, that it may not be possible to induce any large amount of settling if demulsifier is cut to a sufficiently low level; secondly, that unfavourable mixing conditions can yield similar results to insufficient demulsifier addition; thirdly, that optimizing mixing conditions can improve the efficiency of modest doses of demulsifier, and as a result can also lead to decreased demulsifier use.

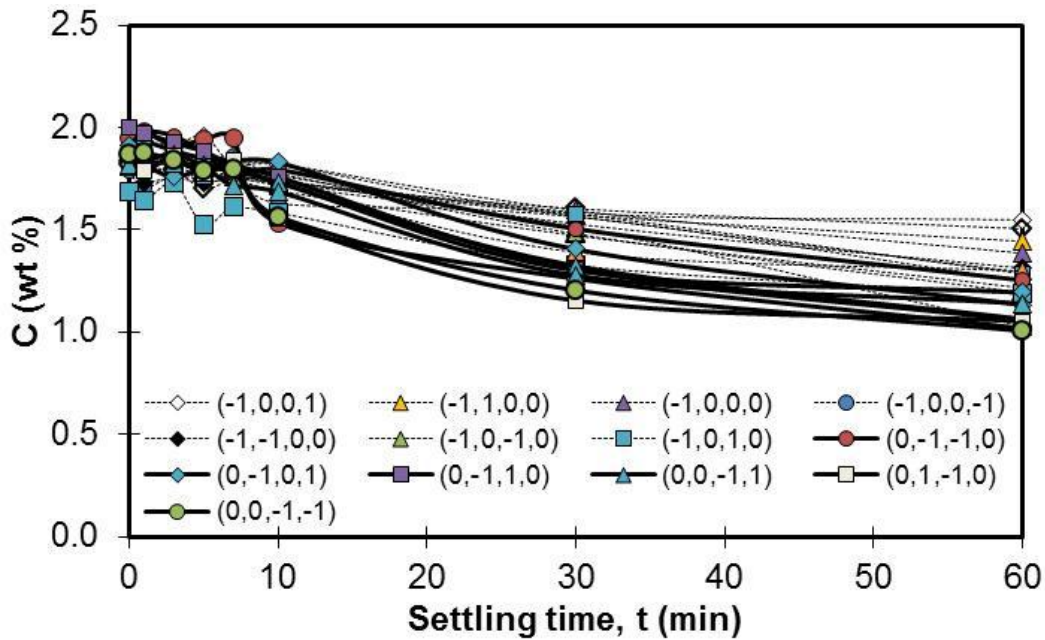


Figure 3-7: Diluted bitumen water content during batch gravity settling, with final water content exceeding 1 wt%. Unfavourable mixing conditions can render 26 ppm of demulsifier as ineffective as 2 ppm demulsifier. Variable order: (X_{BC} , X_{ϵ} , X_t and X_{IC}).

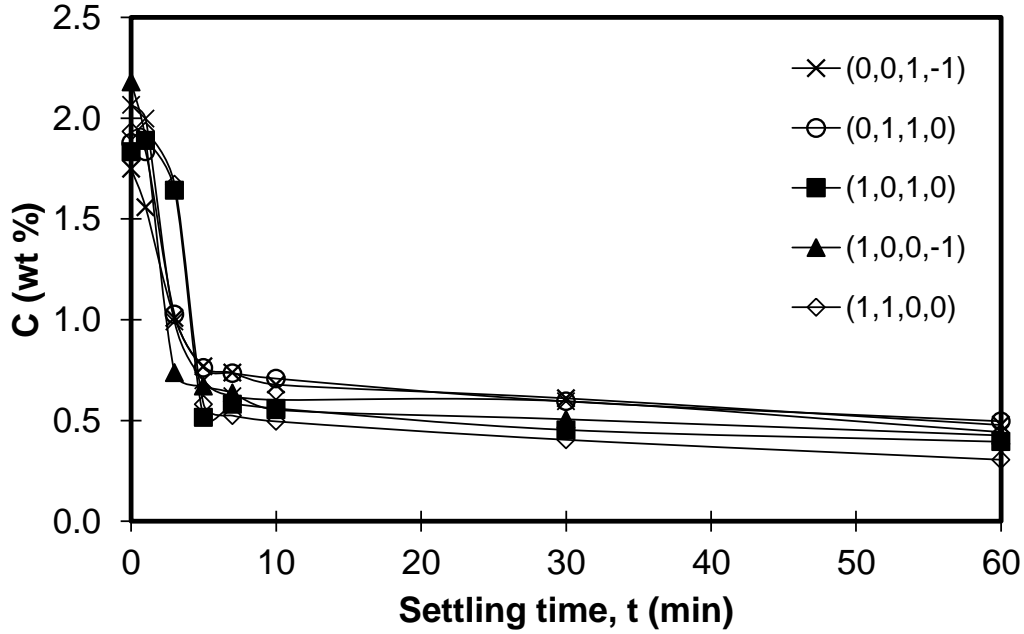


Figure 3-8: Diluted bitumen water content during batch gravity settling, with final water content less than 0.5 wt%; favourable mixing conditions can yield similar results using 26 ppm and 50 ppm of demulsifier. Variable order: (X_{BC} , X_{ϵ} , X_t and X_{IC}).

3.2.1 Mixing and Demulsifier Effects on Settling

The density of the data acquired as well as the multiple factors involved makes it difficult to proceed with a visual analysis of the results. The batch gravity settling data was subjected to a 4-factor multiple linear regression analysis at each instance in time using the regression equation:

$$\begin{aligned}
 C(t) = & \beta_0 + \beta_{BC}x_{BC} + \beta_{\epsilon}x_{\epsilon} + \beta_t x_t + \beta_{IC}x_{IC} \\
 & + \beta_{BC*BC}x_{BC}^2 + \beta_{\epsilon\epsilon}x_{\epsilon}^2 + \beta_{tt}x_t^2 + \beta_{IC*IC}x_{IC}^2 \\
 & + \beta_{BC*\epsilon}x_{BC}x_{\epsilon} + \beta_{BC*t}x_{BC}x_t + \beta_{BC*IC}x_{BC}x_{IC} \\
 & + \beta_{\epsilon*t}x_{\epsilon}x_t + \beta_{\epsilon*IC}x_{\epsilon}x_{IC} + \beta_{t*IC}x_t x_{IC}
 \end{aligned}
 \tag{3-3}$$

where $C(t)$ is the water content in mass percentage as a function of time. The regression was performed iteratively, discarding statistically insignificant effects until all effects evaluated were considered statistically significant. The resulting coefficients and their confidence intervals are shown in Figure 3-9. Settling effects are detected from 3 min settling onward, and all 4 factors are statistically significant for a large range of settling times. Confidence intervals are given for 95% confidence. This analysis confirmed the expected direction of effects (improved performance for low IC, high BC, ϵ , and t), and shows that the BC has twice the impact of the other three variables. Other significant effects include a quadratic effect of bulk concentration (30 and 60 minutes) and a bulk concentration and initial concentration interaction effect (3 minutes). In general, the bulk concentration effect is found to be twice as large as any other mixing effects. The uncertainty on parameter estimates narrows with increasing settling time.

The significance of the results is that, regardless of mechanism, all four variables were found to be relevant over the range of interest. A higher dosage of demulsifier is required to achieve a cleaner product. In addition positive results can also be accomplished with a combination of increasing the mixing intensity, mixing time, and reducing the injection concentration of demulsifier. There are shortcomings with the multiple-linear regression approach. The confidence intervals of the main effects remain large due to high variability in the data. Smaller meaningful interaction effects can escape detection, and the same can be said for quadratic effects.

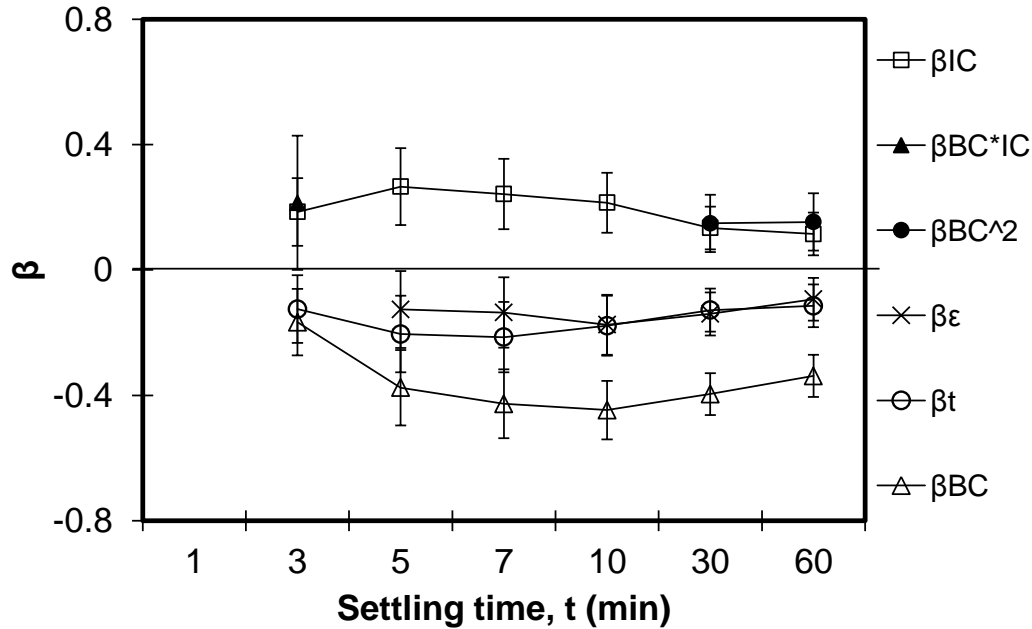


Figure 3-9: Regression coefficients and their confidence intervals for four variable multiple linear regression; significant main effects include bulk concentration (BC), mixing intensity (ϵ), mixing time (t), and injection concentration (IC)

As previously seen in Figure 3-9, the quadratic effect of bulk demulsifier concentration is not shown until the later stages of settling, where confidence intervals are significantly narrowed. This effect makes much physical sense, given that there are often diminishing returns to any surface active chemical. In fact, overdoses of demulsifier are generally known to be neutral or harmful to a process once reaching the critical micelle concentration (CMC) where demulsifier will self-associate. There is no evidence of overdosing in this work, and the CMC remains unknown for this chemical. The factorial results are examined in more detail in Figure 3-10, Figure 3-11, and Figure 3-12. While the linear regression might suggest otherwise, direct observations show no significant correlation between water content and mixing intensity or time at a bulk concentration of 2 ppm demulsifier. A smaller but noticeable increase in process performance is observed with a decrease in injection concentration. The linear fit fails to account for these interaction effects. Despite these

misgivings the large changes in performance are observed at greater bulk concentrations. The main benefit of the linear regression is that all four variables of interest are found to be statistically significant over the range studied, while mechanistic arguments can be made based on this significance. A few additional observations remain. In Figure 3-13 increasing mixing time is observed to have a greater effect at higher mixing intensities. In Figure 3-14, an increase in mixing intensity is observed to be much more important at higher injection concentrations. In Figure 3-11 and Figure 3-15 we see larger than normal variance at lower mixing times. These observations are not captured in the statistical model but are nonetheless meaningful to the application of the results.

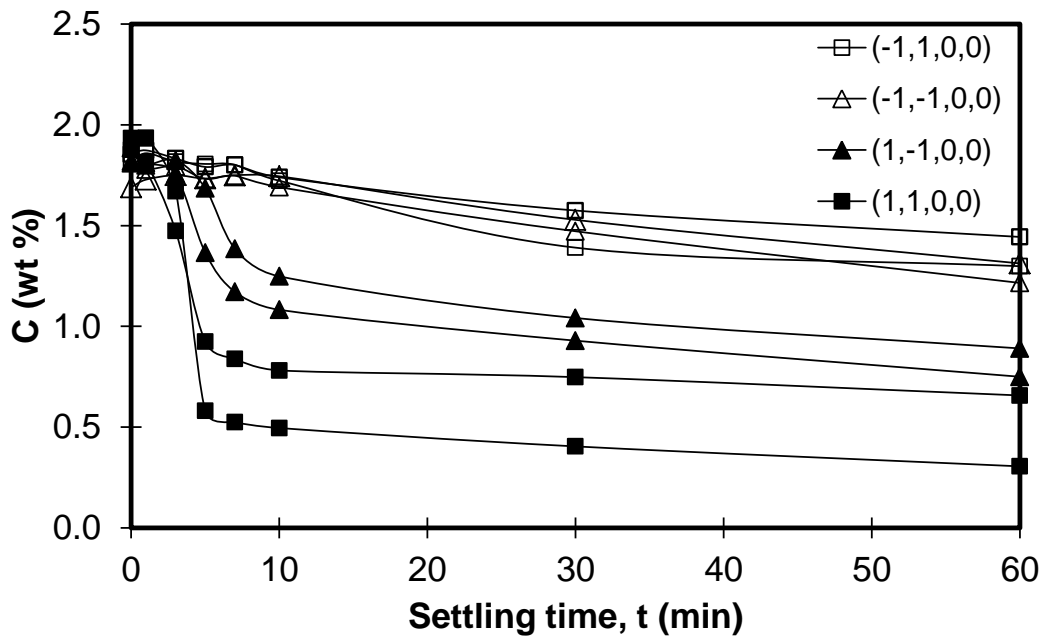


Figure 3-10: Diluted bitumen water content during batch gravity settling, bulk concentration (BC) and mixing intensity (ϵ) block; intense mixing and greater demulsifier dosage are preferred. Variable order: (X_{BC} , X_{ϵ} , X_t and X_{IC}).

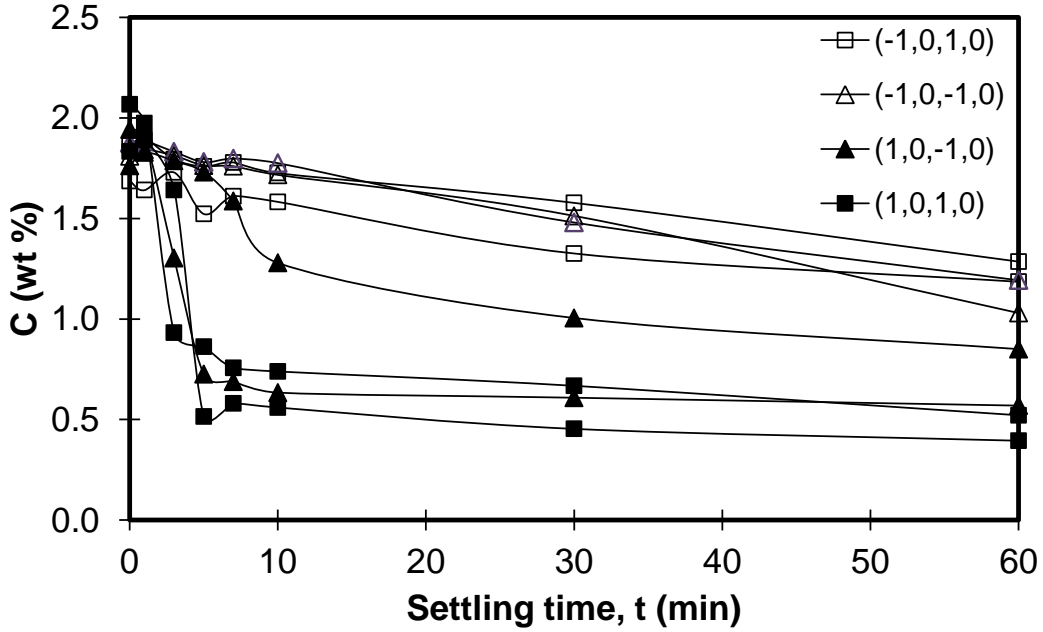


Figure 3-11: Diluted bitumen water content during batch gravity settling, bulk concentration (BC) and mixing time (t) block; longer mixing time and greater demulsifier dosage are preferred. Variable order: (X_{BC} , X_{ε} , X_t and X_{IC}).

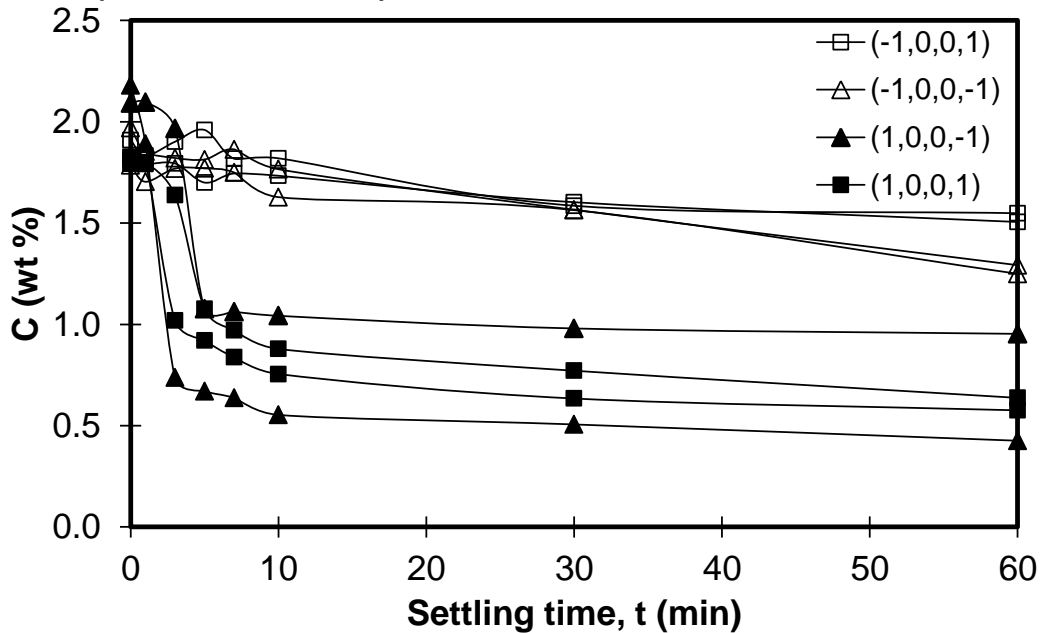


Figure 3-12: Diluted bitumen water content during batch gravity settling, bulk concentration (BC) and injection concentration (IC) block; greater demulsifier dosage is preferred. Variable order: (X_{BC} , X_{ε} , X_t and X_{IC}).

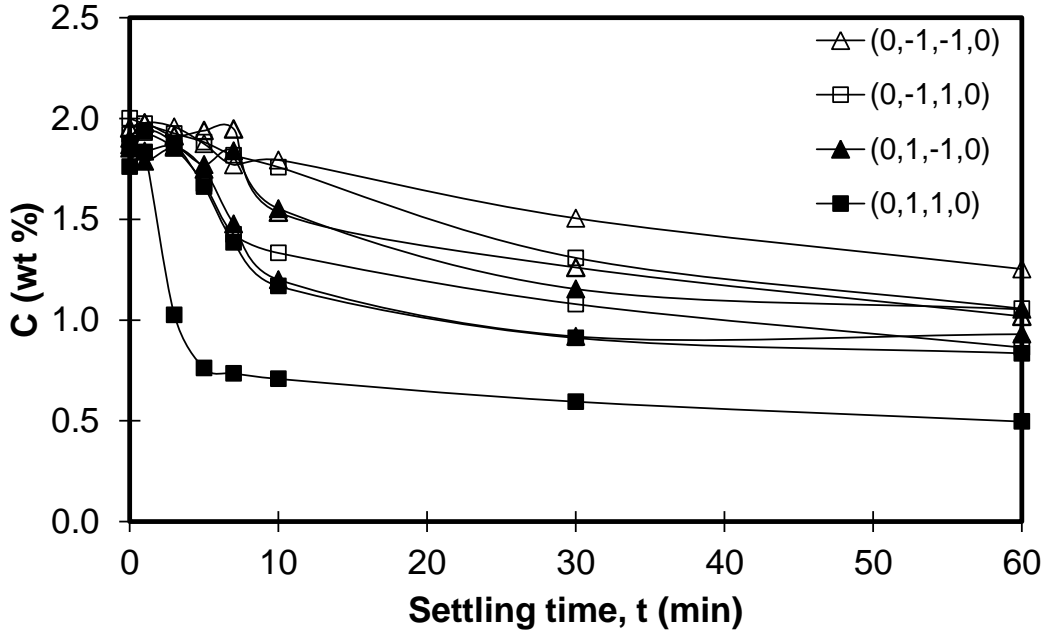


Figure 3-13: Diluted bitumen water content during batch gravity settling, mixing intensity (ϵ) and mixing time (t) block; intense mixing and longer mixing time are preferred. Variable order: (X_{BC} , X_{ϵ} , X_t and X_{IC}).

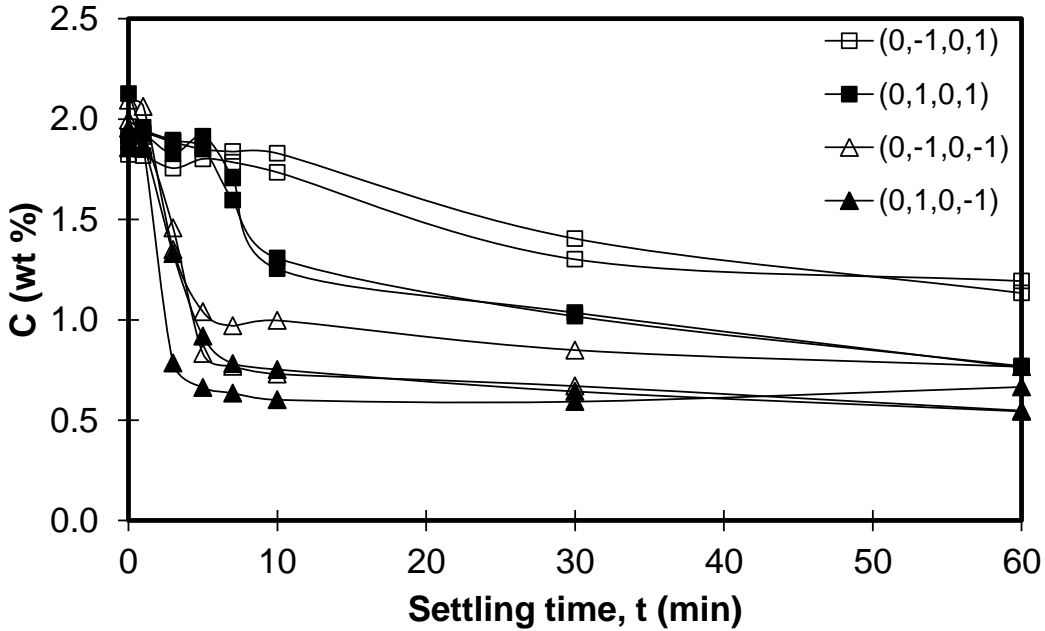


Figure 3-14: Diluted bitumen water content during batch gravity settling, mixing intensity (ϵ) and injection concentration (IC) block; intense mixing and less concentrated injections are preferred. Variable order: (X_{BC} , X_{ϵ} , X_t and X_{IC}).

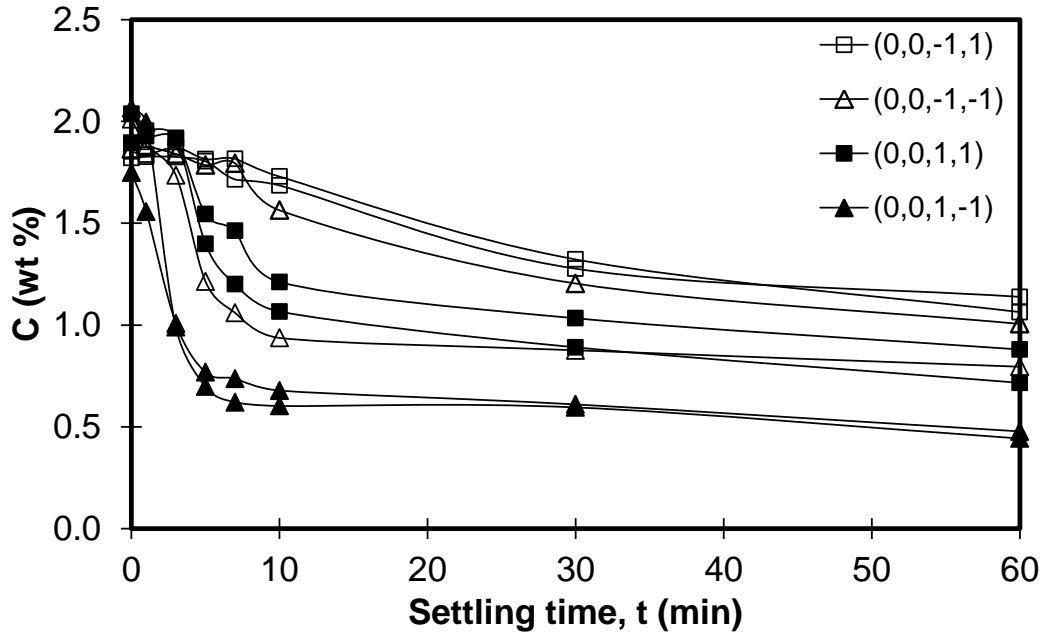


Figure 3-15: Diluted bitumen water content during batch gravity settling, mixing time (t) and injection concentration (IC) block; intense mixing and longer mixing time are preferred. Variable order: (X_{BC} , X_{ϵ} , X_t , and X_{IC}).

Water reduction in this system likely occurs through flocculation and subsequent settling. Figure 3-16 shows microscope images of samples before and after batch gravity settling but after demulsifier dispersion where floc sizes are observed to increase with increasing water removal. Following batch gravity settling there is an observed thick, muddy layer that forms at the bottom of the SSTC. Samples were obtained at the bottom of the SSTC after settling, and representative pictures are shown in Figure 3-17. These images imply an uneven muddy layer due to a combination of high and low water images regardless of product water content. The loose floc structure indicates that at least a large portion of the water and solids settles as flocs. It is possible that additional water is captured by a sweep flocculation mechanism, where large flocs sweep from top to bottom of the cylinder while settling and further reduce water content. While coalescence cannot be discounted, the images suggest that settling occurs in three steps: dissolution of demulsifier, flocculation of water and solids, and settling of flocculated water and solids.

Though the exact mechanism by which flocculation happens was not determined in this study, a quadratic response to demulsifier dosage is not unusual since the solubility limit of demulsifier in the bulk solution will lead to the formation of micelles. Therefore limiting the amount of demulsifier will benefit the system by facilitating the flocculation and possible coalescence of water droplets. Mixing intensity, mixing time, and bulk concentration are known to affect the equilibrium and dynamic floc size. Injection concentration affects the system in two ways: first it affects the dissolution step: that is, the dispersion and distribution of demulsifier to the solid/water-bitumen interphase. Second, it affects the local concentration of demulsifier at the injection point, which can lead to secondary concentration related effects, such as the formation of micelles. The mechanisms affecting dissolution and flocculation are quite complicated, particularly in heavily contaminated systems like diluted bitumen. A simplified mechanism is considered for both cases. The effectiveness of certain demulsifiers in froth treatment has been proposed to be due to a flocculation mechanism as presented in the Oilsands 2011 Conference (Xu et al. 2011; Yang and Melley 2011). This effect is similar to the effect of high froth water and solids content in froth processability (Ng et al. 2011).

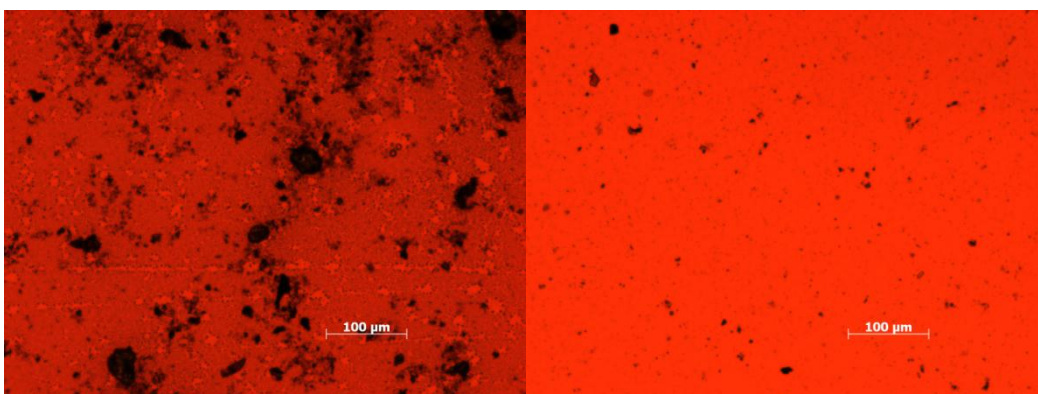
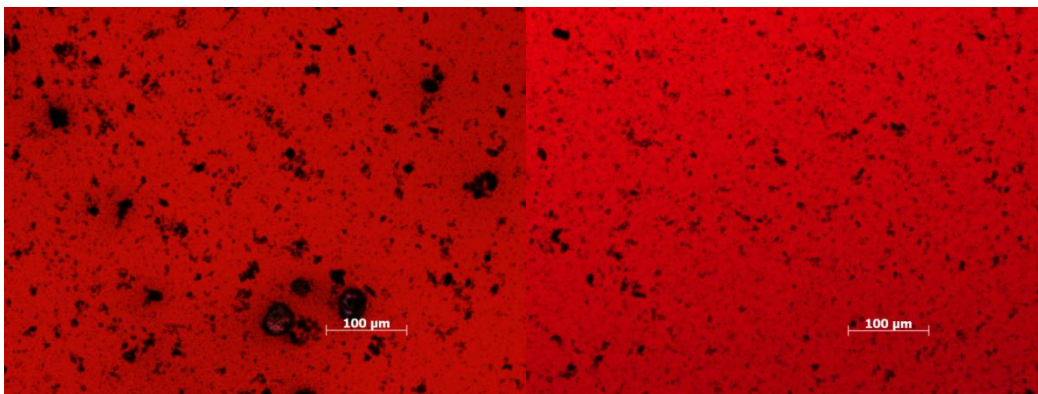
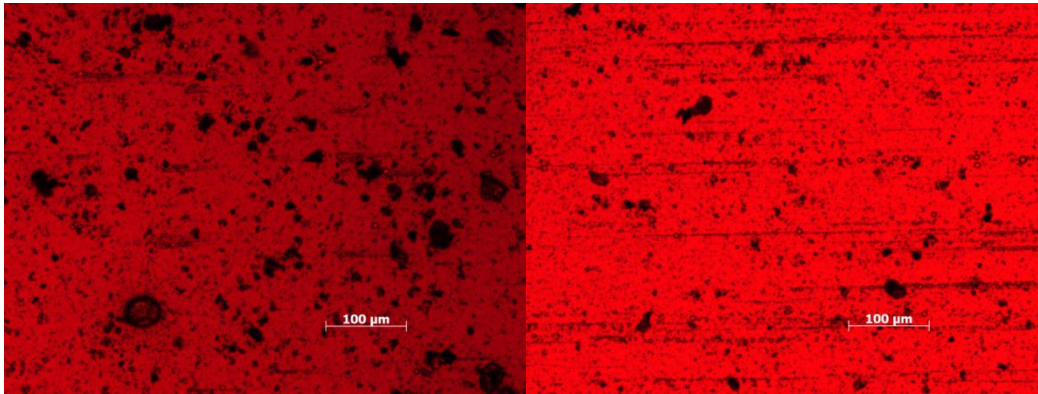


Figure 3-16: Microscope images before and after 60 minutes batch gravity settling at 100x magnification; final water content decreases as floc size increases

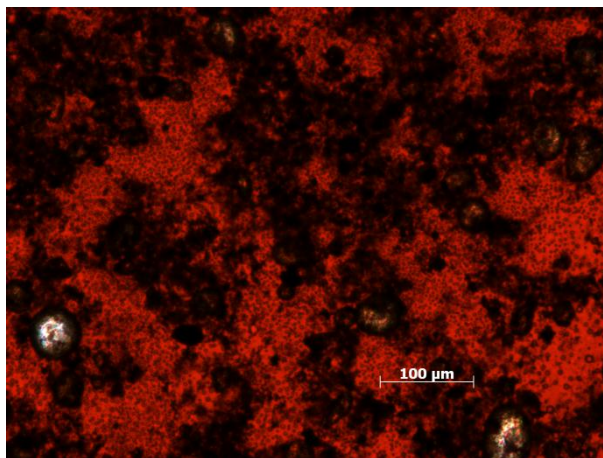
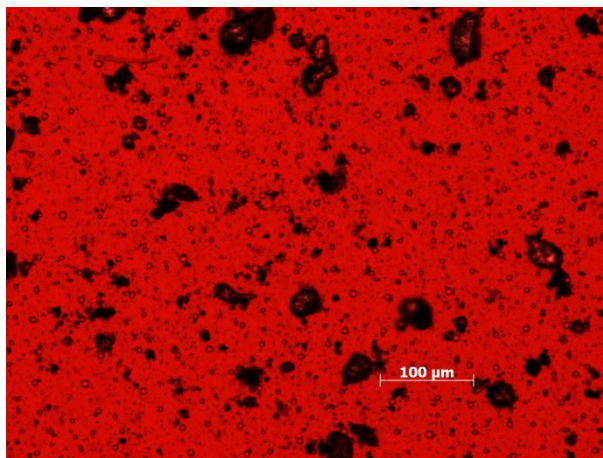
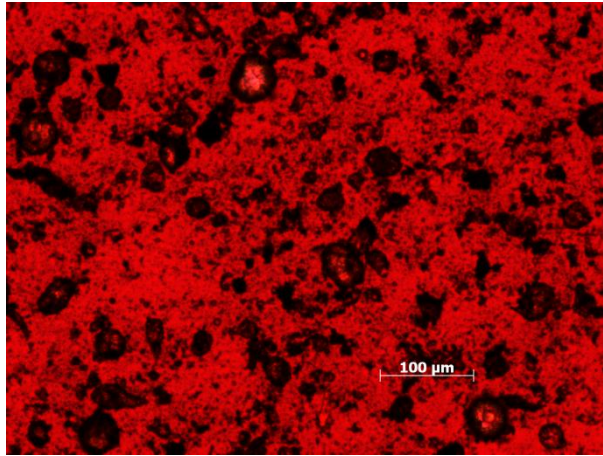


Figure 3-17: Microscope images obtained from samples at the bottom of the SSTC; the sampled bottom is observed to be a combination of normal diluted bitumen product, larger droplets, and packed flocs of water and solids

3.2.2 Lumped Parameter Multiple Linear Regression (MLR)

A second approach to multiple linear regression analysis was taken by lumping mixing intensity and mixing time as a single variable:

$$J = \varepsilon_{max} * t \quad \mathbf{3-4}$$

where J is proportional to the total energy injected at the impeller volume. The results were re-coded as

$$X_J = \left(\frac{2(J - J_{min})}{J_{max} - J_{min}} - 1 \right) \quad \mathbf{3-5}$$

The resulting linear regression is expressed as

$$\begin{aligned} C(t) = & \beta_0 + \beta_{BC}x_{BC} + \beta_Jx_J + \beta_{IC}x_{IC} \\ & + \beta_{BC*BC}x_{BC}^2 + \beta_{JJ}x_J^2 + \beta_{IC*IC}x_{IC}^2 \\ & + \beta_{BC*J}x_{BC}x_J + \beta_{BC*IC}x_{BC}x_{IC} + \beta_{J*IC}x_Jx_{IC} \end{aligned} \quad \mathbf{3-6}$$

Figure 3-18 shows the results of the regression analysis. The combined variable effect β_J is observed to be twice as large as either the mixing intensity or mixing time effects, leading to the conclusion that both variables can be easily combined. β_{J*IC} is observed initially at 3 min although a single unrepeated effect is likely to be insignificant. The β_{BC*J} interaction effect is observed twice, which warrants the plausibility of an interaction effect between total energy added to the system and total demulsifier. The combined 3 variable MLR performed as well as the 4 variable MLR. Figure 3-19 shows that an equal amount of variance is accounted for in both models given the R_{adj}^2 statistic. In both cases, the regressions accounted for over 70% of the variability observed

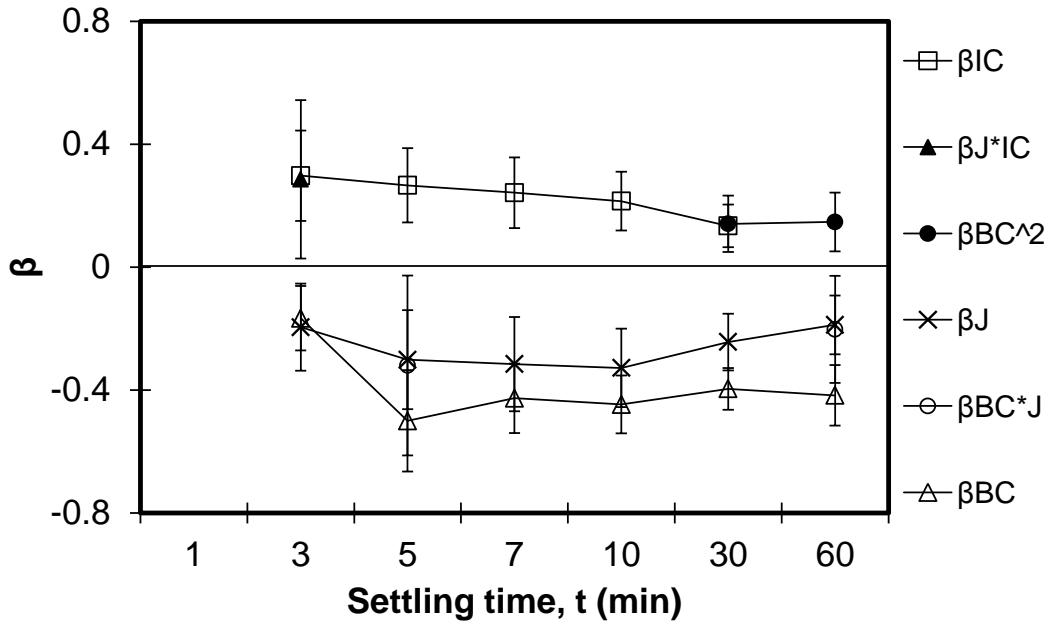


Figure 3-18: Regression coefficients for three variable multiple linear regression; significant main effects include bulk concentration (BC), energy dissipation (w), and injection concentration (IC)

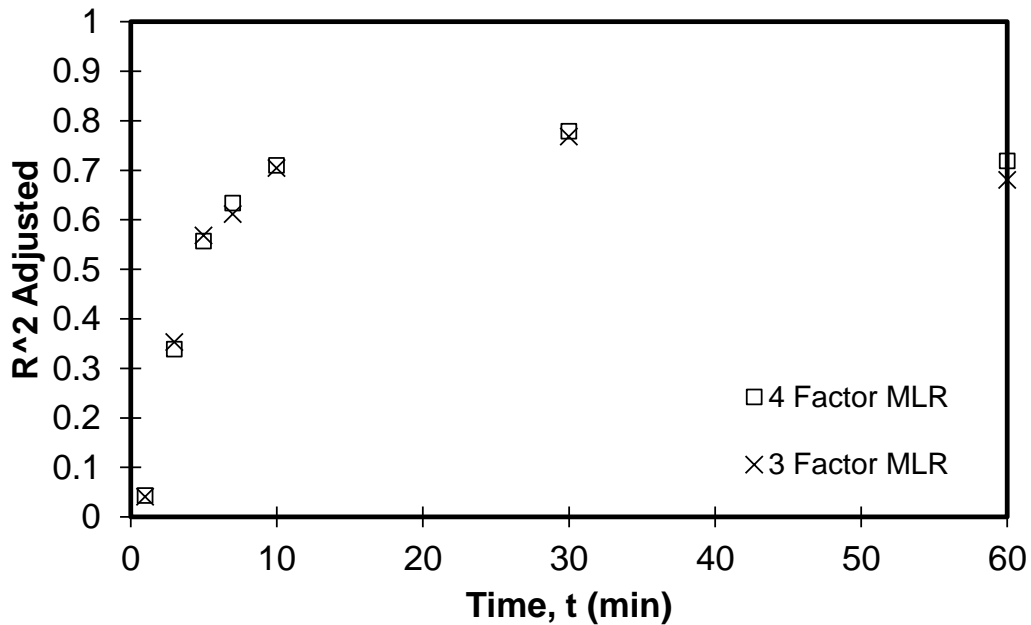


Figure 3-19: Adjusted R² values as a function of time for both 4 and 3 factor multiple linear regressions

experimentally. This consolidated approach may prove useful in lab scale or pilot plant design and scale-up, but it should be used with caution.

3.2.3 Initial Settling and Other Design Considerations

The bulk of settling occurs in the initial stages of settling, at an initial settling rate. A second, slower settling rate would be necessary to satisfy a general material balance over the settling period. The initial settling rate for each experiment was determined using the technique illustrated in Figure 3-20. Linear regions in the settling range are detected by inspection, and the initial rate of water removal is calculated from the initial slope. The water content in the sample following the initial settling period is found by calculating the intercept of the linear regions. Figure 3-21 shows a clear decrease in water content with an increased settling rate, R_i .

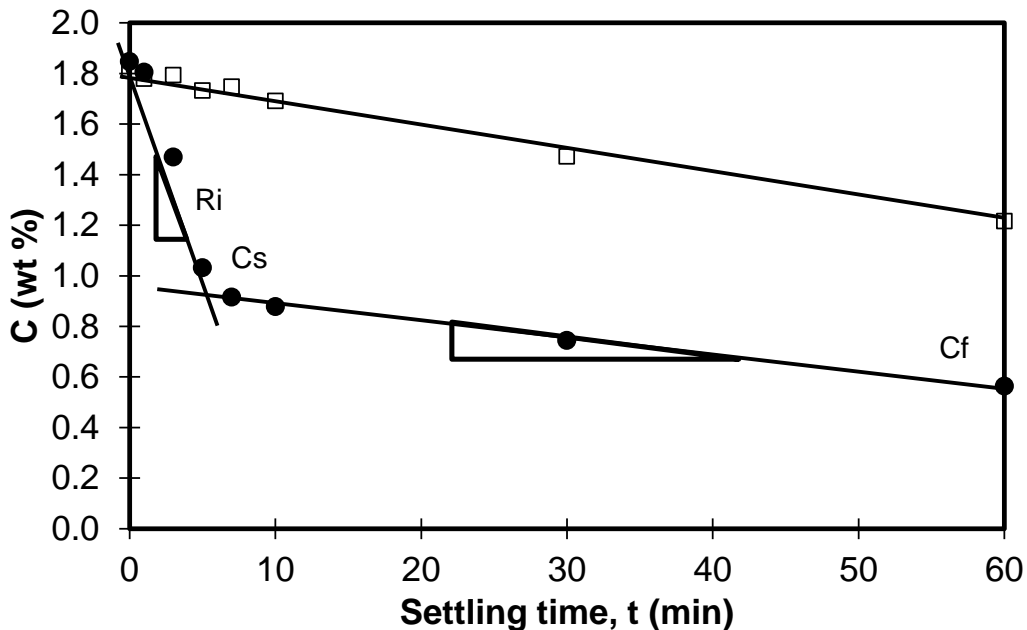


Figure 3-20: Initial water removal rate, water content immediately following initial settling (C_s) and final water content (C_f) can be determined by isolating linear trends in the data

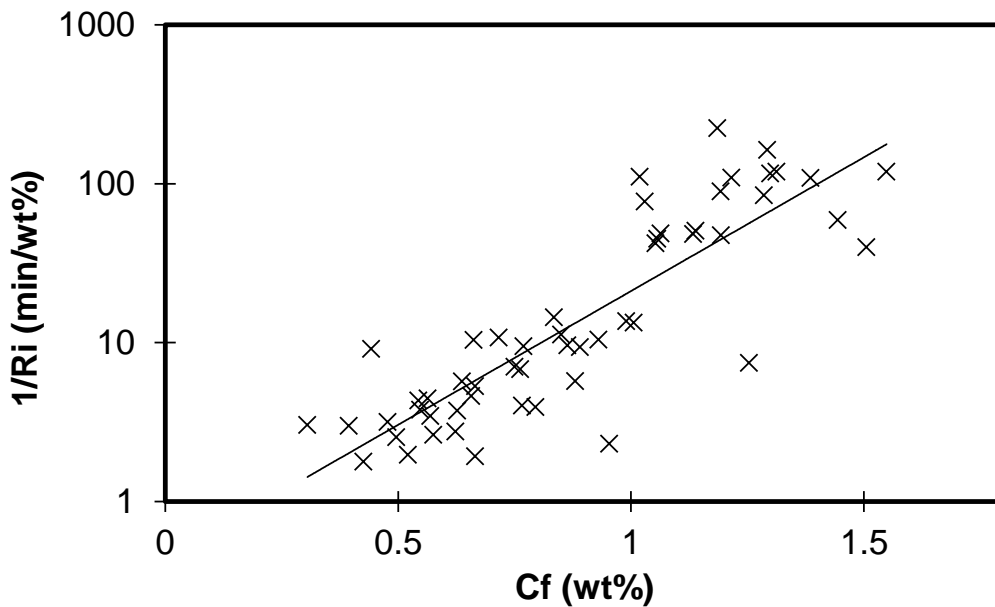


Figure 3-21: Observed initial settling rate as a function of water content; initial settling rate increases drastically with reducing final water content

This result is unsurprising since water is removed through an increase in drop/floc size. Differential settling is favoured by larger initial floc sizes prior to settling. Figure 3-22 confirms that the bulk of settling is achieved at this initial settling rate to within 0.2 wt% of the final settled water content. These results are more readily applied to systems with settling distances equal to 1.25", the settling distance in this system. Measuring water content as a function of settling time as opposed to after 30 or 60 minutes of settling is beneficial, as process equipment can be designed to appropriate settling rates as opposed to a standard settling time.

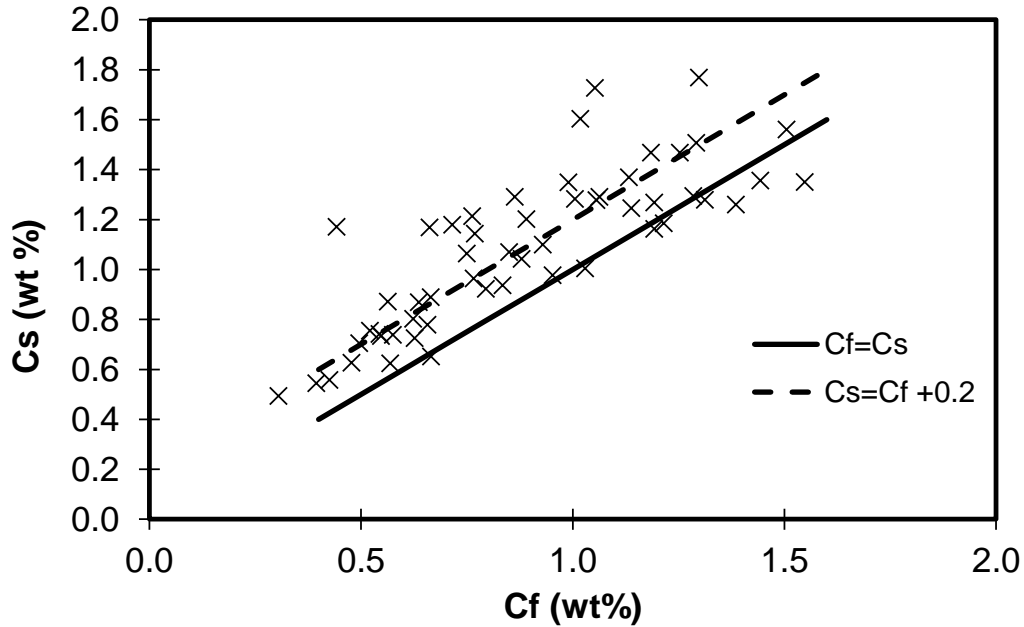


Figure 3-22: Initial settled water content is approximately 0.2 wt% greater than final water content after 60 minutes settling;

3.2.4 The Nature of the Oil-Water Interface

Vertical measurements of water content following batch gravity settling provide insight into the nature of the oil-water interface. While literature on the oil-water interface or “rag layer” is documented (Czarnecki et al. 2008) in froth treatment, it is less abundant for diluted bitumen clarification where the water content is reduced and only fines/fine flocs remain. Vertical concentration profiles from a normalized height h/Z of 0-0.9 were obtained following 60 minutes of settling through sampling and KF titration. The results for normalized heights $h/Z=0.2$, 0.1, and 0 are shown in Figure 3-23, Figure 3-24, Figure 3-25 respectively. The product quality observed in the top 80% of each cylindrical tank was greater than or equal to that observed at the top of the SSTC following batch gravity settling. This implies full settling at a normalized height h/z from the initial BGS sampling point. Figure 3-24 shows that this steep increase in water content is not observed for cases with minimal settling, but rather is a function of the amount of water settled. A rather sharp increase in cases

with elevated water contents is observed with final water contents below 1%, indicating an increase in the height of settled material to $h/z=0.1$. Increasingly high water contents with even lower final water contents shows a gradient ranging between the final water content C_f and 20%. Sampling at the bottom of the SSTC yielded mixed results. As shown in Figure 3-25, elevated water contents become more likely at lower depths, though any relationships between C_f and water content are less clear due to scatter. This is likely due to the nature of the bottom layer of the sample following batch gravity settling; solids and water settled to form an observable muddy layer, which is uneven. It is also likely that this layer would not be thick enough to provide a good sample, and a water/oil mixture from above the sampling point would mix with the muddy layer. Therefore, it is not safe to conclude that the highest local concentration of water is limited to 35%, as suggested by Figure 3-25. These combined results also imply that, despite water occupying at most 2% of the total volume of the cylinder prior to settling (assuming no solids) the settled tailings can occupy as much as 10% of the final volume. This loose packing of flocs may affect design and operations.

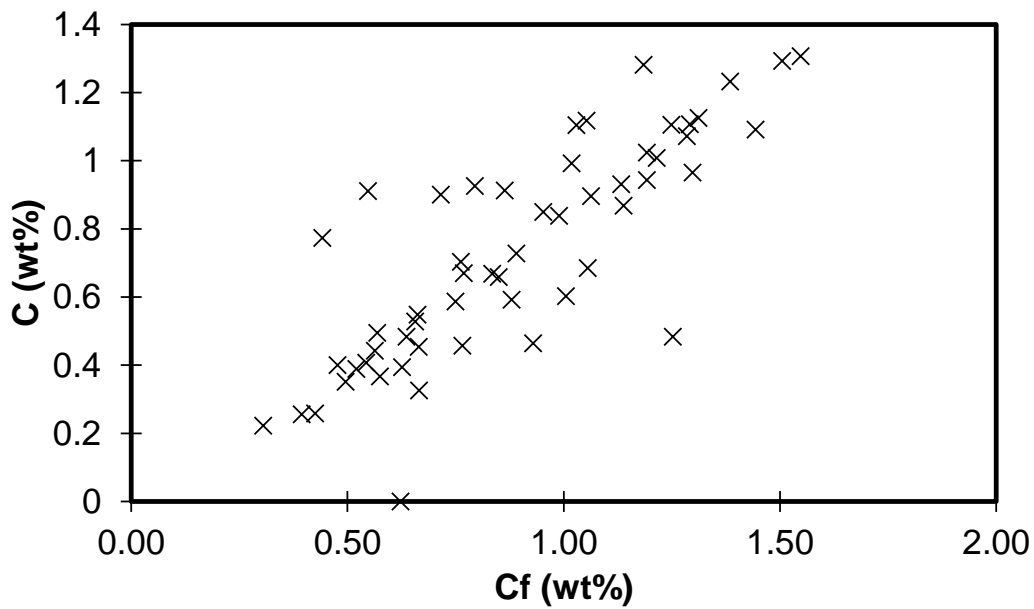


Figure 3-23: Water content at $h/Z=0.2$ following 60 minutes batch gravity settling; water content is approximately equal to final water content as measured from 1.25" from the surface of the SSTC. Solids content correlates with water content.

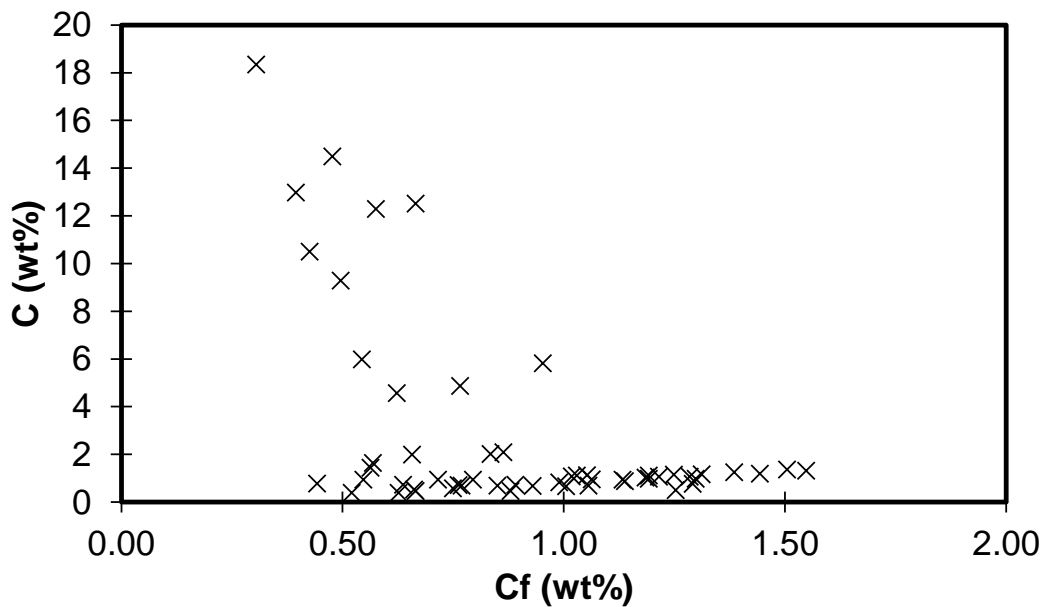


Figure 3-24: Water content at $h/Z=0.1$ following 60 minutes batch gravity settling; there is an abrupt rise in tailings water content following sufficient water content reduction

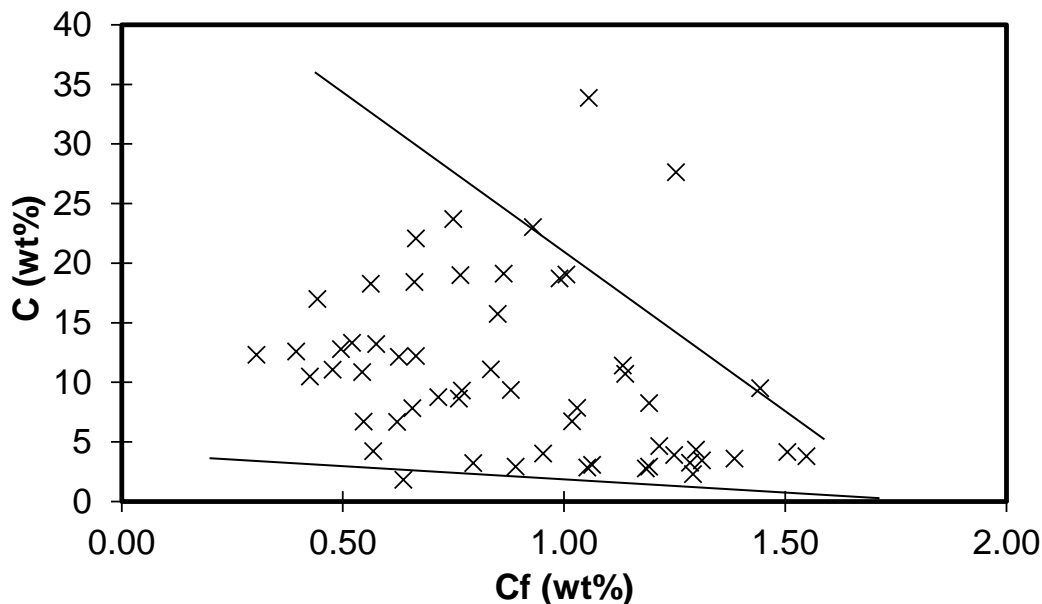


Figure 3-25: Water content at $h/Z=0$ following 60 minutes batch gravity settling; water content increases with decreased final water content in fanning motion (due to high variance in the tailings layer)

3.2.5 Solids Reduction and Characteristics

Diluted bitumen clarification is as much about a reduction in solids as a reduction in water. Initial and final solids content were measured through Dean Stark extraction. The initial solids content for each run is shown in Figure 3-26. There is no initial correlation between water and solids. Figure 3-27 shows a linear trend between final water and solids content following 60 minutes batch gravity settling. The middlings solids content, as obtained by sampling at $h/Z=0.5$, follows a similar trend. Figure 3-29 shows there is no relationship between water and solids at the bottom of the SSTC following batch gravity settling. The solids content is lower than initially present at the bottoms, implying that the solids present in the top 90% of the sample have migrated towards the muddy layer observed at the bottom of the SSTC. The dewatering of diluted bitumen froth appears to be a valid approach to reducing the total suspended solids in the diluted bitumen product.

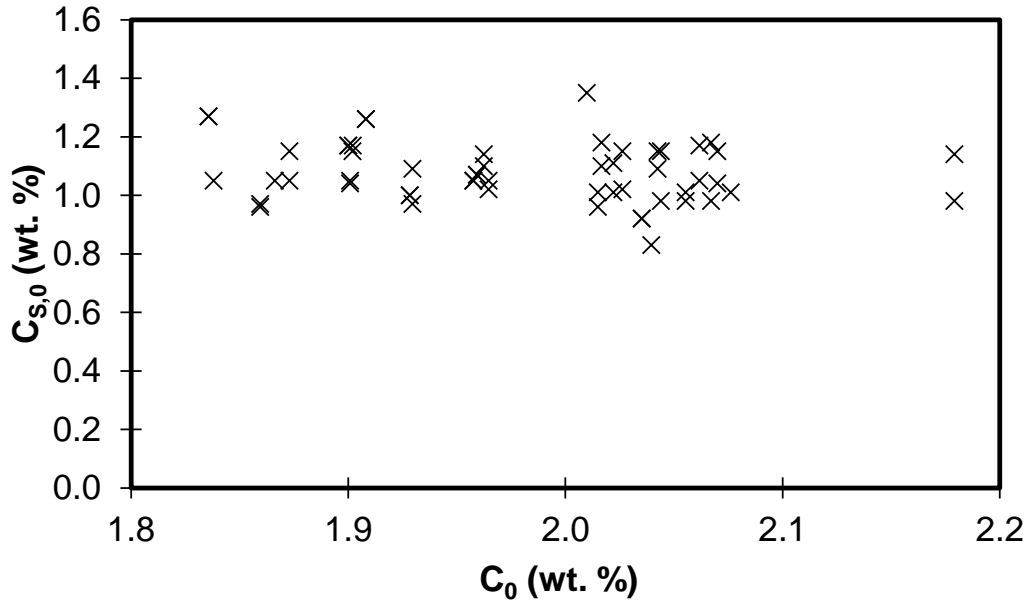


Figure 3-26: Initial solids content as a function of initial water content; initial solids vary from 1-1.2% while initial water varies from 1.8-2.2% with no correlation

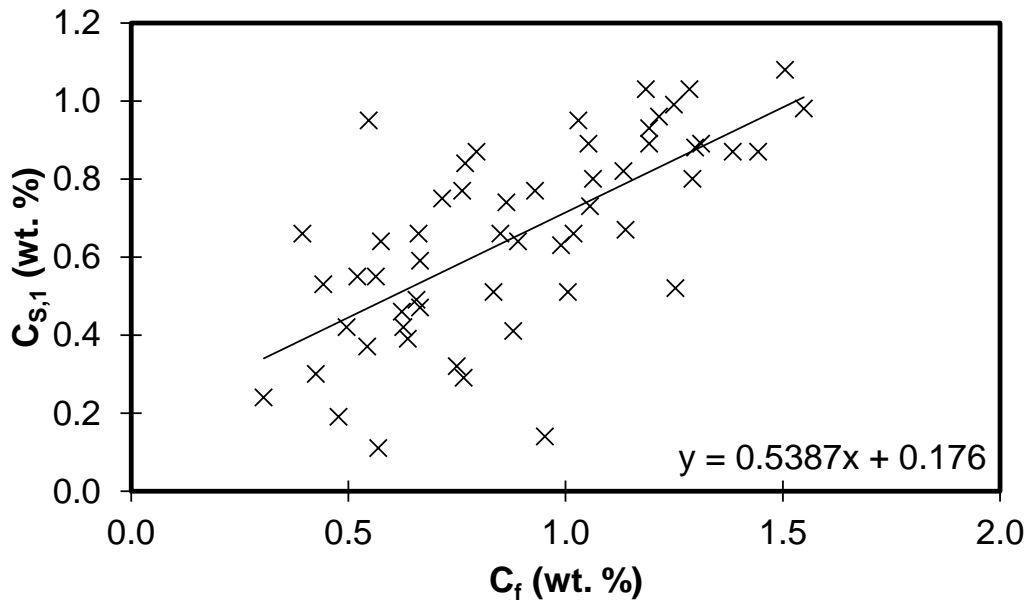


Figure 3-27: Product solids content (product) as a function of final water content; solids content varies linearly with water content

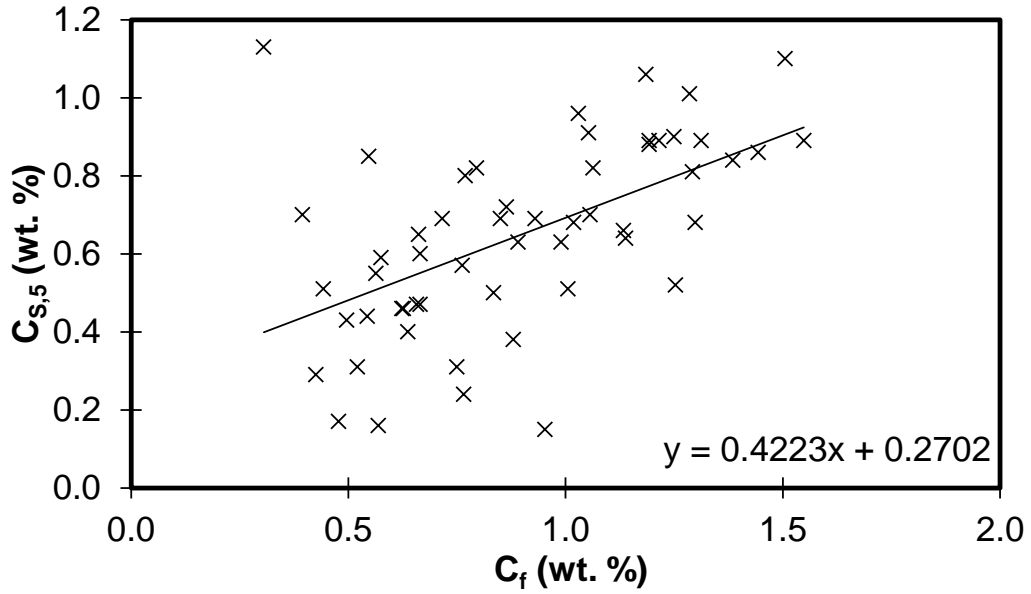


Figure 3-28: Product solids content (middlings) as a function of final water content; solids content varies linearly with water content

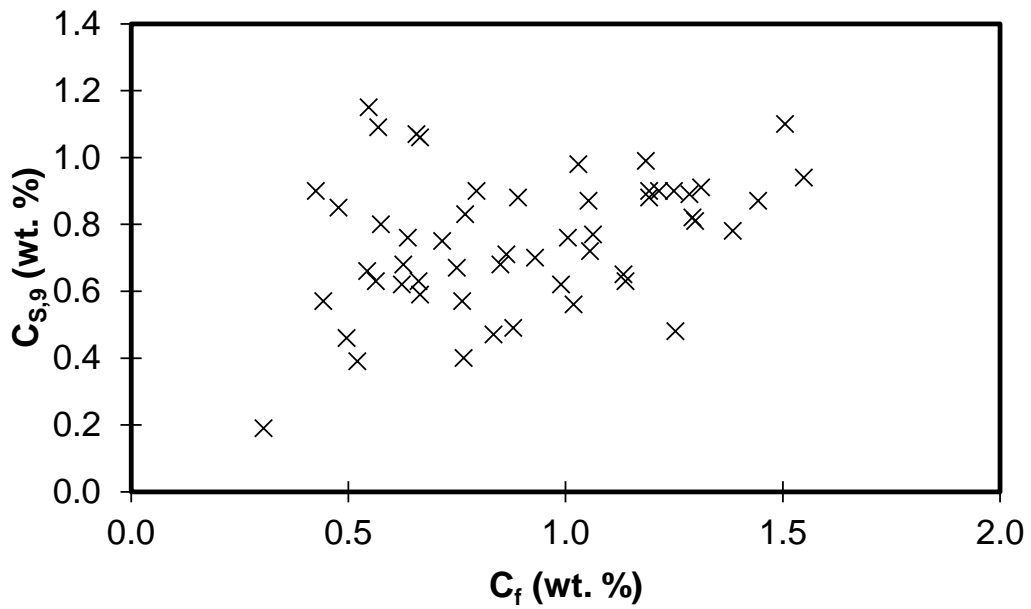


Figure 3-29: Product solids content (bottoms) as a function of final water content; solids do not correlate well with water content

3.3 Conclusions

This study concludes that in diluted bitumen clarification, the bulk concentration of demulsifier has the largest single impact on settling of water and solids. However, sub-optimal mixing conditions can drastically reduce the effectiveness of a given demulsifier dosage. Increasing mixing time and mixing intensity are physical ways to increase the effectiveness of demulsifier, while pre-dilution is shown to be an effective way to enhance demulsifier performance.

An increase in product quality is accompanied by faster initial settling rates, due to increased floc sizes. This increase in settling highlights the importance of lab-scale tests prior to equipment selection. Process designers should note this relationship between product quality and time based effects.

The SSTC was found to be a convenient way to perform mixer-settler experiments, and it eliminated unnecessary transfer steps in the experimental procedure. This study provides a first trial of the SSTC as a standard mixer/settler apparatus.

A. PHASE 1 EXPERIMENTAL DATA

Table A-1: Batch gravity settling data in wt% water (corr.)

Run	Labels	0	1	3	5	10	30	60
P1_004	(+1,+1,0)	3.59	3.43	2.67	1.31	0.67	0.47	0.37
P1_011	(+1,+1,0)	3.80	3.38	3.00	2.05	0.79	0.44	0.33
P1_005	(+1,0,+1)	3.77	3.66	3.40	1.04	0.47	0.32	0.26
P1_007	(+1,0,+1)	3.73	3.65	3.18	2.16	0.44	0.33	0.28
P1_014	(+1,0,-1)	3.46	3.32	2.60	1.43	0.51	0.41	0.34
P1_022	(+1,-1,0)	3.94	3.15	1.98	1.10	0.72	0.56	0.47
P1_019	(0,+1,+1)	3.90	3.22	2.79	1.71	1.01	0.66	0.53
P1_012	(0,+1,-1)	4.57	4.04	3.31	1.92	1.22	0.98	0.83
P1_020	(0,-1,-1)	3.91	2.74	2.27	1.97	1.38	0.90	0.74
P1_021	(0,-1,+1)	3.78	2.31	1.87	1.39	0.86	0.57	0.51
P1_018	(-1,+1,0)	3.96	3.40	3.11	2.30	1.90	1.81	1.68

Table A-1: Batch gravity settling data in wt% water (corr.)

P1_017	(-1,0,+1)	3.77	3.71	3.14	2.70	2.26	2.15	1.82
P1_013	(-1,0,-1)	3.89	3.55	3.27	2.79	2.24	1.90	1.86
P1_023	(-1,-1,0)	3.61	2.17	1.82	1.77	1.67	1.41	1.22
P1_008	(0,0,0)	3.67	3.66	2.41	1.36	0.88	0.80	0.69
P1_015	(0,0,0)	3.59	3.41	1.88	1.21	0.99	0.81	0.70
P1_016	(0,0,0)	4.12	3.72	2.66	2.02	1.20	0.95	0.79

Table A-2: Vertical concentration profile data in wt% water (corr.) at normalized height h/Z

Experiment	$h/Z=1$	0.5	0.4	0.3	0.2	0.1
P1_011	0.36	0.32	0.29	0.27	2.45	10.43
P1_007	0.30	0.30	0.20	0.26	7.34	12.29
P1_014	0.38	0.22	0.27	0.29	4.85	10.84
P1_022	0.46	0.45	0.43	0.42	0.41	10.31

Table A-2: Vertical concentration profile data in wt% water (corr.) at normalized height h/Z

P1_019	0.54	0.53	0.48	0.50	2.51	11.06
P1_012	0.75	0.77	0.72	0.76	0.74	6.62
P1_008	0.71	0.67	0.58	0.56	0.55	2.32
P1_015	0.72	0.67	0.63	0.62	0.71	11.17
P1_016	0.81	0.76	0.70	0.49	0.40	6.42
P1_020	0.71	0.69	0.52	0.75	0.52	1.02
P1_021	0.51	0.49	0.39	0.39	0.44	4.20
P1_018	1.64	1.62	1.47	1.49	1.51	1.50
P1_017	1.64	1.63	1.59	1.44	1.54	1.54
P1_013	2.19	1.73	1.68	1.70	1.67	1.69
P1_023	1.21	1.17	1.37	1.09	1.10	1.16

Table A-3: OWS Data

Run	Sample Source	Wt% Bitumen	Wt% Naphtha	Wt% Water	Wt% Toluene	Sample Weight	Added Toluene (mL)
P1_004	Pre-Mix	46.29	49.12	3.12	1.47	58.923	15
P1_004	T	61.08	36.67	1.88	0.36	96.62	
P1_004	T	61.54	37.2	0.91	0.35	78.422	
P1_004	T	61.53	35.67	2.33	0.47	91.285	
P1_004	T	62.7	34.01	2.75	0.53	86.024	
P1_004	B	52.12	35.62	8.06	4.2	70.096	5
P1_004	B	57.9	33.97	5.21	2.93	108.668	5
P1_004	B	52.13	35.16	8.91	3.8	69.263	5
P1_004	B	53.09	32.99	10.37	3.56	75.633	5
P1_005	Pre-Mix	47.99	45.27	5.09	1.66	59.111	15
P1_005	T	63.95	34.73	0.9	0.42	73.859	
P1_005	T	63.07	35.53	1.03	0.37	80.2	
P1_005	T	64.33	33.39	1.95	0.33	77.968	
P1_005	T	66.63	32.97	0.13	0.27	87.301	
P1_005	B	53.53	36.66	6.67	3.14	89.417	5
P1_005	B	54.39	35.27	6.93	3.42	89.222	5
P1_005	B	54.78	34.27	7.47	3.47	89.244	5
P1_005	B	53.15	36.85	6.38	3.63	91.962	5
P1_006	Pre-Mix	45.04	49.95	3.77	1.25	58.226	15
P1_006	T	62.89	35.2	1.23	0.67	71.835	
P1_006	T	61.84	35.78	1.77	0.62	69.653	
P1_006	T	62.9	35.11	1.36	0.64	71.993	
P1_006	T	63.91	33.8	1.74	0.55	84.582	
P1_006	B	57	34.42	5.72	2.87	79.75	5
P1_006	B	55.76	36.58	4.9	2.76	87.192	5
P1_006	B	55.05	34.97	6.64	3.33	66.254	5
P1_006	B	54.86	36.81	5.54	2.79	68.03	5
P1_007	Pre-Mix	46	49.05	3.57	1.39	61.643	15
P1_007	T	64.19	34.48	1.08	0.24	95.719	
P1_007	T	62.86	35.95	0.88	0.3	73.428	
P1_007	T	63.67	34.42	1.62	0.3	69.503	
P1_007	T	59.7	39.05	0.98	0.27	79.239	
P1_007	B	52.71	34.51	8.85	3.93	81.003	5
P1_007	B	54.21	35.24	7.07	3.49	84.272	5

Table A-3: OWS Data

P1_007	B	55.34	33.78	7.45	3.43	81.533	5
P1_007	B	53.36	34.53	8.33	3.77	79.229	5
P1_008	Pre-Mix	44.32	50.21	3.78	1.69	57.222	15
P1_008	T	60.56	37.42	1.09	0.94	65.391	
P1_008	T	62.29	36.05	0.82	0.84	75.51	
P1_008	T	61.6	35.22	2.39	0.79	75.334	
P1_008	T	62.54	35.72	0.99	0.75	74.278	
P1_008	B	54.38	37.29	5.67	2.66	85.975	5
P1_008	B	55.06	35.22	6.64	3.09	82.571	5
P1_008	B	55.91	34.39	6.69	3.01	83.89	5
P1_008	B	54.3	36.46	6.29	2.95	85.74	5
P1_009	Pre-Mix	60.09	32.76	5.07	2.08	51.33	
P1_009	T	61.59	37.19	0.6	0.61	71.824	
P1_009	T	62.82	36.02	0.55	0.61	75.38	
P1_009	T	62.85	35.84	0.67	0.64	77.459	
P1_009	T	62.15	36.7	0.54	0.62	79.887	
P1_009	B	53.57	36.56	6.52	3.35	86.47	5
P1_009	B	54.12	36.23	6.24	3.42	85.253	5
P1_009	B	53.22	35.25	7.93	3.6	79.413	5
P1_009	B	51.78	37.54	7.06	3.62	79.541	5
P1_010	Pre-Mix	58.86	34.88	4.59	1.67	51.485	
P1_010	T	61.76	33.55	4.15	0.54	89.712	
P1_010	T	62.34	36.41	0.65	0.61	70.113	
P1_010	T	62.42	35.5	1.46	0.62	76.294	
P1_010	T	63.04	35.17	1.09	0.69	76.997	
P1_010	B	56.38	36.83	4.01	2.77	84.491	5
P1_010	B	57.08	39.83	0.61	2.48	86.26	5
P1_010	B	57.93	35.79	3.89	2.4	87.974	5
P1_010	B	56.84	36.16	4.35	2.65	81.203	5
P1_011	Pre-Mix	58.4	34.99	4.41	2.2	46.593	
P1_011	T	61.31	36.72	1.37	0.59	80.18	
P1_011	T	63.52	34.16	1.78	0.54	74.12	
P1_011	T	63.91	34.43	1.08	0.57	79.335	
P1_011	T	67.07	31.47	0.75	0.72	71.383	
P1_011	B	54.19	35.57	6.59	3.65	88.264	5

Table A-3: OWS Data

P1_011	B	54.17	35.59	6.51	3.73	82.014	5
P1_011	B	55.25	33.95	7.1	3.7	89.601	5
P1_011	B	55.71	33.77	7	3.53	87.727	5
P1_012	Pre-Mix	59.08	33.94	4.93	2.05	61.002	
P1_012	T	62.96	34.83	1.27	0.94	72.161	
P1_012	T	62.01	35.2	1.88	0.91	67.831	
P1_012	T	61.71	33.12	4.33	0.84	81.653	
P1_012	T	61.17	37.27	0.7	0.86	78.065	
P1_012	B	53.09	37.73	6.1	3.08	85.682	5
P1_012	B	54.01	37.28	5.7	3	88.329	5
P1_012	B	52.79	36.83	6.96	3.42	79.491	5
P1_012	B	53.77	37.39	6.19	2.64	90.472	5
P1_013	Pre-Mix	59.07	34.73	4.25	1.96	64.994	
P1_013	T	52.83	43.83	1.97	1.37	83.757	
P1_013	T	61.39	35.72	1.75	1.14	77.062	
P1_013	T	61.26	35.23	2.29	1.21	74.705	
P1_013	T	58.81	37.86	2.14	1.18	74.95	
P1_013	B	55.87	36.93	5.07	2.13	84.484	5
P1_013	B	56.52	35.87	5.39	2.22	82.432	5
P1_013	B	55.06	38.03	4.75	2.16	85.41	5
P1_013	B	54.98	39.13	3.72	2.17	87.264	5
P1_014	Pre-Mix	55.43	38.57	4.11	1.9	59.467	
P1_014	T	62.75	35.66	0.94	0.64	72.037	
P1_014	T	61.78	36.47	1.19	0.56	78.461	
P1_014	T	62.38	37.01	0.01	0.59	73.268	
P1_014	T	63.14	35.47	0.88	0.52	78.956	
P1_014	B	53.5	37.12	6.25	3.13	91.195	5
P1_014	B	50.09	39.71	6.74	3.45	78.791	5
P1_014	B	53.8	36.32	6.65	3.24	90.893	5
P1_014	B	53.41	36.51	6.57	3.51	84.146	5
P1_015	Pre-Mix	58.25	35.92	4.23	1.61	68.029	
P1_015	T	61.58	36.34	1.58	0.5	83.372	
P1_015	T	62.06	36.66	0.68	0.59	66.271	
P1_015	T	62.51	36.43	0.52	0.54	76.152	
P1_015	T	62.4	35.11	1.95	0.54	79.409	

Table A-3: OWS Data

P1_015	B	55.32	35.31	6.44	2.93	87.048	5
P1_015	B	54.75	37.03	5.67	2.55	91.451	5
P1_015	B	56.27	34.73	6.35	2.65	91.734	5
P1_015	B	53.99	35.97	7.18	2.86	81.94	5
P1_016	Pre-Mix	59.75	34.5	4.02	1.73	55.785	
P1_016	T	59.86	37.52	1.91	0.71	84.903	
P1_016	T	62.19	35.73	1.37	0.7	83.271	
P1_016	T	61.88	35.95	1.49	0.67	80.095	
P1_016	T	63.48	33.88	1.97	0.66	83.352	
P1_016	B	53.32	37.49	6.51	2.67	85.289	5
P1_016	B	54.92	36.03	6.36	2.7	85.911	5
P1_016	B	54.68	37.48	5.3	2.54	89.294	5
P1_016	B	54.45	36.65	6.43	2.47	91.523	5
P1_017	Pre-Mix	58.88	35.44	4.08	1.6	66.693	
P1_017	T	61.06	35.61	2.29	1.04	81.883	
P1_017	T	61.19	34.41	3.28	1.12	82.772	
P1_017	T	62.61	34.13	2.08	1.18	90.801	
P1_017	T	60.18	37.25	1.53	1.04	79.279	
P1_017	B	56.7	36.45	4.78	2.07	87.607	5
P1_017	B	55.16	37.93	4.86	2.04	84.551	5
P1_017	B	55.36	38.1	4.5	2.04	90.87	5
P1_017	B	55.72	38.19	4.03	2.06	87.364	5
P1_018	Pre-Mix	57.81	35.69	4.95	1.55	57.769	
P1_018	T	59.01	38.18	1.85	0.97	79.534	
P1_018	T	61.14	35.61	2.25	1	82.651	
P1_018	T	60.08	35.77	3.2	0.95	70.644	
P1_018	T	57.74	38.99	2.34	0.93	83.493	
P1_018	B	53.86	39.62	4.65	1.87	88.362	5
P1_018	B	57.05	36.35	4.71	1.89	90.162	5
P1_018	B	58.92	34.38	4.77	1.93	87.035	5
P1_018	B	56.73	36.62	4.67	1.98	85.623	5
P1_019	Pre-Mix	74.22	20.62	3.68	1.48	64.081	
P1_019	T	47.46	50.7	1.47	0.37	79.209	
P1_019	T	60.62	36.97	2.04	0.38	77.194	
P1_019	T	67.78	29.96	1.87	0.39	69.556	

Table A-3: OWS Data

P1_019	T	53.13	45.88	0.61	0.38	81.244	
P1_019	B	54.41	36.67	5.93	2.99	89.288	5
P1_019	B	54.82	37.35	4.95	2.88	91.737	5
P1_019	B	53.63	38.45	5.16	2.76	94.065	5
P1_019	B	64.32	26.5	6.08	3.11	81.209	5
P1_020	Pre-Mix	72.04	22.32	3.96	1.68	62.12	
P1_020	T	42.64	56.01	0.78	0.57	87.57	
P1_020	T	62.45	36.2	0.81	0.53	86.412	
P1_020	T	62.13	36.47	0.83	0.57	74.823	
P1_020	T	63.41	35.36	0.69	0.54	82.198	
P1_020	B	55.24	36.77	5.33	2.66	85.161	5
P1_020	B	55.85	36.51	5.18	2.46	85.529	5
P1_020	B	56.27	36.29	5.01	2.42	90.753	5
P1_020	B	56.14	38.79	3.23	1.84	90.913	5
P1_020	Flask Remainder	53.8	39.24	4.76	2.19	101.717	10
P1_020	Flask Remainder	54.01	40.19	3.92	1.88	89.425	10
P1_021	Pre-Mix	58.82	35.77	3.85	1.56	77.799	
P1_021	T	59.82	39	0.59	0.6	74.145	
P1_021	T	60.54	38.03	0.85	0.58	70.849	
P1_021	T	61.65	37.04	0.76	0.55	72.129	
P1_021	T	61.36	37.4	0.69	0.55	89.699	
P1_021	B	55.16	37.27	5.15	2.43	88.806	5
P1_021	B	55.53	35.93	5.95	2.59	90.334	5
P1_021	B	55.51	36.55	5.5	2.44	82.94	5
P1_021	B	55.09	36.71	5.61	2.59	90.634	5
P1_021	Flask Remainder	53.76	41.85	2.96	1.43	76.402	10
P1_021	Flask Remainder	55.49	39.66	3.24	1.6	87.637	10
P1_022	Pre-Mix	58.72	35.05	4.7	1.53	75.888	
P1_022	T	61.02	37.77	0.82	0.39	84.095	
P1_022	T	62.46	36.68	0.46	0.4	73.851	
P1_022	T	62.03	36.6	1.03	0.35	81.107	
P1_022	T	62.14	36.11	1.43	0.33	79.136	
P1_022	B	54.26	36	6.81	2.92	82.19	5
P1_022	B	55.51	36.07	5.77	2.65	90.009	5
P1_022	B	54.18	36.82	5.99	3.01	84.217	5
P1_022	B	53.79	37.44	5.9	2.87	90.213	5

Table A-3: OWS Data

P1_022	Flask Remainder	55.08	40.42	2.84	1.66	102.599	10
P1_022	Flask Remainder	55.52	38.99	3.62	1.86	101.047	10
P1_023	Pre-Mix	57.84	36.65	3.93	1.58	74.966	
P1_023	T	59.8	37.33	1.79	1.08	83.845	
P1_023	T	60.41	37.32	1.25	1.02	77.275	
P1_023	T	61.23	35.54	2.21	1.02	85.134	
P1_023	T	60.62	37.36	1.1	0.91	89.408	
P1_023	B	53.89	39.05	5.32	1.75	88.679	5
P1_023	B	58	36.94	4.02	1.04	82.833	5
P1_023	B	56.71	36.97	4.07	2.24	82.822	5
P1_023	B	58.51	37.89	2.07	1.54	102.83	5
P1_023	Flask Remainder	51.87	40.83	5.25	2.05	60.996	10
P1_023	Flask Remainder	51.4	38.08	7.86	2.67	78.402	10

B. PHASE 2 EXPERIMENTAL DATA

Table B-1: Batch gravity settling data in wt% water (corr.)

Experiment	Label/Time:	0	1	3	5	7	10	30	60
P1_027	(-1,-1,0,0)	1.69	1.73	1.75	1.73	1.75	1.74	1.53	1.31
P1_050	(-1,-1,0,0)	1.81	1.78	1.79	1.73	1.75	1.69	1.47	1.22
P1_031	(-1,0,-1,0)	1.81	1.84	1.81	1.76	1.76	1.72	1.51	1.03
P1_052	(-1,0,-1,0)	1.88	1.89	1.83	1.78	1.80	1.78	1.48	1.19
P1_020	(-1,0,0,-1)	1.79	1.70	1.77	1.77	1.75	1.63	1.56	1.25
P1_056	(-1,0,0,-1)	1.97	1.85	1.82	1.81	1.86	1.77	1.57	1.29

Table B-1: Batch gravity settling data in wt% water (corr.)

P1_022	(-1,0,0,0)	1.86	1.92	1.90	1.80	1.83	1.82	1.59	1.39
P1_015	(-1,0,0,1)	1.91	1.83	1.90	1.96	1.82	1.82	1.59	1.55
P1_047	(-1,0,0,1)	1.81	1.79	1.79	1.70	1.74	1.73	1.60	1.51
P1_034	(-1,0,1,0)	1.69	1.64	1.73	1.52	1.61	1.58	1.33	1.19
P1_042	(-1,0,1,0)	1.86	1.90	1.79	1.76	1.78	1.73	1.58	1.29
P1_029	(-1,1,0,0)	1.81	1.86	1.82	1.81	1.80	1.72	1.39	1.30
P1_053	(-1,1,0,0)	1.85	1.87	1.83	1.79	1.80	1.74	1.57	1.44
P1_060	(0,-1,-1,0)	1.95	1.98	1.91	1.94	1.95	1.53	1.26	1.02
P1_021	(0,-1,-1,0)	1.90	1.98	1.96	1.87	1.77	1.79	1.50	1.25
P1_007	(0,-1,0,-1)	2.09	2.06	1.35	1.04	0.97	1.00	0.85	0.77
P1_057	(0,-1,0,-1)	1.99	1.92	1.46	0.83	0.77	0.73	0.67	0.55
P1_006	(0,-1,0,1)	1.82	1.82	1.76	1.80	1.78	1.73	1.30	1.19
P1_041	(0,-1,0,1)	1.91	1.93	1.89	1.85	1.84	1.83	1.40	1.13
P1_024	(0,-1,1,0)	2.00	1.97	1.93	1.88	1.82	1.76	1.31	1.06
P1_038	(0,-1,1,0)	1.92	1.93	1.85	1.68	1.42	1.33	1.08	0.86
P1_013	(0,0,-1,-1)	1.87	1.88	1.84	1.79	1.79	1.56	1.20	1.01
P1_043	(0,0,-1,-1)	2.01	1.88	1.74	1.21	1.06	0.94	0.88	0.80

Table B-1: Batch gravity settling data in wt% water (corr.)

P1_023	(0,0,-1,1)	1.85	1.84	1.87	1.82	1.82	1.73	1.32	1.06
P1_054	(0,0,-1,1)	1.82	1.83	1.83	1.80	1.72	1.69	1.28	1.14
P1_009	(0,0,0,0)	1.90	1.97	1.96	1.93	1.78	1.57	1.19	0.99
P1_018	(0,0,0,0)	1.80	1.79	1.87	1.78	1.55	1.37	1.11	0.66
P1_026	(0,0,0,0)	1.76	1.78	1.75	1.67	1.36	1.23	0.90	0.67
P1_033	(0,0,0,0)	1.85	1.80	1.47	1.03	0.92	0.88	0.74	0.56
P1_039	(0,0,0,0)	1.89	1.97	1.63	1.05	0.94	0.86	0.79	0.62
P1_051	(0,0,0,0)	1.94	1.91	1.16	0.89	0.82	0.81	0.71	0.63
P1_032	(0,0,1,-1)	1.75	1.56	1.01	0.77	0.74	0.68	0.61	0.48
P1_059	(0,0,1,-1)	2.07	2.00	0.99	0.70	0.62	0.60	0.60	0.44
P1_011	(0,0,1,1)	2.04	1.93	1.91	1.55	1.46	1.21	1.03	0.88
P1_058	(0,0,1,1)	1.90	1.95	1.92	1.40	1.20	1.07	0.89	0.72
P1_016	(0,1,-1,0)	1.87	1.79	1.86	1.77	1.84	1.55	1.15	1.05
P1_049	(0,1,-1,0)	1.85	1.84	1.86	1.75	1.48	1.20	0.92	0.93
P1_025	(0,1,0,-1)	1.86	1.87	1.33	0.92	0.78	0.75	0.64	0.54
P1_045	(0,1,0,-1)	1.95	1.85	0.79	0.66	0.63	0.60	0.59	0.67
P1_012	(0,1,0,1)	1.88	1.92	1.83	1.91	1.71	1.25	1.04	0.76

Table B-1: Batch gravity settling data in wt% water (corr.)

P1_044	(0,1,0,1)	2.13	1.96	1.89	1.85	1.60	1.31	1.02	0.77
P1_010	(0,1,1,0)	1.76	1.94	1.87	1.66	1.38	1.17	0.91	0.83
P1_040	(0,1,1,0)	1.88	1.83	1.03	0.76	0.73	0.71	0.59	0.50
P1_019	(1,-1,0,0)	1.82	1.80	1.82	1.69	1.39	1.25	1.04	0.89
P1_036	(1,-1,0,0)	1.89	1.81	1.75	1.37	1.17	1.08	0.93	0.75
P1_028	(1,0,-1,0)	1.76	1.83	1.79	1.73	1.59	1.28	1.01	0.85
P1_061	(1,0,-1,0)	1.94	1.91	1.30	0.73	0.69	0.63	0.61	0.57
P1_005	(1,0,0,-1)	2.18	1.89	0.74	0.67	0.64	0.55	0.51	0.43
P1_055	(1,0,0,-1)	2.09	2.10	1.97	1.08	1.06	1.04	0.98	0.95
P1_030	(1,0,0,1)	1.79	1.80	1.64	1.08	0.97	0.88	0.77	0.64
P1_048	(1,0,0,1)	1.83	1.80	1.02	0.92	0.84	0.75	0.63	0.58
P1_008	(1,0,1,0)	2.07	1.97	0.93	0.86	0.76	0.74	0.67	0.52
P1_035	(1,0,1,0)	1.83	1.89	1.64	0.52	0.58	0.56	0.45	0.39
P1_014	(1,1,0,0)	1.88	1.81	1.47	0.92	0.84	0.78	0.75	0.66
P1_037	(1,1,0,0)	1.93	1.94	1.67	0.58	0.52	0.50	0.40	0.31

Table B-2: Vertical concentration profile data in wt% water (corr.)

Experiment / (h/Z)	0.9	0.8	0.7	0.6	0.5	0.4	0.3	0.2	0.1	0
P1_027 (-1,-1,0,0)	1.18	1.18	1.24	1.24	1.25	1.18	1.14	1.13	1.15	3.43
P1_050 (-1,-1,0,0)	1.84	1.09	1.07	1.09	1.07	0.99	1.00	1.01	1.06	4.63
P1_031 (-1,0,-1,0)	1.13	1.13	1.18	1.17	1.16	1.10	1.13	1.10	1.11	7.84
P1_052 (-1,0,-1,0)	1.37	1.13	1.12	1.10	1.10	0.99	0.99	1.02	1.11	2.92
P1_020 (-1,0,0,-1)	1.78	1.21	1.20	1.31	1.20	1.17	1.12	1.11	1.14	3.90
P1_056 (-1,0,0,-1)	2.01	1.16	1.23	1.23	1.23	1.11	1.13	1.11	0.76	2.29
P1_022 (-1,0,0,0)	1.43	2.30	1.33	1.30	1.33	1.24	1.86	1.23	1.24	3.60
P1_015 (-1,0,0,1)	1.33	1.42	1.42	1.40	1.41	1.23	1.30	1.31	1.30	3.79
P1_047 (-1,0,0,1)	1.34	1.34	1.40	1.40	1.31	1.25	1.29	1.29	1.35	4.15
P1_034 (-1,0,1,0)	1.26	1.03	1.11	1.09	1.14	0.99	1.01	1.28	1.03	2.76
P1_042 (-1,0,1,0)	1.38	1.07	1.19	1.16	1.16	1.08	1.09	1.07	1.06	3.24
P1_029 (-1,1,0,0)	1.09	1.13	1.09	1.08	1.10	0.96	0.97	0.97	0.98	4.35
P1_053 (-1,1,0,0)	1.28	1.20	1.24	1.24	0.67	1.13	1.12	1.09	1.18	9.50
P1_060 (0,-1,-1,0)	1.05	1.05	1.08	1.12	1.06	0.94	0.97	0.99	1.07	6.72

Table B-2: Vertical concentration profile data in wt% water (corr.)

P1_021	(0,-1,-1,0)	0.58	0.58	0.59	0.57	0.58	0.49	0.48	0.48	0.49	27.62
P1_007	(0,-1,0,-1)	0.51	0.52	0.54	0.53	0.52	0.47	0.44	0.46	4.87	18.98
P1_057	(0,-1,0,-1)	0.00	0.00	0.00	0.00	0.90	0.92	0.96	0.91	0.93	6.68
P1_006	(0,-1,0,1)	0.93	0.92	0.94	0.93	0.76	0.96	0.95	0.94	0.97	8.26
P1_041	(0,-1,0,1)	1.30	1.00	1.08	1.07	1.08	0.92	0.92	0.93	0.93	11.40
P1_024	(0,-1,1,0)	0.88	0.82	0.81	0.80	0.79	0.68	0.68	0.68	0.68	33.84
P1_038	(0,-1,1,0)	0.98	0.97	1.01	1.00	0.98	0.93	0.92	0.91	2.08	19.12
P1_013	(0,0,-1,-1)	0.60	0.58	0.59	0.59	0.59	0.63	0.61	0.60	0.65	19.03
P1_043	(0,0,-1,-1)	1.11	0.90	0.96	1.15	1.01	0.93	0.92	0.93	0.93	3.22
P1_023	(0,0,-1,1)	0.98	0.99	1.00	0.96	0.98	0.86	0.91	0.90	0.95	3.08
P1_054	(0,0,-1,1)	0.93	0.94	1.00	0.98	0.96	0.87	0.87	0.87	0.86	10.70
P1_009	(0,0,0,0)	0.91	1.25	0.90	0.90	0.92	0.82	0.84	0.84	0.82	18.71
P1_018	(0,0,0,0)	0.74	0.61	0.65	0.66	0.64	0.54	0.54	0.55	0.52	18.41
P1_026	(0,0,0,0)	0.53	0.62	0.57	0.56	0.53	0.45	0.44	0.45	0.46	22.06
P1_033	(0,0,0,0)	0.46	0.43	0.48	0.64	0.43	0.44	0.88	0.44	1.43	18.25

Table B-2: Vertical concentration profile data in wt% water (corr.)

P1_039	(0,0,0,0)	0.53	0.55	0.55	0.55	0.56	0.47	0.45	0.00	4.56	6.68
P1_051	(0,0,0,0)	0.74	0.44	0.46	0.43	0.42	0.37	0.39	0.39	0.39	12.12
P1_032	(0,0,1,-1)	0.48	0.39	0.44	0.42	0.42	0.40	0.42	0.40	14.49	11.04
P1_059	(0,0,1,-1)	0.85	0.86	0.89	0.84	0.86	0.79	0.76	0.77	0.77	16.99
P1_011	(0,0,1,1)	0.94	0.68	0.68	0.69	0.69	0.59	0.60	0.59	0.46	9.35
P1_058	(0,0,1,1)	1.10	0.99	1.04	0.99	1.01	0.93	0.92	0.90	0.94	8.75
P1_016	(0,1,-1,0)	1.20	1.18	1.21	1.24	1.25	1.13	1.11	1.12	1.13	2.84
P1_049	(0,1,-1,0)	0.56	0.54	0.56	0.56	0.56	0.63	0.61	0.46	0.67	23.00
P1_025	(0,1,0,-1)	0.48	0.47	0.50	0.51	0.55	0.41	0.39	0.41	5.97	10.86
P1_045	(0,1,0,-1)	0.30	0.33	0.31	0.31	0.35	0.38	0.31	0.33	12.50	12.21
P1_012	(0,1,0,1)	0.77	0.81	0.76	0.78	0.78	0.49	0.71	0.70	0.71	8.62
P1_044	(0,1,0,1)	1.72	0.80	0.85	0.75	0.76	0.67	0.66	0.67	0.69	9.29
P1_010	(0,1,1,0)	0.77	0.71	0.77	0.35	0.76	0.69	0.68	0.67	2.01	11.07
P1_040	(0,1,1,0)	0.47	0.46	0.45	0.49	0.43	0.37	0.36	0.35	9.27	12.77
P1_019	(1,-1,0,0)	0.81	0.79	0.79	0.79	0.80	0.70	0.72	0.73	0.72	2.93

Table B-2: Vertical concentration profile data in wt% water (corr.)

P1_036	(1,-1,0,0)	0.81	0.66	0.67	0.67	0.70	0.54	0.60	0.59	0.57	23.68
P1_028	(1,0,-1,0)	0.75	0.75	0.76	0.75	0.78	0.68	0.68	0.66	0.68	15.72
P1_061	(1,0,-1,0)	0.53	0.50	0.48	0.50	0.49	0.49	0.51	0.49	1.64	4.21
P1_005	(1,0,0,-1)	0.00	0.00	0.00	0.00	0.25	0.27	0.29	0.26	10.49	10.47
P1_055	(1,0,0,-1)	0.88	0.88	0.92	0.85	0.81	0.99	0.83	0.85	5.81	4.02
P1_030	(1,0,0,1)	0.62	0.55	0.58	0.58	0.59	0.48	0.48	0.48	0.72	1.81
P1_048	(1,0,0,1)	0.44	0.44	0.46	0.44	0.46	0.40	0.39	0.37	12.29	13.22
P1_008	(1,0,1,0)	0.32	0.36	0.30	0.38	0.39	0.39	0.39	0.39	0.39	13.31
P1_035	(1,0,1,0)	0.31	0.29	0.26	0.28	0.28	0.27	0.26	0.26	12.97	12.57
P1_014	(1,1,0,0)	0.76	0.59	0.60	0.58	0.61	0.56	0.56	0.53	1.98	7.82
P1_037	(1,1,0,0)	0.27	0.31	0.28	0.28	0.27	0.21	0.23	0.22	18.34	12.31

Table B-3: Solids Content Data

Experiment	Label / Solids Content	Pre-Mix	0.1	0.5	0.9
P1_027	(-1,-1,0,0)	1.07	0.89	0.89	0.91
P1_050	(-1,-1,0,0)	1.26	0.96	0.89	0.9
P1_031	(-1,0,-1,0)	0.97	0.95	0.96	0.98
P1_052	(-1,0,-1,0)	1.09	0.93	0.89	0.9
P1_020	(-1,0,0,-1)	1	0.99	0.9	0.9
P1_056	(-1,0,0,-1)	0.92	0.8	0.81	0.82
P1_022	(-1,0,0,0)	1.1	0.87	0.84	0.78
P1_015	(-1,0,0,1)	1.18	0.98	0.89	0.94
P1_047	(-1,0,0,1)	1.27	1.08	1.1	1.1
P1_034	(-1,0,1,0)	1.17	1.03	1.06	0.99
P1_042	(-1,0,1,0)	1.15	1.03	1.01	0.89
P1_029	(-1,1,0,0)	1.05	0.88	0.68	0.81
P1_053	(-1,1,0,0)	1.05	0.87	0.86	0.87
P1_060	(0,-1,-1,0)	0.96	0.66	0.68	0.56

Table B-3: Solids Content Data

P1_007	(0,-1,0,-1)	1.14	0.52	0.52	0.48
P1_057	(0,-1,0,-1)	0.98	0.29	0.24	0.4
P1_006	(0,-1,0,1)	0.98	0.95	0.85	1.15
P1_041	(0,-1,0,1)	1.15	0.89	0.88	0.88
P1_024	(0,-1,1,0)	1.02	0.82	0.66	0.65
P1_038	(0,-1,1,0)	1.04	0.73	0.7	0.72
P1_013	(0,0,-1,-1)	1.15	0.74	0.72	0.71
P1_043	(0,0,-1,-1)	1.05	0.51	0.51	0.76
P1_023	(0,0,-1,1)	1.02	0.87	0.82	0.9
P1_054	(0,0,-1,1)	1.05	0.8	0.82	0.77
P1_009	(0,0,0,0)	1.01	0.67	0.64	0.63
P1_018	(0,0,0,0)	1.11	0.63	0.63	0.62
P1_026	(0,0,0,0)	1.05	0.66	0.65	0.63
P1_033	(0,0,0,0)	1.17	0.59	0.6	0.59
P1_039	(0,0,0,0)	1.15	0.55	0.55	0.63

Table B-3: Solids Content Data

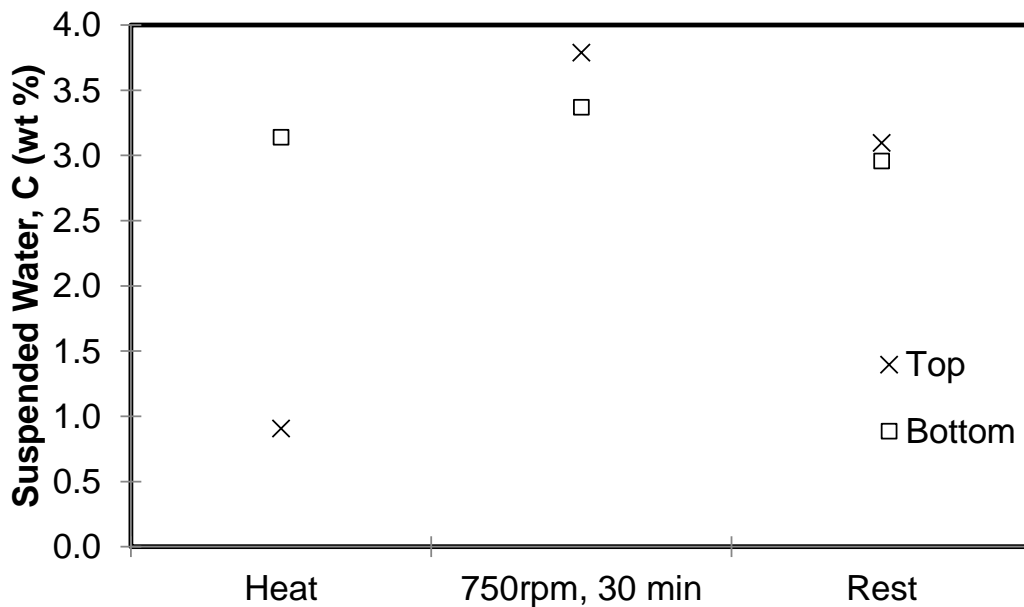
P1_051	(0,0,0,0)	1.09	0.46	0.46	0.62
P1_032	(0,0,1,-1)	0.97	0.42	0.46	0.68
P1_059	(0,0,1,-1)	0.96	0.19	0.17	0.85
P1_011	(0,0,1,1)	1.01	0.53	0.51	0.57
P1_058	(0,0,1,1)	0.98	0.41	0.38	0.49
P1_016	(0,1,-1,0)	1.18	0.75	0.69	0.75
P1_021	(0,-1,-1,0)	1.1	0.89	0.91	0.87
P1_049	(0,1,-1,0)	1.26	0.77	0.69	0.7
P1_025	(0,1,0,-1)	1.05	0.37	0.44	0.66
P1_045	(0,1,0,-1)	1.35	0.47	0.47	1.06
P1_012	(0,1,0,1)	1.01	0.77	0.57	0.57
P1_044	(0,1,0,1)	1.05	0.84	0.8	0.83
P1_010	(0,1,1,0)	1.01	0.51	0.5	0.47
P1_040	(0,1,1,0)	1.15	0.42	0.43	0.46
P1_019	(1,-1,0,0)	1	0.64	0.63	0.88

Table B-3: Solids Content Data

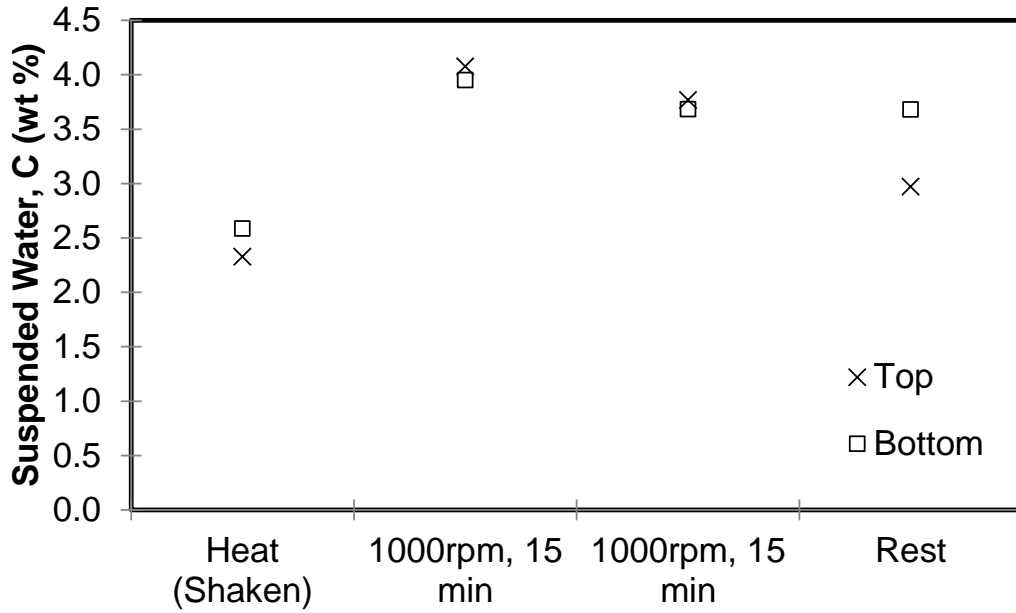
P1_036	(1,-1,0,0)	1.17	0.32	0.31	0.67
P1_028	(1,0,-1,0)	1.07	0.66	0.69	0.68
P1_061	(1,0,-1,0)	0.83	0.11	0.16	1.09
P1_005	(1,0,0,-1)	0.98	0.3	0.29	0.9
P1_055	(1,0,0,-1)	0.92	0.14	0.15	
P1_030	(1,0,0,1)	1.05	0.39	0.4	0.76
P1_048	(1,0,0,1)	1.27	0.64	0.59	0.8
P1_008	(1,0,1,0)	1.14	0.55	0.31	0.39
P1_035	(1,0,1,0)	1.17	0.66	0.7	
P1_014	(1,1,0,0)	1.15	0.49	0.47	1.07
P1_037	(1,1,0,0)	1.04	0.24	1.13	0.19

C. PRE-MIXING EXPERIMENTS

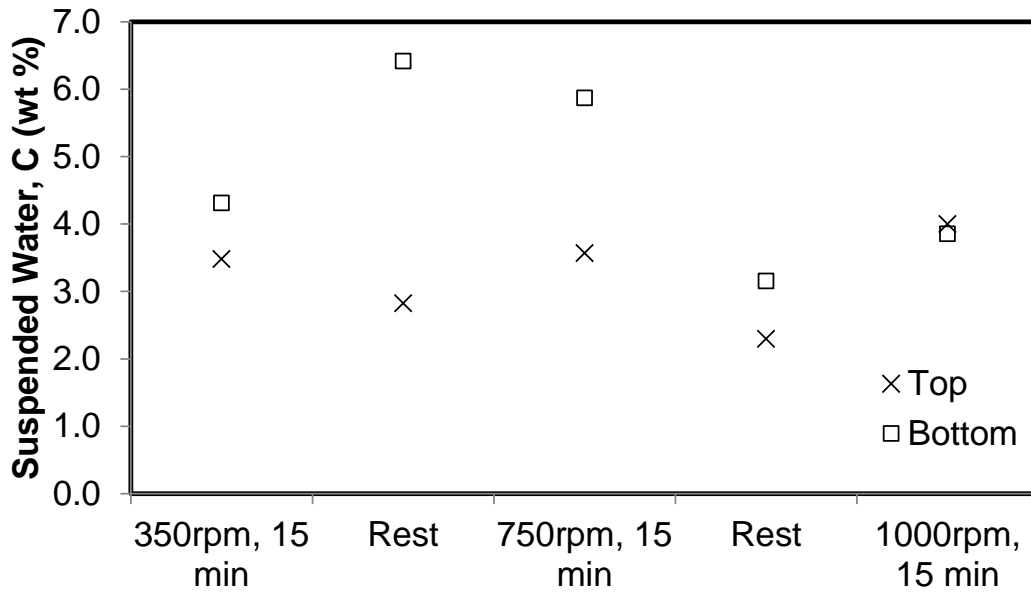
Experiments were conducted to evaluate the appropriateness of the pre-mixing protocol. Main concerns: will most of the sample be re-suspended? How stable is it? Is the sample fairly uniform from top to bottom?



Mixing for 30 minutes at 750 rpm after heating was not sufficiently stable; there is still a large gap in water content from the top to the bottom. Shaking the sample, then heating it to temperature, then pre-mixing the sample for 15 minute suspended a lot of solids. No difference was observed after mixing for 15 more minutes.



The next step was to see if it is possible to obtain sufficiently high solids at lower agitation, if shaken by hand before any impeller agitation or heating takes place. The best case was still at 1000 rpm for 15 minutes. As a note, 1000 rpm seemed to be the limits at which the sample could be agitated.



References

Bhardwaj, A. and S. Hartland (1993). "Study of demulsification of water-in-crude oil emulsion." Journal of Dispersion Science and Technology **14**(5): 541-557.

Bhardwaj, A. and S. Hartland (1994). "Dynamics of emulsification and demulsification of water in crude oil emulsions." Industrial & Engineering Chemistry Research **33**(5): 1271-1279.

Bhardwaj, A. and S. Hartland (1994). "Kinetics of coalescence of water droplets in water-in-crude oil emulsions." Journal of Dispersion Science and Technology **15**(2): 133-146.

Borges, B., M. Rondón, O. Sereno and J. Asuaje (2009). "Breaking of water-in-crude-oil emulsions. 3. influence of salinity and water-oil ratio on demulsifier action." Energy and Fuels **23**(3): 1568-1574.

Chen, H. T. and S. Middleman (1967). "Drop size distribution in agitated liquid-liquid systems." AIChE J. **13**(5): 989-995.

Chin, C. J., S. Yiaccoumi and C. Tsouris (1998). "Shear-induced flocculation of colloidal particles in stirred tanks." Journal of Colloid and Interface Science **206**(2): 532-545.

Czarnecki, J., K. Moran and X. Yang (2007). "On the "rag layer" and diluted bitumen froth dewatering." Canadian Journal of Chemical Engineering **85**(5): 748-755.

Czarnecki, J., K. Moran and X. Yang (2008). "On the "Rag Layer" and Diluted Bitumen Froth Dewatering." CJChE **85**: 748-755.

Davies, J. T. (1987). "A physical interpretation of drop sizes in homogenizers and agitated tanks, including the dispersion of viscous oils." Chem. Eng. Sci. **42**: 1671-1676.

ERCB (2011). ST98-2011: Alberta's Energy Reserves 2010 and Supply/Demand Outlook 2011-2020. Calgary.

Feng, X., P. Mussone, S. Gao, S. Wang, S. Y. Wu, J. H. Masliyah and Z. Xu (2010). "Mechanistic study on demulsification of water-in-diluted bitumen emulsions by ethylcellulose." Langmuir **26**(5): 3050-3057.

Feng, X., Z. Xu and J. Masliyah (2009). "Biodegradable polymer for demulsification of water-in-bitumen emulsions." Energy and Fuels **23**(1): 451-456.

Grenville, R. K. (1992). Blending of viscous Newtonian and pseudo-plastic fluids, Ph.D. dissertation. Cranfield, Bedfordshire, England, Cranfield Institute of Technology.

Gu, G., Z. Xu, K. Nandakumar and J. H. Masliyah (2002). "Influence of water-soluble and water-insoluble natural surface active components on the stability of water-in-toluene-diluted bitumen emulsion." Fuel **81**(14): 1859-1869.

Ibemere, S. and S. Kresta (2007). "Modelling the mixing and dissolution kinetics of partially miscible liquids." Chemical Engineering Research and Design **85**(5 A): 710-720.

Kaku, V., M. Boufadel and A. Venosa (2006). "Evaluation of mixing energy in flasks used for dispersant effectiveness testing." Journal of Environmental Engineering: 93-101.

Khristov, K., S. D. Taylor, J. Czarnecki and J. Masliyah (2000). "Thin liquid film technique - Application to water-oil-water bitumen emulsion films." Colloids and Surfaces A: Physicochemical and Engineering Aspects **174**(1-2): 183-196.

Kim, Y. H. and D. T. Wasan (1996). "Effect of Demulsifier Partitioning on the Destabilization of Water-in-Oil Emulsions." Industrial and Engineering Chemistry Research **35**(4): 1141-1149.

Krawczyk, M. A., D. T. Wasan and C. S. Shetty (1991). "Chemical demulsification of petroleum emulsions using oil-soluble demulsifiers." Industrial and Engineering Chemistry Research **30**(2): 367-375.

Kresta, S. M. (2010). Mixing in the Process Industry, CH E 620. Edmonton, Alberta, Canada, University of Alberta.

Kukukova, A., J. Aubin and S. M. Kresta (2009). "A new definition of mixing and segregation: Three dimensions of a key process variable." Chemical Engineering Research and Design **87**(4): 633-647.

Liu, J., Z. Xu and J. Masliyah (2005). "Processability of oil sand ores in Alberta." Energy and Fuels **19**(5): 2056-2063.

Long, Y., T. Dabros and H. Hamza (2002). "Stability and settling characteristics of solvent-diluted bitumen emulsions." Fuel **81**(15): 1945-1952.

Machado, M. and S. Kresta (2011). Unpublished Data.

Masliyah, J., Z. Zhou, Z. Xu, J. Czarnecki and H. Hamza (2004). "Understanding water-based bitumen extraction from athabasca oil sands." Canadian Journal of Chemical Engineering **82**(4): 628-654.

Mason, S. L., K. May and S. Hartland (1995). "Drop size and concentration profile determination in petroleum emulsion separation." Colloids and Surfaces A: Physicochemical and Engineering Aspects **96**(1-2): 85-92.

Menon, V. B. and D. T. Wasan (1988). "Characterization of oil-water interfaces containing finely divided solids with applications to the coalescence of water-in-oil Emulsions: A review." Colloids and Surfaces **29**(1): 7-27.

Ng, S., M. Lu, J. Kresta, P. H. J. Mercier, L. S. Kotlyar, B. D. Sparks and T. McCracken (2011). Impact of Froth Quality on Its Processability for Naphtha Based Froth Treatment Processes. Oilsands 2011 Conference, Edmonton, Alberta, Canada.

Pacheco, V. F., L. Spinelli, E. F. Lucas and C. R. E. Mansur (2011). "Destabilization of petroleum emulsions: Evaluation of the influence of the solvent on additives." Energy and Fuels **25**(4): 1659-1666.

Paul, E. L., V. A. Atiemo-Obeng and S. M. Kresta (2004). Handbook of Industrial Mixing : Science and Practice. Hoboken, New Jersey, John Wiley & Sons, Inc.

Peña, A. A., G. J. Hirasaki and C. A. Miller (2005). "Chemically induced destabilization of water-in-crude oil emulsions." Industrial and Engineering Chemistry Research **44**(5): 1139-1149.

Radler, M. (2006). "Oil production, reserves increase slightly in 2006." Oil and Gas Journal **104**(47): 20-21.

Rahmani, N. H. G., T. Dabros and J. H. Masliyah (2004). "Evolution of asphaltene floc size distribution in organic solvents under shear." Chemical Engineering Science **59**(3): 685-697.

Rahmani, N. H. G., T. Dabros and J. H. Masliyah (2005). "Settling properties of asphaltene aggregates." Energy and Fuels **19**(3): 1099-1108.

Rahmani, N. H. G., J. H. Masliyah and T. Dabros (2003). "Characterization of asphaltenes aggregation and fragmentation in a shear field." AIChE Journal **49**(7): 1645-1655.

Ramakrishna (2001). Population Balances. New York, Wiley.

Rashidnia, N. and R. Balasubramaniam (2004). "Measurement of the mass diffusivity of miscible liquids as a function of concentration using a common path shearing interferometer." Experiments in Fluids **36**(4): 619-626.

Rastegari, K., W. Y. Svrcek and H. W. Yarranton (2004). "Kinetics of asphaltene flocculation." Industrial and Engineering Chemistry Research **43**(21): 6861-6870.

Saadatmand, M., H. W. Yarranton and K. Moran (2008). "Rag layers in oil sand froths." Industrial and Engineering Chemistry Research **47**(22): 8828-8839.

Seyer, F. A. and G. W. Gyte (1989). Viscosity. AOSTRA Technical Handbook on Oil Sands, Bitumens, and Heavy Oils. L. E. Hepler and C. His, AOSTRA Technical Publication Series #6.

Shelfantook, W. E. (2004). "A perspective on the selection of froth treatment processes." Canadian Journal of Chemical Engineering **82**(4): 704-709.

Skelland, A. H. P. and R. Seksaria (1978). "Minimum impeller speeds for liquid-liquid dispersion in baffled vessels." Ind. Eng. Chem. Process. Des. Dev. **17**: 56-61.

Sztukowski, D. M. and H. W. Yarranton (2005). "Oilfield solids and water-in-oil emulsion stability." Journal of Colloid And Interface Science **285**(2): 821-833.

Tavlarides, L. L. and C. Tsouris (1994). "Breakage and Coalescence Models for Drops in Turbulent Dispersions." AICHE J. **40(3)**: 395-406.

Xia, L., S. Lu and G. Cao (2004). "Stability and demulsification of emulsions stabilized by asphaltenes or resins." Journal of Colloid And Interface Science **271(2)**: 504-506.

Xu, Z., Q. Liu, J. Peng and J. Masliyah (2011). A Novel Magnetic Demulsifier for Removal of Water in Diluted Bitumen. Oilsands 2011 Conference, Edmonton, Alberta, Canada.

Yan, N., M. R. Gray and J. H. Masliyah (2001). "On water-in-oil emulsions stabilized by fine solids." Colloids and Surfaces A: Physicochemical and Engineering Aspects **193(1-3)**: 97-107.

Yang, X. and R. Melley (2011). Case Studies in Chemical Application in Naphtha Froth Treatment Systems. Oilsands 2011 Conference, Edmonton, Alberta, Canada.

Yarranton, H. W., H. Hussein and J. H. Masliyah (2000). "Water-in-hydrocarbon emulsions stabilized by asphaltenes at low concentrations." Journal of Colloid And Interface Science **228(1)**: 52-63.

Yeung, A., T. Dabros and J. Czarnecki (1999). "On the interfacial properties of micrometre-sized water droplets in crude oil." Proceedings of the Royal Society A: Mathematical, Physical and Engineering Sciences **455(1990)**: 3709-3723.

Zhang, J. J. and X. Y. Li (2003). "Modeling particle-size distribution dynamics in a flocculation system." AICHE Journal **49(7)**: 1870-1882.

Zhou, G. and S. M. Kresta (1996). "Distribution of energy between convective and turbulent flow for three frequently used impellers." AICHE J. **74A**: 2476-2490.

Zhou, G. and S. M. Kresta (1996). "Impact of geometry on the maximum turbulence energy dissipation rate for various impellers." AICHE J. **42**: 2476-2490.

Zhou, G. and S. M. Kresta (1998). "Evolution of drop size distribution in liquid-liquid dispersions for various impellers." Chem. Eng. Sci. **53**: 2099-2113.

Zweitering, T. N. (1958). "Suspending of solid particles in liquid by agitators." Chem. Eng. Sci. **8**: 244.